2-Substituted vs 4-substituted-9,9'-spirobifluorene host materials for green and blue phosphorescent OLEDs: a structure-property relationship study

Sebastien Thiery, Céline Declairieux, Denis Tondelier, Gijun Seo, Bernard Geffroy, Olivier Jeannin, Rémi Métivier, Joëlle Rault-Berthelot, Cyril Poriel

2-substituted vs 4-substituted-9,9'-spirobifluorene host materials for green and blue phosphorescent OLEDs: A Structure-Property Relationship Study

*Sébastien Thiery,[a] Céline Declairieux,[c] Denis Tondelier,[c] Gijun Seo,[c] Bernard Geffroy,[c,d] Olivier Jeannin,[a] Rémi Métivier,[b] Joëlle Rault-Berthelot,[*a] Cyril Poriel[*a]*

a. Université de Rennes 1-UMR CNRS 6226, "Institut des Sciences Chimiques de Rennes" MaCSE group. Bat 10C, Campus de Beaulieu, 35042 Rennes, France
b. PPSM, Institut d'Alembert, ENS Cachan, UMR CNRS 8531, 61 Avenue du Président Wilson, 94235 Cachan, France
c. LPICM, Ecole Polytechnique, UMR CNRS 7647, Route de Saclay, 91128, Palaiseau
d. LICSEN, CEA Saclay, IRAMIS/NIMBE, 91191 Gif sur Yvette

Abstract

We report a structure-property relationship study of four 9,9'-spirobifluorene (SBF) derivatives (4-5Pm-SBF, 2-5Pm-SBF, 4-Ph-SBF and 2-Ph-SBF), substituted with either phenyl or pyrimidine at the C2 or C4 position of the SBF core. Structural, thermal, electrochemical and photophysical properties have been examined and correlated to theoretical calculations in order to study the influence of the nature and the position of the substituent. The emission properties of 4- vs 2-substituted SBFs are noticeably different highlighting, in the excited state, the remarkable effect of substitution in *ortho* position of SBF. All compounds have been used as host material for green dopant in PhOLEDs with very high performances (2-5Pm-SBF: CE > 58 cd/A, PE > 35 lm/W, EQE > 14 %). More importantly, the two 4-substituted SBFs have been used as host materials in blue PhOLEDs, displaying high performance and a decrease of V_{TH} for 4-5Pm-SBF due to the incorporation of the electron-withdrawing pyrimidine.

Grpahical Abstract

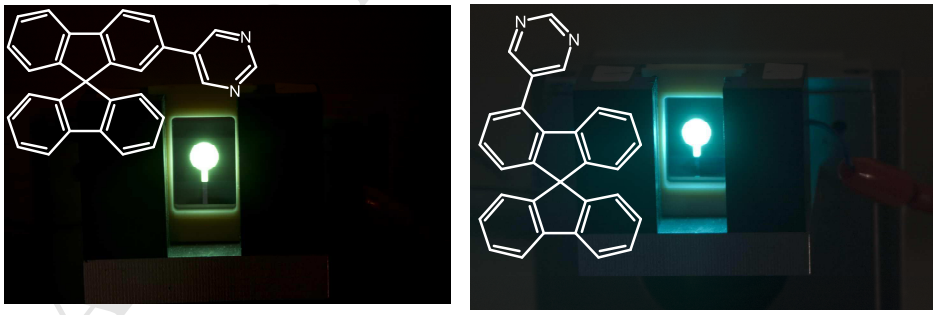

Introduction

In the past twenty years, the use of organic semiconducting materials for applications in "plastic electronics", such as field effect transistors (FETs),[1] organic light emitting diodes (OLEDs),[2,3] and organic photovoltaic (OPVs),[4,5] has gained fantastic interest.[6-8] Particularly, OLEDs have attracted much scientific and commercial interest because of their potential applications in organic flat-panel displays and solid-state lighting. However, as full colour displays and white lighting require materials that emit over a broad range of colour, the weak link of the technology remains the lack of efficient and stable blue light emitters. Moreover, due to the triplet exciton/singlet exciton ratio of 3/1, the maximum achievable emission quantum yield is limited to 25% for fluorescent emitters. Among the significant progress recently made, phosphorescent organic emitting-diodes (PHOLEDs) which use heavy-metal complexes as emitters to harvest both singlet and triplet excitons are considered as the most promising technology because, theoretically the internal quantum efficiencies of these devices may reach 100 %. The fabrication of blue phosphorescent devices is however still challenging because the prerequisites for designing organic host materials are (i) a high triplet energy level (higher than E_T of the blue dopant), (ii) a high glass-transition temperature (Tg) and (iii) matching HOMO/LUMO levels for hole and electron injection/transport. In this context, most of host materials for blue PhOLEDs are based on carbazole, triphenylamines, phosphine oxides or fluorene derivatives.[9-11] However, novel host materials with good thermal and morphological stabilities to afford blue PhOLEDs with high efficiencies, stability and colour purity are still desirable. In this context, 9,9'-spirobifluorene (SBF) based semiconductors have experienced a fantastic development during the last thirty years, due to their use as chiral ligand,[12,13] as electropolymerizable building block,[14-17] as solid state laser[18], in third-order nonlinear optics,[19] in Metal Organic Frameworks[20] but more importantly in organic electronics, leading to fantastic breakthroughs in the field.[21-23] Thus, numbers of electron donating and /or withdrawing functionalities have been introduced on the SBF scaffold in order to make the electronic properties of the resulting dyes fitting with an application.[21] For that purpose, electron-deficient heterocycles such as 1,3,4-oxadiazoles,[24] pyridine[25], quinoline,[26] quinoxaline[27] and pyridopyrazine[28] connected at C2 and C7 positions of SBF were reported in literature. Among those electron-deficient heterocycles, only few examples describing the fluorene substitution by pyrimidine units (see chart 1) have been reported to date. However, pyrimidine possesses many striking characteristics, as it is notably more electron-deficient than pyridine, which has been widely studied.[29] Thus Bryce's group has for example demonstrated in 2003, that fluorene fluorophore F3 emits a pure blue emission in solution and thin films.[30] However the electroluminescent spectrum of F3-based OLED mainly presents the known parasite green emission of dialkylfluorenes.[31-33] A similar green emission is observed on PL spectrum of the liquid crystal F4.[34] The introduction of a 9,9' Spirobifluorene unit (SBF) in TBPSF leads to improve the thermal, optical and electronic properties and this new blue emitter has been used as host for fluorescent blue, red or green organic dopants leading to efficient devices.[35,36]

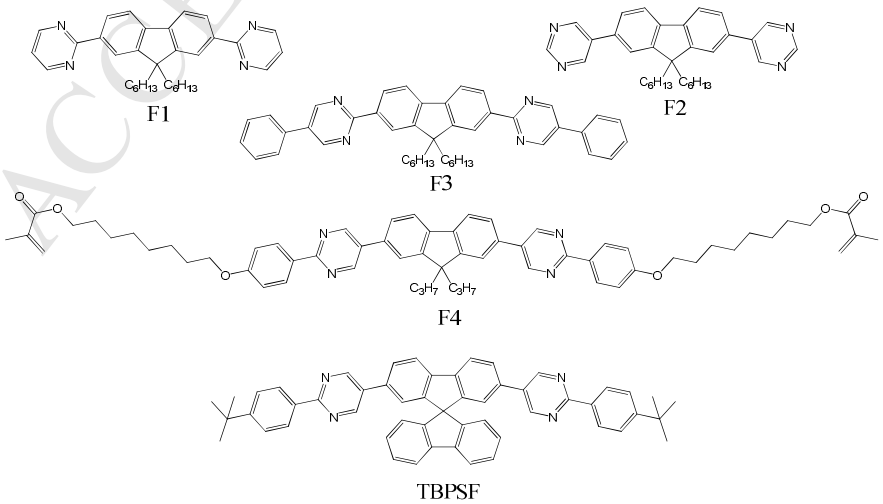

Chart 1. Literature report of fluorene substitution by pyrimidine units

However, if 2-substituted SBFs have been impressively investigated for the last decades, it is far to be the case of the three other positional isomers, that are 1-, 3- or 4-substituted SBFs. Thus, for example, 4-substituted SBFs have only been reported in a few instances[37-42] but appears as a very appealing scaffold to design rigid SBF-based organic host materials for PhOLEDs. In our quest for robust derivatives with high E_T which can be used as host materials for green and blue phosphorescent dyes,[43] we wish to report herein the synthesis and the detailed study of the properties of two pyrimidine-substituted SBFs (**4-5Pm-SBF** and **2-5Pm-SBF**, see chart 2). Moreover, in order to give a detailed description of the influence of the pyrimidine unit, the 2- and 4-phenyl-substituted SBFs (**2-Ph-SBF** and **4-Ph-SBF**) have been also studied in detail (**4-Ph-SBF** has been previously reported).[44] Thus, after synthetic considerations, the electrochemical, thermal and photo-physical properties will be discussed and coupled to a theoretical approach. The influence of the nature of the substituent (pyrimidine *vs* phenyl) and of its position (2- *vs* 4-) will be notably carefully investigated. Finally, the incorporation of these four semiconductors as host material for green and blue PhOLEDs will be presented.

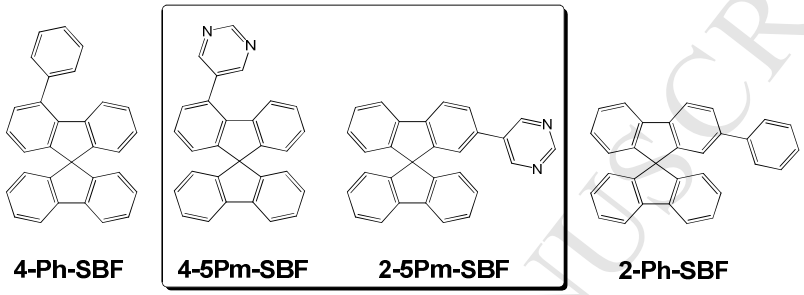

Chart 2. Molecules studied in this work

Results and discussion

The first step towards the synthesis of 4- and 2-substituted SBF was the access of the two key platforms 4- and 2-bromo-9,9'-spirobifluorene (see structures of **4-Br-SBF** and **2-Br-SBF** in scheme 1). As reported previously,[37,44] **4-Br-SBF** was synthesized by the mono lithium-halogen exchange of 2,2'-dibromobiphenyl followed by the trapping of the corresponding lithiated intermediate with 9-fluorenone. The intramolecular electrophilic ring closure of the corresponding fluorenol (not isolated), in acidic media (AcOH/HCl), further provides **4-Br-SBF** with 75 % yield (2 steps). Finally, a subsequent Suzuki cross-coupling between **4-Br-SBF** and either 5-pyrimidine boronic acid or phenylboronic acid was performed ($Pd(dppf)Cl_2/K_2CO_3$/DMF) providing **4-5Pm-SBF** or **4-Ph-SBF** with significant good yields (94% and 91% respectively). Similarly, access to **2-Br-SBF** was performed by the lithium-halogen exchange of 2-bromobiphenyl followed by the trapping of the corresponding lithiated intermediate with 2-bromo-9-fluorenone.[45] The intramolecular electrophilic ring closure of the corresponding fluorenol, in acidic media (AcOH/HCl), further provides **2-Br-SBF** with 67% yield (2 steps), involved in a final Suzuki cross-coupling with either 5-pyrimidine boronic acid or phenylboronic acid to lead the corresponding **2-5Pm-SBF** or **2-Ph-SBF** with high yields (77% and 78% respectively).

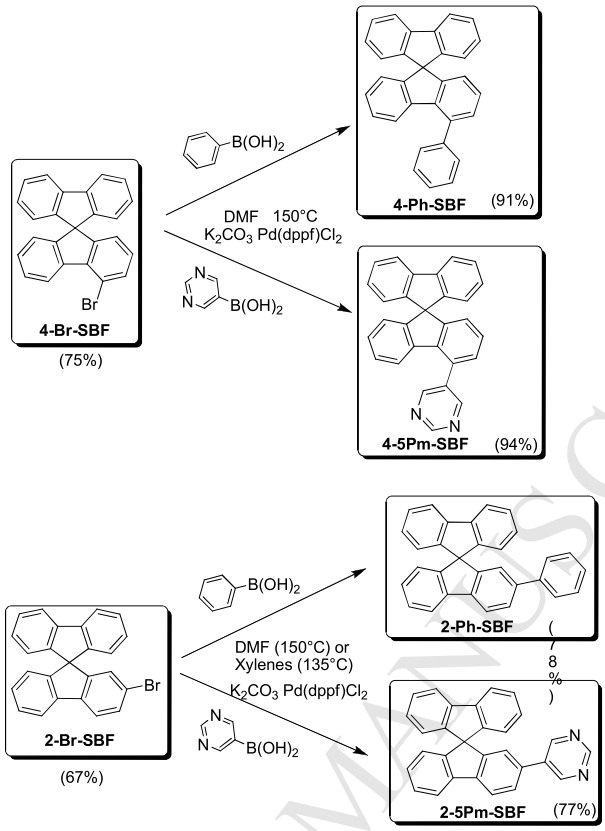

Scheme 1. Synthesis of the four dyes, **4-Ph-SBF**, **4-5Pm-SBF, 2-Ph-SBF** and **2-5Pm-SBF**

Structural Properties

Molecular structure of the four dyes was further confirmed by X-ray crystallography. The X-ray diffraction data of single crystals of **2-Ph-SBF** (Figure 1, left) and **4-Ph-SBF** (Figure 1, right) reveal an asymmetric unit containing two independent molecules 1 and 2. As previously reported,[44] in **4-Ph-SBF**, the angle between the mean plane of the pendant phenyl ring and that of its attached phenyl ring of the fluorene is as large as 51.2° in molecule 1 and 56.6° in molecule 2.

In **2-Ph-SBF**, the same angle appears to be noticeably smaller, ie 37.4° for molecule 1. Similar values have been reported in literature for 2-substituted SBF (ca 30°)[46,47] and seems hence to be a characteristic of such family of 2-substituted SBFs. This difference between the angle observed in **2-Ph-SBF** and **4-Ph-SBF** may be at the origin of the restricted π-conjugation of the latter and will have remarkable consequences on the electronic properties (see below). In addition, we note that the fluorene unit bearing the pendant phenyl ring in the molecule 1 of **2-Ph-SBF** is folded with a deformation of ca 7.1° between the mean planes of each phenyl unit. However, in the case of molecule 2 of **2-Ph-SBF,** we surprisingly note that the pendant phenyl unit is almost coplanar with the fluorene unit with an angle between the mean plane of the pendant phenyl ring and that of its attached phenyl ring of the fluorene unit as low as 4.6°. In addition and oppositely to what was observed for molecule 1, the fluorene bearing the phenyl unit is now almost perfectly flat with only a small deformation of 1.5° (7.1° measured in molecule 1, see above). Such structural feature appears highly surprising and is assigned to the packing of the molecule. Indeed, numbers of short CH and CC distances are detected in the packing diagram of **2-Ph-SBF** and especially two short intermolecular CH distances of ca 2.8 Å between the pendant phenyl ring and its close neighbours (see SI).

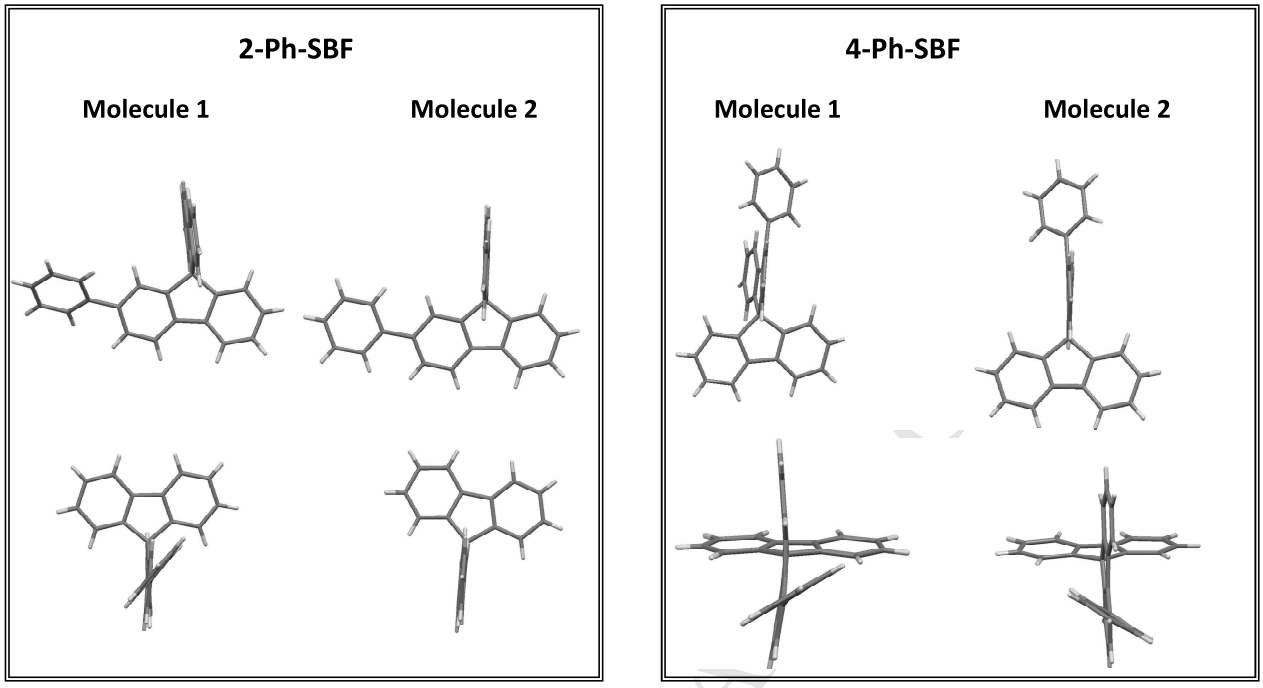

Figure 1. Molecular structure of the two molecules (molecule 1 and molecule 2) contained in **2-Ph-SBF** (left) and **4-Ph-SBF**[44] (right) single crystal asymmetric unit.

However, in the case pyrimidine based SBFs, ie **4-5Pm-SBF** and **2-5Pm-SBF**, we only managed to obtain single crystals of **2-5Pm-SBF** good enough for X-Ray diffraction and hence the direct comparison is not possible. However, we are convinced that similar structural features structures occur in both **4-5Pm-SBF** and **2-5Pm-SBF**. Indeed, in **2-5Pm-SBF**, the angle between the mean plane of the pyrimidine plane and that of its attached phenyl ring is recorded at 23.7° (See SI), lower than that recorded for its phenyl analogue **2-Ph-SBF** (37.4°).

Electrochemical Properties

Electrochemical properties have been investigated by cyclic voltammetry (CV) in CH_2Cl_2 in oxidation and reduction and are summarized in table 1. Pyrimidine-substituted SBF were studied in absence of Al_2O_3 as their rapid adsorption on Al_2O_3 leads to a strong decrease of the intensity of the oxidation and reduction waves.

All compounds present at least two successive oxidation waves (with maxima E^1 and E^2) before 2.2 V (figure 2). Except for **2-5Pm-SBF**, the oxidation is accompanied by an electropolymerization process signed on the present CVs by a reduction wave at the back sweep. This polymerization process is more clearly observed along recurrent sweeps (see CVs in SI). Compared one to another, polymerization process is highly efficient for **2-Ph-SBF** and **4-Ph-SBF** and largely less efficient for **4-5Pm-SBF**. Moreover, the electroactivity of the corresponding polymers, ie **Poly(2-Ph-SBF)** and **Poly(4-Ph-SBF)** are similar with onset oxidation potentials at ca 1.1 V vs SCE (polymers HOMO: -5.5 eV). In addition, the p-doping process reversibility of the two polymers occurs in a large potential range between 1 and 2 V. Oppositely, **Poly(4-5Pm-SBF**) presents a p-

doping process only occurring since 1.35 V (polymer HOMO : -5.75 eV) and appearing less intense and reversible.

Table1. Selected electrochemical, theoretical and optical data

	Electrochemical studies					Theoretical calculations			Optical studies
	E^1, E^2 oxidation peaks/ E_{onset}^{ox} (V)[a]	Reduction peak/ E_{onset}^{red} (V)[a]	HOMO[b] (eV)	LUMO[c] (eV)	ΔE^{el} (eV)[d]	HOMO (eV)	LUMO (eV)	ΔE^{theo} (eV) / E_T	ΔE^{opt} (eV)[e]
4-5Pm-SBF	1.82, 2.23/ 1.57	-2.38/ -2.17	-5.97	-2.23	3.74	-6.16	-1.65	4.51/2.80	3.72
4-Ph-SBF	1.68, 1.88/ 1.55	-2.75/ -2.45	-5.95	-1.95	4.00	-5.97	-1.27	4.70/2.82	3.82
2-5Pm-SBF	1.75, 2.00/ 1.56	-2.33/ -2.10	-5.96	-2.30	3.66	-6.13	-1.85	4.29/2.63	3.66
2-Ph-SBF	1.60, 1.93/ 1.48	No peak in CH_2Cl_2/ -2.3	-5.88	-2.10	3.78	-5.87	-1.48	4.39/2.62	3.70

a. Measured in CH_2Cl_2 + Bu_4NPF_6 0.2 M at 100 mV/s, b. Calculated from the onset oxidation potential E_{onset}^{ox}, c. Calculated from the onset reduction potential E_{onset}^{red}, d: ΔE^{el} = |HOMO-LUMO|, e: Calculated from the onset of the absorption spectrum in solution in cyclohexane (see spectra figure 5 left) by using ΔE^{opt} = hc/λ (ΔE^{opt}(eV)=1237.5/λ(nm).

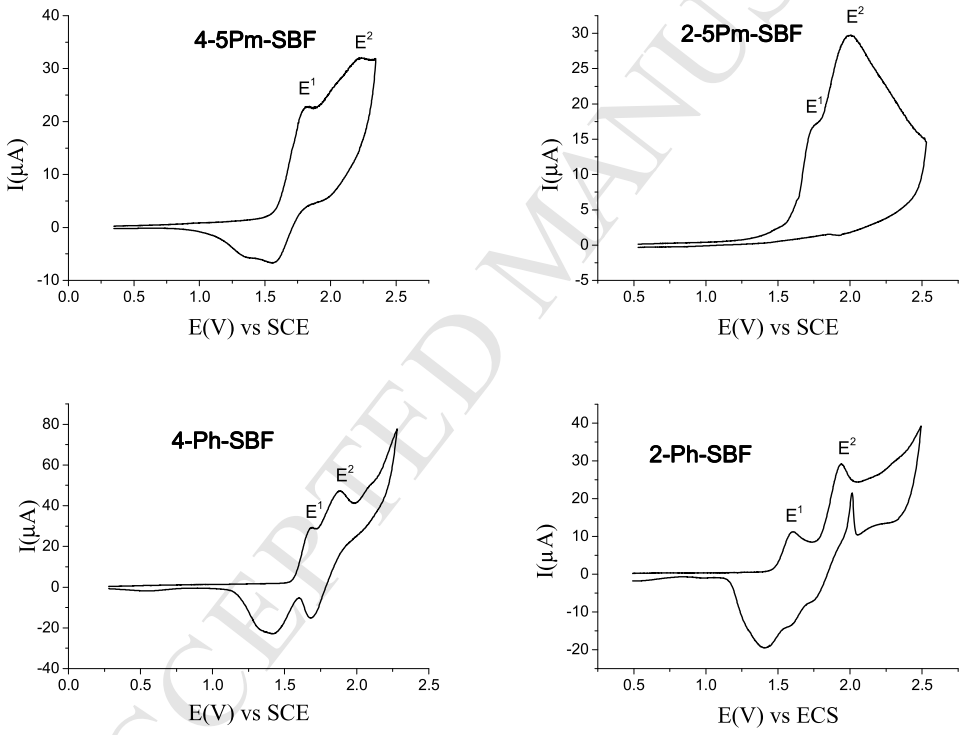

Figure 2. Cyclic voltammetry of **4-5Pm-SBF** (5×10^{-3} M) and **2-5Pm-SBF** (2×10^{-3} M) (top) and of **4-Ph-SBF** (5×10^{-3} M) and **2-Ph-SBF** ($5\ 10^{-3}$ M) (bottom) solutions in CH_2Cl_2 + Bu_4NPF_6 0.2 M, sweep-rate 100 mV.s^{-1}. Platinum disk (Ø: 1mm) working electrode.

From the onset oxidation of the CVs, we determined the HOMO levels[48] of **4-5Pm-SBF** at -6.0 V close to that of **4-Ph-SBF** (HOMO: -5.95 eV) and of its constituting building block **SBF** (HOMO: -5.94 eV)[49] indicating that the substitution in *ortho* position leads to a π-conjugation interruption surely due to the large angle observed in the X-ray structure between the pendant unit and the fluorene core. In addition, we note that the substitution by a 5-pyrimidine or a phenyl group have both very weak effects on the HOMO level of the 4-substituted-SBFs. Indeed, as seen in theoretical calculations, the pendant substituent is not involved in the HOMO character of 4-substituted SBFs (Figure 3) being hence in accordance with our electrochemical conclusions. On the other hand, HOMO levels of **2-5Pm-SBF** and **2-Ph-SBF** calculated from their respective onset oxidation potentials are estimated at -5.96 eV and -5.88 eV. The highest HOMO of **2-**

Ph-SBF compared to that of **SBF** signs an extension of the π-conjugation between the fluorene and the phenyl group in **2-Ph-SBF**. This effect is however neutralized in **2-5Pm-SBF** by the electron withdrawing effect of the pyrimidine group leading to an HOMO level identical to that of **SBF**. Thus, in the case of **2-Ph-SBF**, the substituent is involved in the character of the HOMO (Figure 3), which is not the case for the HOMO of **2-5Pm-SBF**. Cathodic exploration in dichloromethane, reveal that all compounds are reduced at negative potential in a non-reversible process close to the electrolytic medium reduction (see CVs in SI). However, when studied in THF, allowing reaching a more cathodic potential range, one or two reduction waves are observed before the reduction of the electrolytic solution (see CVs in SI). LUMO levels were determined from the onset reduction potential in CH_2Cl_2 at -2.23 ; -1.95 ; -2.30 and -2.10 eV for **4-5Pm-SBF** ; **4-Ph-SBF** : **2-5Pm-SBF** and **2-Ph-SBF** respectively (these values are close to that measured in THF, see in SI).

The lowest LUMO level is recorded for **2-5Pm-SBF** as low as -2.3 eV, 0.41 eV lower than the LUMO of **SBF** (-1.89 eV)[44] signing the double effect of the extension of conjugation due to the substitution at the C2 of **SBF** and to the electron-withdrawing effect of the electron-deficient pyrimidinium group. Thus, we note that the pyrimidine unit is strongly involved in the LUMO character of **2-5Pm-SBF** and even more strongly involved in the case of **4-5Pm-SBF** (Figure 3). Thus, the LUMO level of **4-5Pm-SBF** (-2.23 eV) is shifted by 0.07 eV compared to that of **2-5Pm-SBF**. In addition, the LUMO level of **4-5Pm-SBF** is shifted by 0.27 eV compared to that of **SBF**, (-1.96 eV) due to the effect of the incorporation of the electron-withdrawing pyrimidine fragment. Finally, due to the absence of π-conjugation between the phenyl and the C4-fluorene,[44] LUMO levels of **4-Ph-SBF** is the highest of the present series, ie -1.96 eV, and very close to that of **SBF**.

Finally, HOMO-LUMO gaps (ΔE^{el}) extend between 3.66 eV for **2-5Pm-SBF** to 4.00 eV for **4-Ph-SBF**. This trend in HOMO-LUMO gap changes is well reproduced by theoretical calculations (figure 3) with nevertheless a deviation of ca 0.7 eV.

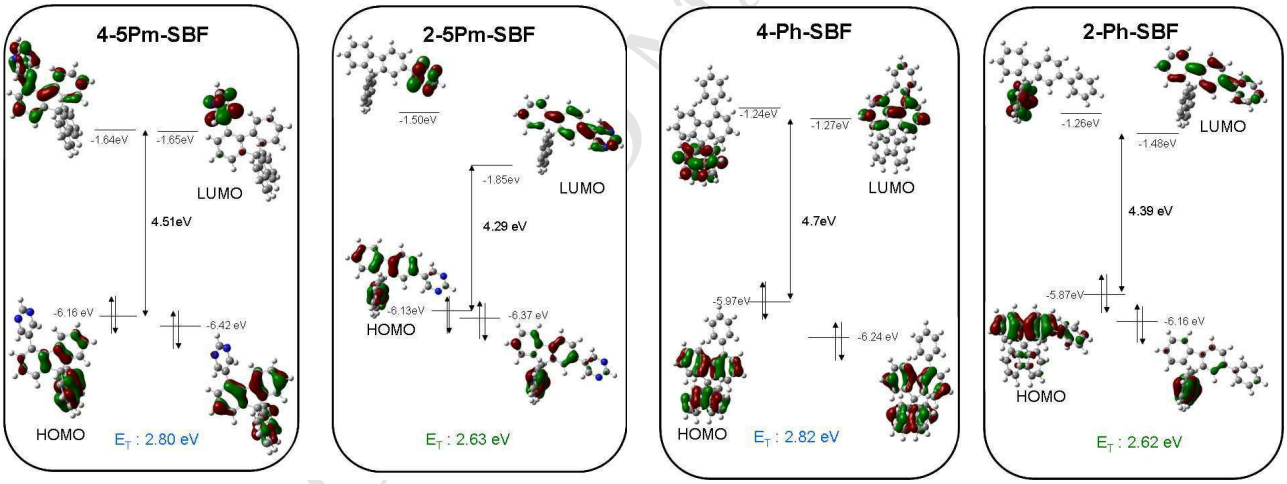

Figure 3. Calculated frontier molecular orbitals by DFT of **4-5Pm-SBF** ; **4-Ph-SBF** : **2-5Pm-SBF** and **2-Ph-SBF**, after geometry optimization at the B3LYP/6-311G+(d,p) level of theory, shown with an isovalue of 0.04 .

Geometry optimization of the four substituted dyes in the singlet and triplet states was performed using Density Functional Theory (DFT) at the Gaussian09 B3LYP/6-311+G(d,p) level of theory. There is a clear resemblance between the HOMO values determined by CVs and by theoretical calculations. **2-Ph-SBF** is the easiest oxidizable molecule due to the extension of conjugation between the phenyl and the 2-substituted fluorene unit and its HOMO presents a phenyl-fluorene character, perfectly translating this extension of conjugation. **4-5Pm-SBF** is the more difficult oxidizible molecule due to the withdrawing effect of the pyrimidine group on the fluorenyl core. However, it should be noted that **2-5Pm-SBF** and **4-5Pm-SBF** presents almost identical HOMO character and HOMO energy level (-6.13 eV vs -6.16 eV resp) clearly meaning that the position of the pyrimidine group only has a weak influence on the HOMO energy levels and distribution. As exposed above, the more easily reduced molecule is **2-5Pm-SBF** due to the double effect of the extension of conjugation and of the electron-accepting properties of the pyrimidine unit, its LUMO has hence a clear pyrimidine-fluorene character. In **4-5Pm-SBF**, the LUMO exclusively has a pyrimidine character and its energy level is 0.2 eV higher than that of **2-5Pm-SBF** due to the absence of

conjugation between the fluorene and the pyrimidine unit. This is a very important feature of the present chemical design and clearly highlights its efficiency. Thus, in 4-substituted SBFs, the HOMO character is almost identical with no (or weak) contribution of the substituent in accordance with our electrochemical conclusions (see above). In addition, it must be pointed out that the LUMO+1 of **4-5Pm-SBF** is very close to its LUMO (0.01 eV) with a 4-5Pm-fluorenyl and 4,5Pm character respectively. Thus, both **2-5Pm-SBF** and **4-5Pm-SBF** have a clear fluorene/pyrimidine character in their LUMO and LUMO+1 (almost degenerated with the LUMO which exclusively possess a pyrimidine character) respectively but present different energy levels. This highlights the importance of the torsion angle between the fluorene and the pyrimidine, which is surely at the origin of these different energy values. The computed triplet adiabatic S_0 to T_1 excitation energies, defined as the energy difference between total energy of the molecule in their respective singlet and triplet states, is of 2.80 and 2.82 eV **for 4-5Pm-SBF** and **4-Ph-SBF** and of 2.63 and 2.62 eV for **2-5Pm-SBF** and **2-Ph-SBF** respectively. These calculations predict that **4-5Pm-SBF** will be, as **4-Ph-SBF**,[44] a good candidate as host for blue and green phosphorescent dyes and both **2-5Pm-SBF** and **2-Ph-SBF** will be both only adapted to green dopants.

The thermal properties of all **SBF** derivatives were investigated by thermogravimetric analysis (TGA) and differential scanning calorimetry (DSC) and the results are summarized in table 2. The *Td* is defined as the temperature at which the sample has lost the first 5% of mass during heating.

Table 2. Thermal properties (melting point: m.p., decomposition temperature: T_d, glass transition: T_g, crystallization temperature: T_c, all obtained from the tangent to the transition peak) of the four SBF dyes.

	4-5Pm-SBF	**4-Ph-SBF**	**2-5PmSBF**	**2-Ph-SBF**
m.p.(°C)	173	213[b]	197-198	100-108[a]
T_d (°C)	277	254	242	238
T_g (°C)	85	76	94	78
T_c (°C)	-	115	-	-

a: This transition appears to be not very clear, occurring on a large range. b. from reference 44

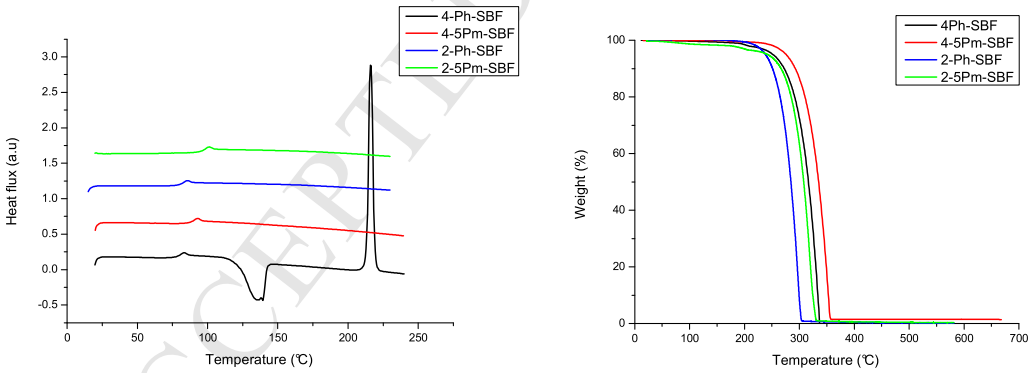

Figure 4. DSC curves from second heating cycle (Left) and TGA curves (right) of **4-Ph-SBF** (black line), **4-5Pm-SBF** (red line), **2-Ph-SBF** (blue line), **2-5Pm-SBF** (green line)

5% decomposition (T_d) of **4-Ph-SBF** (Figure 4 right, black line) and **4-5Pm-SBF** (Figure 4 right, red line) respectively occurs at 254°C and 277°C, higher than the T_d of **SBF** (234°C)[44] showing the interest of the incorporation of a pendant phenyl or pyrimidine unit at the C4 of SBF. Decomposition temperature of the 2-substituted-SBF occurs at 242°C (**2-5Pm-SBF**) and 238°C (**2-Ph-SBF**) close to the T_d of **SBF**, clearly highlighting that the substitution in position 2 only has a weak effect on the thermal stability, whereas the substitution in position 4 leads to a more stiff structure being hence more thermally stable. Thus, we note that the position of the substitution has a clear influence on the T_d. On the other hand, **4-5Pm-SBF** and **4-Ph-SBF** respectively present melting transitions at 173 and 206°C, whereas that of **2-5Pm-SBF** is detected at ca 197/198° (see SI). It should be noted that the fusion of **2-Ph-SBF** was very surprising appearing on a wide

range of temperature. The substituent also has a clear influence on the whole thermal properties as the replacement of phenyl by pyrimidine leads to different glass transitions (T_g). Thus, we note that lower T_g (Figure 4, left) are detected (recorded on the second heating cycle of DSC, Figure 4 left) for phenyl-substituted SBF (76 and 78°C for **4-Ph-SBF** and **2-Ph-SBF** respectively) compared to pyrimidine-substituted SBF (85 and 94°C for **4-5Pm-SBF** and **2-5Pm-SBF** respectively). The slightly higher Tg of pyrimidine-substituted compounds compared to phenyl-substituted compounds may be the consequence of stronger intermolecular interactions due to CH···N hydrogens bonding interactions.[50] It is important to stress that all compounds present T_g higher than those of classical host materials for PhOLEDs such as CBP (62°C)[51] or *m*-CP (55°C).[10] Finally, it should be mentioned that **4-5Pm-SBF**, **2-5Pm-SBF** and **2-Ph-SBF** do no present any cristallization phenomena,T_c, being hence highly promising for devices incorporation. A cristallization transition was only recorded for **4-Ph-SBF** but at high temperature, 115°C, during the second heating cycle in DSC.

Photophysical studies

The UV-Vis absorption and emission spectra recorded in cyclohexane are presented figure 5. All compounds present similar absorption bands in the range 260-315 with the same maxima at 308 nm similar to the main absorption band of **SBF** attributed to π–π* transition of the fluorene unit in **SBF**.[37,38,44]

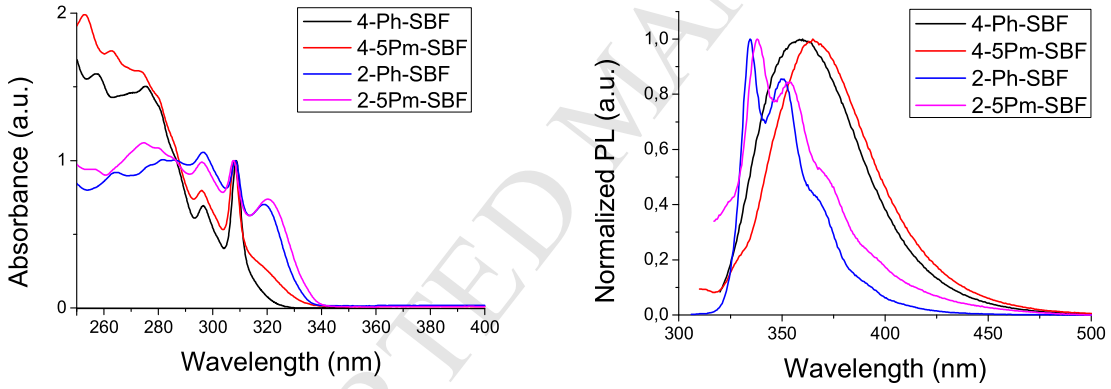

Figure 5. Normalized absorption (left) and emission (right, λ_{exc}=300 nm for **4-Ph-SBF**, **4-5Pm-SBF** and **2-Ph-SBF** and 305 nm for **2-5Pm-SBF**) spectra of the four dyes recorded in cyclohexane, C=10^{-6} M.

At higher wavelength, each compound possesses its own signature with a clear supplemental absorption peak at 320 or 319 nm for **2-5Pm-SBF** or **2-Ph-SBF** signing an extension of the conjugation between the fluorene and the pyrimidine or the phenyl rings when the fluorene is substituted at C2 position. Literature reports a λ_{max} of 328 nm (CH_2Cl_2) for the disubstituted analogue 2,7-di-5Pm-9,9-dihexylfluorene (compound F2 in chart 1) clearly showing an even more important extension of π-conjugation due to the presence of two pyrimidine units.[30] It means that efficient π-conjugation occurs between fluorene and pyrimidine unit leading to a red shift of ca 8/10 nm per pyrimidine unit. In the case of 4-substituted SBF, we note the presence of wavelength tail between 315 and 340 nm, which appears to be larger in the case of **4-5Pm-SBF** than in the case of **4-Ph-SBF**. This tail may be due to a more limited π-conjugation between the pyrimidine or the phenyl ring and the fluorene when substituted at the C4 position. It could also reflect a minor proportion of conformers of the molecules with a more planar structure, allowing a certain degree of π-conjugation between the pyrimidine or phenyl rings and the fluorene moiety. As these bands at low energy seem to be more intense for pyrimidine-based dyes than for phenyl-based dyes, one may conclude that more efficient π-conjugation seems to occur between fluorene and pyrimidine units.

From the onset absorption wavelength, optical energy gap (ΔE^{opt}) varying from 3.66 eV for **2-5Pm-SBF** to 3.82 eV for **4-Ph-SBF** were determined (see table 1) with a variation following the same trend as that obtained from electrochemical measurement and theoretical calculations.

The experimental UV-vis spectra of the four dyes have been compared with predicted electronic absorption spectrum from TD-DFT calculations (see figures in SI) and compared to that of its constituting building block **SBF**. From those calculations one may observe that except **4-Ph-SBF**, all compounds present an additional absorption band at a lower energy than that the main band observed in **SBF** (see Figures in SI). This additional band presents an oscillator strength value as high as 0.3552 for **2-Ph-SBF** and 0.1677 for **2-5Pm-SBF**, similar to that calculated for the neighbouring band (0.3346 for **2-Ph-SBF** and 0.1553 for **2-5Pm-SBF**), itself calculated close to the lowest energy band of **SBF**. This is in accordance with the experimental conclusions from absorption spectroscopy presented above. Looking at the detailed transitions, for **2-Ph-SBF** and **2-5Pm-SBF**, the lowest energy absorption band corresponds to an HOMO-LUMO transition involving the 2-substituted-fluorene unit (see figure 3). For **4-5Pm-SBF**, the two calculated lowest energy bands present strongly less intense oscillator strength (0.0198 and 0.0303 for excited state 1 and 2 respectively) and the more important transitions involved in these two bands correspond to (i) HOMO *vs* LUMO transition (65 % in excited state 1) involving two different molecular fragments of the fluorophore (HOMO possessing a spirobifluorenyl character and LUMO possessing a pyrimidine character) presenting very low orbital overlap and hence a very strong charge transfer character and (ii) HOMO *vs* LUMO+1 transition (58.7% in excited excited state 2) involving two fluorenyl units and hence an orbital overlap between them (HOMO possessing a spirobifluorenyl character and LUMO+1 possessing a pyrimidine/fluorenyl character). Finally, calculated UV-spectrum of **4-Ph-SBF** is very similar to that calculated for **SBF** (see SI) and the lowest energy absorption bands with very weak oscillator strength (0.06 and 0.059 for calculated excited states 1 and 2) correspond to the HOMO *vs* LUMO and HOMO *vs* LUMO+1 transitions, corresponding mainly to fluorene-fluorene transitions.

Fluorescence spectra of the four dyes (figure 5, right) clearly show drastically different emission spectra depending on the substitution. The first type of emission spectra recorded for the 2-substituted-SBFs presents a well resolved emission spectra with maxima at 338/355 and 335/351 nm for **2-5Pm-SBF** and **2-Ph-SBF** respectively, signing the extension of π-conjugation compared to **SBF** (λ_{max} = 311/323 nm).[49] Structured emission spectrum was also reported for 2,7-di-5Pm-9,9-dihexylfluorene (compound F2 in chart 1) with maxima at 361 and 378 nm due to an even more important extension of conjugation in the disubstituted-fluorenyl core.[30] 4-substituted SBFs presents structureless and large emission spectra centred at 365 nm for **4-5Pm-SBF** and 358 nm for **4-Ph-SBF**. This surprising loss of resolution was also observed for the rare examples of 4-substituted **SBF** found in literature, ie 4-diphenylphosphine oxide-SBF (λ_{max}: 346 nm)[39], 4-dibenzofuran-SBF (λ_{max}: 369 nm)[41] and 4-dibenzothiophene-SBF (λ_{max}: 355 nm).[42] This feature appears hence to be a unique characteristic of 4-substituted SBF derivatives as 2-substituted SBF analogues (and 9,9'dialkylfluorene as well) always present well resolved emission bands assigned to the double bond character of the C-C bond linking the pendant substituent and the fluorene core in the excited state.[52-55]

In addition, there is also an intriguing red shift observed between 4-substituted-SBF and 2-substituted-SBF derivatives (shift of 27 nm for 5Pm-SBFs and of 23 nm for Ph-SBFs). It is clear that the position of the substitution (C2 vs C4) is at the origin of this spectacular effect. We could assume that the C4 substitution of phenyl or pyrimidine fragments on the fluorene do not affect dramatically the π-conjugation in the ground state (absorption spectra are only slightly altered with a low energy tail, as described above), but contribute to a strong planarization in the excited state leading to an impressive Stokes shift. More detailed theoretical and spectroscopic investigations need to be conducted to unravel this critical issue.

The emission quantum yields (Φsol) were determined in cyclohexane by using standard procedures with quinine sulphate as reference. On one hand, phenyl-substituted SBFs appear to be efficiently fluorescent with Φsol of 0.42 and 0.87 and lifetimes of 4.20 ns and 1.56 ns for **4-Ph-SBF** and **2-Ph-SBF**, respectively. On the other hand, a quenching of fluorescence is observed for pyrimidine-substituted SBFs with Φsol of 0.04 and 0.02 and lifetimes of 0.61 ns and 0.44 ns for **4-5Pm-SBF** and **2-5Pm-SBF**, respectively. It should be

noted that in other solvents, such as THF, the quantum yields of **4-5Pm-SBF** and **2-5Pm-SBF** remain very low and the solvent can hence not be responsible of these low values. It must be noted that such a decrease of the fluorescence was not observed for previously reported compounds with pyrimidine units such as **TBPSF** (Φsol=1 in solution)[35] and **F3** (Φsol=0.85 in solution)[30] (see structures in chart 1) bearing respectively either a 5 pyrimidine or a 2 pyrimidine unit, both being also substituted with a phenyl ring. The presence of this phenyl ring on the pyrimidine unit appears hence to be very important and we believe that, in our case, the absence of this phenyl ring and hence the presence of the aromatic NCHN fragment in the 5-pyrimidine unit has a strong impact on the deactivation rates of the excited state. Indeed, pyrimidine substituted derivatives **4-5Pm-SBF** and **2-5Pm-SBF** show a lower radiative rate constant k_r and a much higher non-radiative rate constant k_{nr} compared to phenyl-substituted derivatives **4-Ph-SBF** and **2-Ph-SBF**, as mentioned in Table 3.

Table 3. Optical properties of the four SBF dyes.

	4-5Pm-SBF	**4-Ph-SBF**	**2-5Pm-SBF**	**2-Ph-SBF**
λabs, solution (nm) ε (10^4, $L.mol^{-1}.m^{-2}$)[a]	297 (0.5), 308 (0.6), 318 (sh)	297 (0.7), 308 (1.4), 318 (sh)	296 (2.5), 308 (2.5), 320 (1.8)	297 (2.4), 308 (2.2), 319 (1.6)
λabs, thin-film (nm)[b]	298, 311	298, 311	301, 312, 326	301, 312, 329
λem, solution (nm)[a]	365	358	338, 355	335, 351
λem, thin-film (nm)[b]	372	363	355, 366	343, 359
Φsol[a,c]	0.04	0.42	0.02	0.87
τ (ns)[a]	0.61	4.20	0.44	1.56
k_r (s^{-1})[a]	6.6×10^7	1.0×10^8	4.6×10^7	5.6×10^8
k_{nr} (s^{-1})[a]	1.6×10^9	1.4×10^8	2.2×10^9	8.3×10^7

a. in cyclohexane, b. Spin-coated thin film from a solution in THF, [solution] = 10 mg/mL), c. Quantum yields in solution (Φsol) were calculated relative to quinine sulfate (Φsol = 0.546 in H_2SO_4 1N)

From a careful inspection of the dependence of the absorption behaviour of the four dyes on solvent polarity, we note that the absorption maximum is almost insensitive to the dielectric constant of the environment (see Figures in SI). This indicates that the electronic and structural characteristics of the ground and Franck Condon excited states do not differ much with a change in solvent polarity.[56]

While phenyl-substituted SBFs showed minor differences of the PL spectra in various solvents (Figure 6, top), distinct fluorescence solvatochromism was observed in pyrimidine-substituted SBF when the solvent polarity increases from cyclohexane to ethanol (Figure 6, bottom). Indeed, both dyes are highly sensitive to the solvent polarity with fluorescence maxima ranging from 366 and 338 nm in cyclohexane to 390 and 375 nm in ethanol for **4-5Pm-SBF** and **2-5Pm-SBF** respectively. This dependence of the emission wavelength on the solvent polarity is indicative of dipole-dipole interactions between Pm-substituted SBFs and polar solvent molecules and hence of a photoinduced intramolecular charge transfer between the donor (fluorene) and the acceptor part (pyrimidine) of the dye.[57]

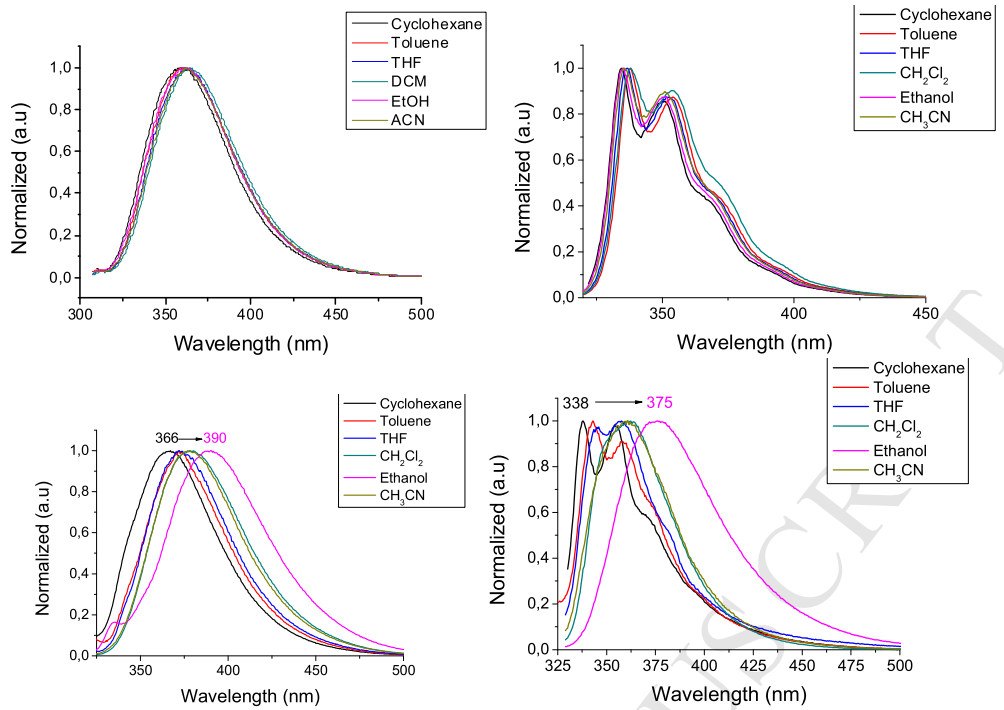

Figure 6. Normalized PL spectra of solutions of **4-Ph-SBF** (top left) and **2-Ph-SBF** (top right) and of **4-5Pm-SBF** (bottom left) and **2-5Pm-SBF** (bottom right) in cyclohexane, toluene, THF, CH_2Cl_2, ethanol and CH_3CN

The solid state absorption spectra of all dyes (figure 7, left) appear very similar to those in solution (figure 5 left) with only a small red shift of less than 8 nm detected and a slight increase of the lowest energy band intensity (compared to the band at 310 nm) for the 2-substituted-SBFs. Such similarity between absorption spectra in solution and in solid state clearly signs that there are minimal intermolecular interactions in the ground state in thin films.

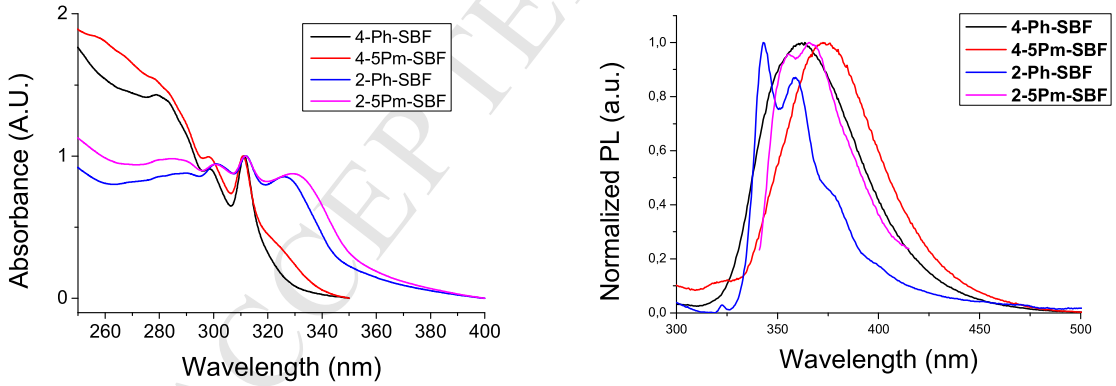

Figure 7. Absorption (left) and Emission (right) spectra of the four dyes recorded in solid state (spin-coated thin film from a solution in THF, [solution] = 10 mg/mL).

Regarding the solid-state fluorescent properties (figure 7, right), except for **2-5Pm-SBF**, they are almost identical to those recorded in solution (figure 5, right) with only a small red shift ranging from 3 nm for **4-Ph-SBF** to 8 nm for **4-5Pm-SBF** and **2-Ph-SBF**. Solid-state fluorescent spectrum of **2-5Pm-SBF** (figure 7, right, pink line) nevertheless appears poorly resolved with two maxima recorded at 355/366 nm, red shifted by 17/11 nm compared to that in solution. Finally, to examine the suitability of the four dyes as host materials for phosphorescent green and/or blue dopant, the phosphorescence of the molecules was recorded at 77 K in a methylcyclohexane/2-methylpentane mixture (1:1), Figure 8. From those spectra, E_T values of the molecules were calculated from the lowest phosphorescent peak of 2.75 eV for **4-5Pm-SBF** and 2.56 eV for

2-Ph-SBF. Compared to the E_T value of **4-Ph-SBF** (2.77 eV) and of **SBF** (2.87 eV) reported by our group recently,[44] we note that the E_T level of **4-5-Pm-SBF** is sufficiently high for its use as host material for both green and blue phosphorescent dyes. The E_T of **2-Ph-SBF** (2.56 eV) and that of **2-5-Pm-SBF** (2.58 eV) is lower than that of the blue dopant FIrpic (E_T: 2.62 eV[58]) and these molecules may be used as host material for green dopant $Irppy_3$ (E_T: 2.42 eV[59]).

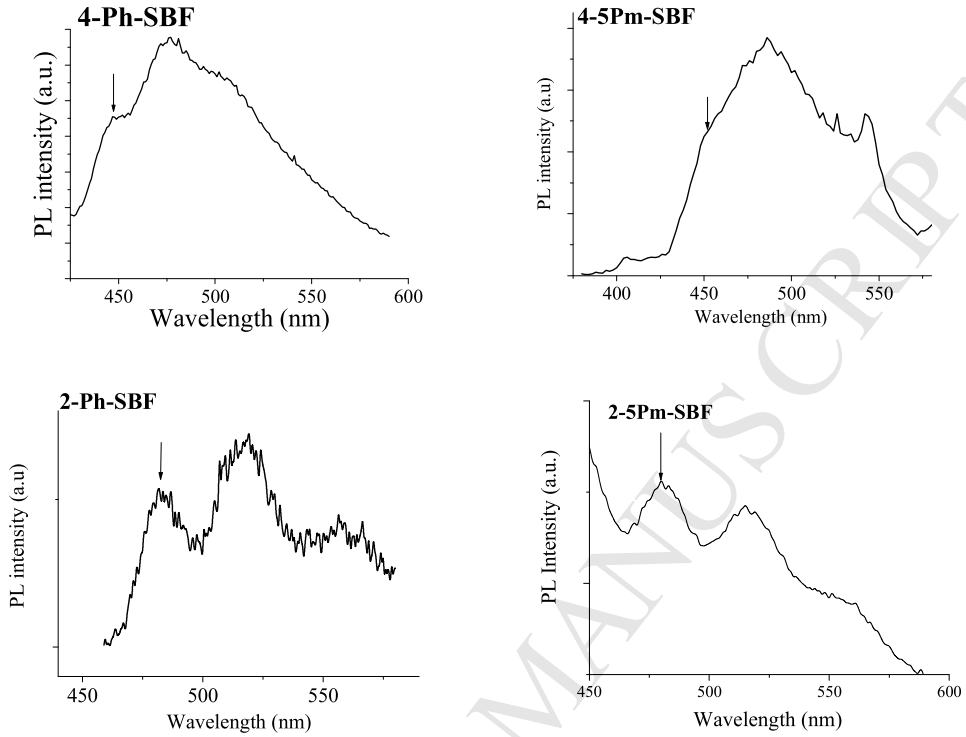

Figure 8. Emission spectra at 77 K in a methylcyclohexane/2-methylpentane mixture (1:1) of **4-Ph-SBF** (λ_{exc}= 300 nm, **4-5Pm-SBF** (λ_{exc}= 300 nm) and **2-Ph-SBF** (λ_{exc}= 250 nm) and **2-5PmSBF** (λ_{exc}= 250 nm). The determination of the Et value has been done at from the lowest phosphorescent peak (black arrow)

In conclusion of the above presented photophysical and physico-chemical analysis, the position (C2 *vs* C4) and the nature of the substituent (phenyl *vs* pyrimidine) on the SBF core leads to drastic alterations of the resulting properties. Substitution at the C2 leads to an increase of the conjugation length and therefore to a decrease of the singlet and triplet state energy level, while the substitution at the C4 only has a weak influence on these two key parameters, keeping them almost identical to those of their constituting building block **SBF**. This has been assigned to π-conjugation breaking induced by the large torsion angle made by the substituents in C4. This chemical design allows hence obtaining organic semiconductors based on a C4-substituted SBF with high singlet and triplet state energy level with excellent thermal/morphological properties. On the other hand, the substitution by the pyrimidine group leads to a decrease of the LUMO level due to the pyrimidine electron affinity, which should lead in principle to a decrease of the threshold voltage of the resulting devices. Thus, the four dyes possess the prerequisites for their uses as host in PhOLEDs that is, a high T_g and T*d*, HOMO/LUMO levels adapted for hole and electron injection/transport in the devices and E_T higher that of the green phosphorescent emitter $Ir(ppy)_3$ (2.42 eV[59]) and in the case of **4-Ph-SBF** and **4-5Pm-SBF** for the blue phosphorescent emitter FIrpic (2.62 eV[58]).

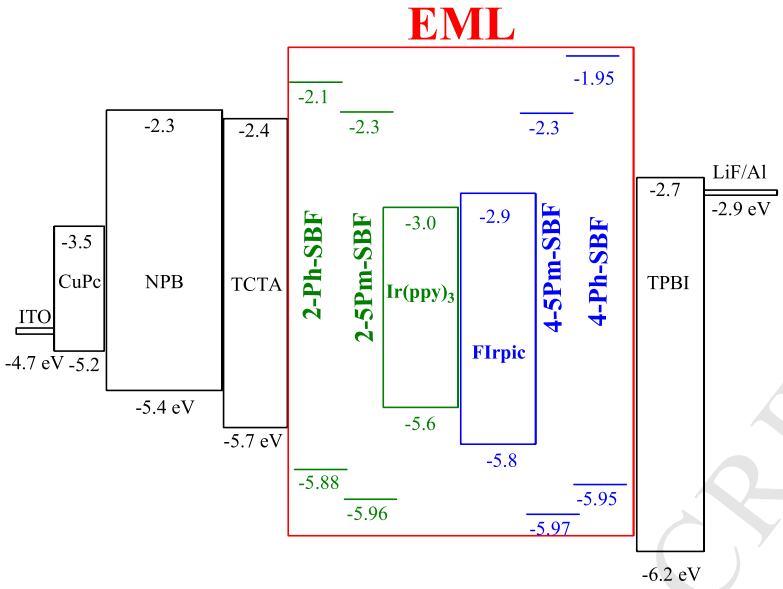

Scheme 2. Energy level diagram of the devices.

In order to explore the potential of the present semi-conductors as host for triplet emitters, green ($Ir(ppy)_3$) and blue (FIrpic) PhOLEDs were fabricated. The device configuration was ITO/CuPc(10 nm)/NPB (40 nm)/TCTA (10 nm)/ **EML**:dopant (20 nm)/TPBi (40 nm)/LiF (1.2 nm)/Al (100 nm). ITO is used as the anode, CuPc (copper phtalocyanine) is the hole injecting layer, NPB (N,N'-di(1-naphtyl)-N,N'-diphenyl-[1,1'-biphenyl]-4,4'-diamine) is the hole-transporting layer, TCTA (4,4',4''-Tris(carbazol-9-yl)-triphenylamine) is the electron/exciton blocking layer, TPBI (1,3,5-Tris(1-phenyl-1H-benzimidazol-2-yl)benzene) is both the electron transporting layer and the hole blocking layer and a thin film of lithium fluoride covered with aluminum is the cathode. $Ir(PPy)_3$ and FIrpic are used as dopant for green and blue OLEDs respectively. The relative energy levels of the successive layers of the devices are reported in scheme 2. Table 4 gathers selected data obtained from the average of two experiments.

Due to their E_T values higher than that of $Ir(ppy)_3$, the four substituted-SBFs were used as host for $Ir(ppy)_3$ green dopant. Performance of the best green PhOLEDs is presented in figure 9 (left) and average parameters are gathered in table 4. The best green PhOLED performance was obtained with **2-5Pm-SBF** and **4-5Pm-SBF** host materials doped with 10% $Ir(ppy)_3$. As shown in figure 9 (left), maximum current and power efficiencies of 58 cd/A and 35 lm/W are obtained respectively for the pyrimidine substituted SBF. Maximum luminance as high as 30 000 cd/m^2 is reached for these devices as shown in table 4. Phenyl substituted dyes, **4-Ph-SBF** and **2-Ph-SBF** presents lower performance with EQE of 10.4% and 11.3 %, highlighting the great interest of the incorporation of the pyrimidine unit in SBF scaffold. The threshold voltage for all devices appears to be low and as low as 2.5 eV for **2-5Pm-SBF**.

The EL spectra of the four devices based on the different host materials are identical, exclusively showing the emission of the green dopant at 516/540 nm (figure 9 right) close to the PL emission of pure $Ir(ppy)_3$ film (509/540 nm)[57] with no parasite emission in the range of the undoped device. This result demonstrates an efficient energy transfer from the four SBF-derivatives to $Ir(ppy)_3$, due to their high triplet energy levels.

The device performance obtained with small pure hydrocarbon host molecules **4-Ph-SBF** and **2-Ph-SBF** are comparable to those obtained with more complicated pure-hydrocarbon-based host materials recently reported,[38,37,58] Performances obtained with pyrimidine-substituted SBF are even more interesting with lowest turn-on voltages and highest EQE (close to 14%) and clearly demonstrate the interest of the pyrimidine substitution in notably favouring the injection of electron.

Table 4. Selected EL data of green and bue devices (average values calculated from two experiments).

		at J= 10 mA/cm²				
Host /Guest (%)	V_{on} (V)	EQE (%)	Current efficiency (cd.A^{-1})	Power efficiency (lm/W)	L^{max} (cd.m^{-2}) at current density (mA.cm^{-2})	CIE (x ; y) at 10 mA.cm^{-2}
Green Phosphorescent OLEDs						
2-Ph-SBF /Ir(ppy)$_3$ (10)	2.6	11.3	42.7	17.8	27 990 (210)	0.33 ; 0.62
2-5Pm-SBF /Ir(ppy)$_3$ (9)	2.5	13.3	49.2	21.5	30 000 (160)	0.33 ; 0.61
4-Ph-SBF[44] /Ir(ppy)$_3$ (10)	3.5	10.4	40.3	16.7	25 700 (230)	0.32 ; 0.62
4-5Pm-SBF /Ir(ppy)$_3$ (10)	3.3	13.7	49.9	17.6	28 000 (150)	0.34 ; 0.61
Blue Phosphorescent OLEDs						
4-Ph-SBF[44] /FIrPic (19)	4.0	5.7	16.2	6.0	3800 (70)	0.20 ; 0.44
4-5Pm-SBF /FIrPic (19)	3.3	4.8	14.1	5.5	2030 (50)	0.20 ; 0.45

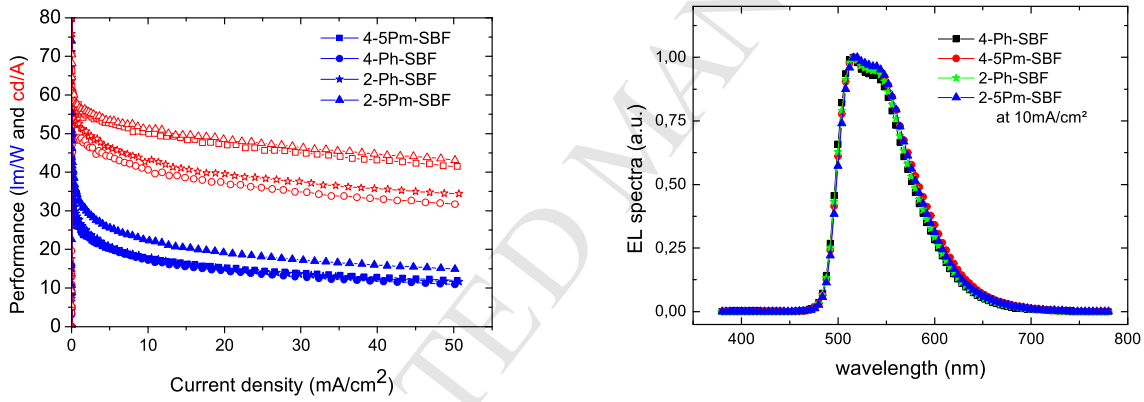

Figure 9. Current (empty symbol) and power efficiencies (filled symbol) versus current density of the green devices using **4-Ph-SBF**, **4-5Pm-SBF**, **2-Ph-SBF** and **2-5Pm-SBF** doped with Ir(ppy)$_3$ (10% in mass) as emitting layer (left). Corresponding EL spectra recorded at 10 mA/cm^2 (right).

Due to their high E_T values (2.77 eV for **4-Ph-SBF** and 2.75 eV for **4-5Pm-SBF**), higher than that of FIrpic (E_T: 2.62 eV), the two 4-substituted-SBFs were used as host for this blue dopant. Characteristics of the two blue devices are presented in figure 10. The best performance is obtained with **4-Ph-SBF** with an EQE of 5.7 %, a LE of 16.2 cd/A and a threshold voltage of 4 V while blue PhOLEDs with **4-5Pm-SBF** as host reach an EQE of 4.8 %, a LE of 14.1 cd/A and a threshold voltage of 3.3 V reported at a current density value of 10 mA/cm^2 (Figure 10 left and Table 4). The threshold voltage of **4-5Pm-SBF** is hence decreased by ca 0.7 V compared to that of **4-Ph-SBF** due to the incorporation of the pyrimidinium group in the former (which leads to a decrease of the LUMO level and hence an easier injection of the electron in the device). This highlights the efficiency of the chemical design investigated in this work. Both devices, reach brightness of 3800 / 2030 cd/m^2 for **4-Ph-SBF** / **4-5Pm-SBF** based devices respectively.

EL spectra of the devices (Figure 10 right) point a main emission of the blue dopant with maxima at 473 and 500 nm close to the PL emission of pure FIrpic film (475/500 nm)[59] but also, in the case of **4-PhSBF** of an additional tiny emission in the range of the undoped device (360/440 nm). This emission may be due to a small amount of recombination in the other organic layers and especially in TCTA. CIE coordinates of **4-Ph-SBF**-based device (0.20 ; 0.44) and of **4-5Pm-SBF**-based device (0.20 ; 0.45) appear nevertheless almost identical as shown in Table 4.

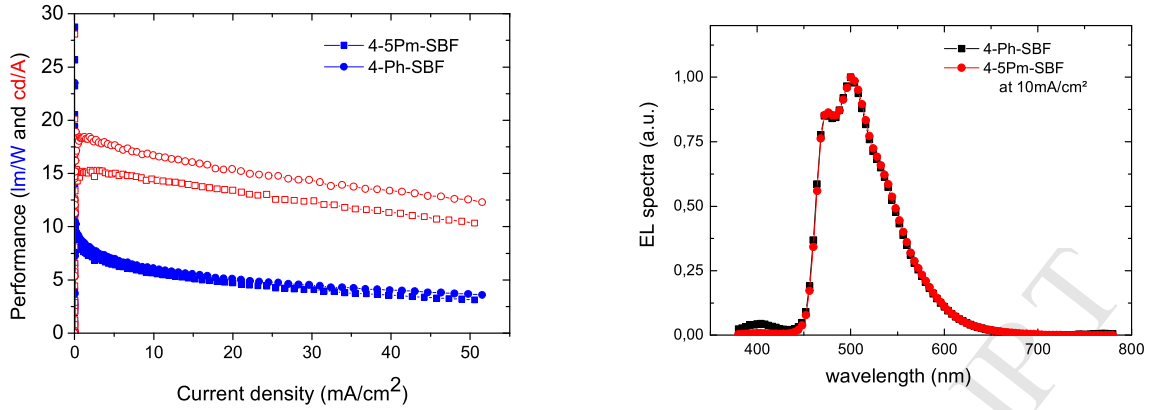

Figure 10. Current (empty symbol) and power efficiencies (filled symbol) versus current density of the blue devices using **4-Ph-SBF** and **4-5Pm-SBF** doped with FIrPic (19% in mass) as emitting layer (left). Corresponding EL spectra recorded at a current density of 10 mA/cm^2 (right).

Conclusion

In summary, four substituted SBF dyes have been synthesized and their thermal, electrochemical and photophysical properties have been scrutinized and compared to the properties of their constituting **SBF** unit. From these studies it has been demonstrated that, compare to **SBF**, the substitution by a phenyl unit at the C4 position of **SBF** leads to weaker modification of the HOMO and LUMO levels compared to the phenyl substitution at the C2 position, which leads to a conjugation extension and hence a decrease of the HOMO-LUMO gap. On the other hand, the substitution by the electro-deficient pyrimidine unit compared to the substitution by the phenyl unit leads to a significant lowering of the LUMO level. Overall, the combination of the two effects (lowering of the HOMO through the extension of conjugation, lowering of the LUMO through pyrimidine electro deficient effect) in **2-5Pm-SBF** leads to the highest modification of the optical energy gap (from 4.05 eV in **SBF** to 3.66 eV in **2-5Pm-SBF**). Thus, the optical energy gap of the four compounds is finely tuned from 4 eV for **4-Ph-SBF** to 3.66 eV for **2-5Pm-SBF**. In addition, the substitution in C2 or in C4 has an impressive influence on the E_T. Indeed, the C2-substituted dyes have E_T values at ca 2.42 eV, whereas the C4 substituted dyes have an E_T as high as 2.7 eV due to the π-conjugation disruption. This structure properties relationship study clearly highlights how a different substitution may lead to very different properties keeping others intact. As all compounds possess a triplet energy level higher than 2.42 eV, they have been used as host for green dopant in PhOLEDs. Remarkable performance has been obtained with **2-5Pm-SBF** as host (CE > 58 cd/A, PE > 35 lm/W, EQE > 14 % and threshold voltage of 2.5 V). Furthermore, the two 4-substituted SBF with triplet energy levels as high as 2.8 eV have also been successfully used as host materials for blue PhOLEDs with high performance. The effect of the pyrimidine substituent leads to a lowering of the threshold working voltage of the device from 4 V for **4-Ph-SBF** based blue device to 3.3 V for **4-5Pm-SBF** based blue device.

Acknowledgements

S.T. and G. S. thank ANR (HOME-OLED Project n°ANR-11-BS07-020-01) for a studentship. C. D thanks ANR (HOME-OLED Project n°ANR-11-BS07-020-01) for a financial support as postdoctoral position. We wish to thank the C.R.M.P.O (Centre Régional de Mesures Physiques de l'Ouest, Rennes) for high resolution mass measurements, Service de Microanalyse-CNRS (Gif sur Yvette) for CHN analyses, CINES (Montpellier) for computing time, the CDIFX (Rennes) for X-Ray data collection, the "Institut des Sciences Analytiques" (UMR CNRS 5280, Villeurbanne) for TGA. Arnaud Brosseau (Cachan) is thanked for his precious assistance in photophysical measurements. Dr Franck Camerel (Rennes) is warmly acknowledged for his help and advice

in the understanding of thermal properties. Prof. Abdou Boucekkine is also warmly thanked for his help in DFT and TD-DFT calculations.

Experimental Section

Synthesis:

All manipulations of oxygen- and moisture-sensitive materials were conducted with a standard Schlenk technique. Commercially available reagents and solvents were used without further purification other than those detailed below. THF was distilled from sodium/benzophenone prior to use. Light petroleum refers to the fraction with bp 40-60°C. 2.5 M solutions of n-BuLi in hexanes or THF were purchased from Sigma Aldrich. 2,2'-dibromobiphenyl was purchased from Fluorochem. Reactions were stirred magnetically, unless otherwise indicated. Analytical thin layer chromatography was carried out using aluminum backed plates coated with Merck Kieselgel 60 GF254 and visualized under UV light (at 254 and 360 nm). Chromatography was carried out using Teledyne Isco CombiFlash® Rf 400 (UV detection 200-360nm), over standard silica cartridges (Redisep® Isco, GraceResolv™ Grace or Puriflash® columns Interchim). ^{1}H and ^{13}C NMR spectra were recorded using Bruker 300 MHz instruments (^{1}H frequency, corresponding ^{13}C frequency: 75 MHz); chemical shifts were recorded in ppm and J values in Hz. In the ^{13}C NMR spectra, signals corresponding to C, CH, CH_2 or Me groups, assigned from DEPT, are noted. The residual signals for the NMR solvents are: $CDCl_3$; 7.26 ppm for the proton and 77.00 ppm for the carbon, CD_2Cl_2; 5.32 ppm for the proton and 53.80 ppm for the carbon. The following abbreviations have been used for the NMR assignment: s for singlet, d for doublet, t for triplet and m for multiplet. High resolution mass spectra were recorded at the Centre Régional de Mesures Physiques de l'Ouest (Rennes) on (i) Bruker MicrO-Tof-Q II (Source: Atmospheric Pressure Chemical Ionization (APCI - direct introduction) (ASAP– Atmospheric Solids Analysis Probe) at a temperature of 30°C - positive mode) or on (ii) Waters Q-Tof II. The synthesis of **4-bromo-9,9'-spirobi[fluorene]** (**1**) and of **4-Ph-SBF** have been previously described[44]

2-bromo-9,9'-spirobi[fluorene] (2)[63] 2-bromo-1,1'-biphenyl (2.16 g, 9.27 mmol, 1.15 eq) was dissolved in dry THF (40 mL) under argon atmosphere, cooled at -78°C, and stirred during 10 minutes at this temperature. A 2.5 M n-BuLi solution in THF (4.31 mL, 10.78 mmol, 1.34 eq) was then slowly injected via a seringue, at -78°C. The resulting yellow mixture was stirred at the same temperature for 30 min. 2-bromo-9H-fluoren-9-one (2.08 g, 8.03 mmol) in dry THF (35 mL) was then added dropwise, and the mixture was stirred for another 30 min at -78°C, and allows warming up to room temperature gradually and stirred overnight. Saturated brine solution (10 mL) was added, and the mixture was extracted twice with ethyl acetate (2x30 mL). The combined organic extracts were dried over anhydrous magnesium sulfate, filtered, and concentrated under reduced pressure. Without other purification, the crude was dissolved into a mixture of acetic acid/hydrochloric acid (50 mL/5 mL) and warmed at 70°C during 2 h under stirring. Then, the mixture was poured into water/ice (200 mL), and the solution was neutralized with solid sodium hydroxide until pH 7. Then the organic layer was extracted three times with dichloromethane (3x50 mL). The combined organic extracts were dried over magnesium sulfate, filtered, and concentrated under reduced pressure. The residue was purified by flash chromatography on silica gel (light petroleum/dichloromethane 95/5) to afford a colorless solid (2.14 g). [column conditions: Silica cartridge 40 g (Serlabo); solid deposit on Celite®; $\lambda_{detection}$: (254 nm, 280 nm); light petroleum/dichloromethane (95/5) at 25 mL/min; collected fraction: 18-42 min]. Yield: 67%. mp: 168-170°C (lit. 160 °C);[64] ^{1}H NMR (300 MHz, CD_2Cl_2): δ 7.89 (m, 3H, ArH), 7.76 (d, J= 8.1 Hz, 1H, ArH), 7.52 (dd, J = 8.1, 1.8 Hz; 1H, ArH), 7.42 (m, 3H, ArH), 7.15 (m, 3H, ArH), 6.87 (m, 1H, ArH), 6.71 (m, 3H, ArH); ^{13}C NMR (75 MHz, CD_2Cl_2): δ 151.5 (C), 149.1 (C), 148.5 (C), 142.4 (C), 141.4 (C), 141.3 (C), 131.4 (CH), 128.8 (CH), 128.6 (CH), 128.54 (CH), 128.48 (CH), 127.6 (CH), 124.37 (CH), 124.35 (CH), 122.1 (CH), 121.8 (C), 120.8 (2xCH seen from HSQC), 66.4 (Spiro C).

General procedure for Suzuki coupling

9,9'-spirobi[fluorene] brominated compound, boronic acid compound, K_2CO_3 and $Pd(dppf)Cl_2$* were dissolved in dry DMF or xylenes. The mixture was warmed to 150°C (DMF) and 135°C (xylenes) stirred overnight. After cooling to room temperature, saturated solution of ammonium chloride (50 mL) was ad-

* $Pd(dppf)Cl_2$: [1,1'-Bis(diphenylphosphino)ferrocene]palladium(II) dichloride complex with dichloromethane

ded, and organic layer was extracted three times with dichloromethane (3x30 mL) and washed with brine (3x30 mL). The combined organic extracts were dried over magnesium sulfate, filtered, and concentrated under reduced pressure. The residue was purified by flash chromatography on silica gel using Teledyne Isco CombiFlash® Rf 400. Column conditions can be found in each compounds description below.

5-(9,9'-spirobi[fluoren]-4-yl)pyrimidine (4-5Pm-SBF). 5-(9,9'-spirobi[fluoren]-4-yl)pyrimidine was synthesized according to the general coupling procedure between 4-bromo-9,9'-spirobi[fluorene] (**1**)[44] (0.808 g, 2.045 mmol), pyrimidin-5-yl-boronic acid (0.333 g, 2.688 mmol, 1.31 eq), K_2CO_3 (2.800 g, 20.260 mmol, 9.91 eq) and Pd(dppf)Cl_2 (0.088 g, 0.108 mmol, 0.05 eq) in dry DMF (30 mL). The residue was purified by flash chromatography on silica gel (light petroleum/ethyl acetate 85/15) to afford a colorless solid (0.759 mg, 1.924 mmol) [column conditions: Silica cartridge 12 g (Serlabo); solid deposit on Celite®; $\lambda_{detection}$: (254 nm, 280 nm); ethyl acetate in ligth petroleum (85/15) at 20 mL/min; collected fraction: 8-17 min]. Yield: 94%. mp: 167°C; IR (ATR, cm^{-1}) ν = 593, 646, 723, 752, 908, 1030, 1157, 1282 1405, 1444, 1545, 3020, 3072; ^{1}H NMR (300Mhz, CD_2Cl_2): δ 9.36 (s, 1H, ArH), 9.04 (s, 2H, ArH), 7.89 (m, 2H, ArH), 7.41 (td, J = 7.5, 1.2 Hz, 2H, ArH), 7.22-7.01 (m, 7H, ArH), 6.76 (m, 3H, ArH), 6.68 (s, 1H, ArH); ^{13}C NMR (75MHz, CD_2Cl_2): δ 158.6 (CH), 157.4 (CH), 150.7 (C), 149.9 (C), 149.0 (C), 142.5 (C), 141.3 (C), 139.7 (C), 135.1 (C), 130.8 (C), 130.7 (CH), 128.7 (CH), 128.53 (CH), 128.48 (CH), 128.3 (CH), 128.2 (CH), 124.9 (CH), 124.7 (CH), 124.3 (CH), 123.0 (CH), 120.8 (CH), 66.24 (Spiro C) ; HRMS calculated for $C_{29}H_{19}N_2$ 395.1542, found 395.1542 $[M+H]^+$; Elemental analysis calculated for $C_{29}H_{18}N_2$: C, 88.30 %; H, 4.60 %; N, 7.10 %. Found: C, 87.81 %; H, 4.81 %; N, 6.81 %; λ_{abs} [nm] (ε[10^4.L.mol^{-1}.cm^{-1}]) = 297 (0.5), 308 (0.6).

2-phenyl-9,9'-spirobi[fluorene] (2-Ph-SBF). 2-phenyl-9,9'-spirobi[fluorene] was synthesized according to the general procedure between 2-bromo-9,9'-spirobi[fluorene] **(2)** (0.751 g, 1.901 mmol), phenylboronic acid (0.304 g, 2.488 mmol, 1.31 eq), K_2CO_3 (1.227 g, 8.883 mmol, 4.67 eq) and Pd(dppf)Cl_2 (0.061 g, 0.076 mmol, 0.04 eq) in xylenes (20 mL). The residue was purified by flash chromatography on silica gel (light petroleum/dichloromethane 9/1) to afford a colorless solid (0.581 g, 1.482 mmol), [column conditions: Silica cartridge 24 g (Serlabo); solid deposit on Celite®; $\lambda_{detection}$: (254 nm, 280 nm); dichloromethane in light petroleum (9/1) at 20 mL/min; collected fraction: 35-45 min]. Yield: 78 %.mp:100-108* IR (ATR, cm^{-1}) ν = 476, 494, 617, 634, 650, 692, 727, 748, 829, 1020, 1155, 1280, 1444, 1597, 3014, 3059; ^{1}H NMR (300 MHz, CD_2Cl_2): δ 7.96 (dd, *J* = 8.0, 0.6 Hz, 1H, ArH), 7.93 – 7.88 (m, 3H, ArH), 7.66 (dd, *J* = 8.0, 1.7 Hz, 1H, ArH), 7.45 – 7.36 (m, 5H, ArH), 7.35 – 7.20 (m, 3H, ArH), 7.13 (td, *J* = 7.5, 1.1 Hz, 3H, ArH), 6.94 (dd, *J* = 1.7, 0.6 Hz, 1H, ArH), 6.78 – 6.72 (m, 2H, ArH), 6.72 – 6.67 (m, 1H, ArH); ^{13}C NMR (75 MHz, CD_2Cl_2): δ 150.1 (C), 149.7 (C), 149.2 (C), 142.4 (C), 142.0 (C), 141.7 (C), 141.4 (C), 141.3 (C), 129.1 (CH), 128.40 (2xCH†), 128.38 (CH), 128.37 (CH), 127.8 (CH), 127.43 (CH), 127.38 (CH), 124.4 (CH), 124.3 (CH), 123.0 (CH), 121.0 (CH), 120.8 (CH), 120.7 (CH), 66.6 (Spiro C); HRMS calculated for $C_{31}H_{21}$ 393.1643, found 393.1646 $[M+H]^+$; Elemental analysis calculated for $C_{31}H_{20}$: C, 94.86 %; H, 5.14 %. Found: C, 94.93 %; H, 5.24 %; λ_{abs} [nm] (ε[10^4.L.mol^{-1}.cm^{-1}]) = 297 (2.4), 308 (2.2), 319 (1.6).

5-(9,9'-spirobi[fluoren]-2-yl)pyrimidine (2-5Pm-SBF). 5-(9,9'-spirobi[fluoren]-2-yl)pyrimidine was synthesized according to the general procedure between 2-bromo-9,9'-spirobi[fluorene] **(2)** (0.749 g, 1.897 mmol), pyrimidin-5-yl-boronic acid (0.312 g, 2.519 mmol, 1.33 eq), K_2CO_3 (1.226 g, 8.872 mmol, 4.68 eq) and Pd(dppf)Cl_2 (0.059 g, 0.073 mmol, 0.04 eq) in dry DMF (20 mL). The residue was purified by flash chromatography on silica gel (light petroleum/ethyl acetate 8/2) to afford a colorless solid (0.5743 g, 1.456 mmol) [column conditions: Silica cartridge 24 g (Serlabo); solid deposit on Celite®; $\lambda_{detection}$: (254 nm, 280 nm); ethyl acetate in light petroleum (8/2) at 20 mL/min; collected fraction: 34-50 min]. Yield (77 %). mp: 197-198°C; IR (ATR, cm^{-1}) ν = 491, 604, 619, 636, 721, 731, 750, 833, 862, 1018, 1105, 1153, 1186, 1267, 1400, 1414, 1446, 1554, 3016, 3039, 3053; ^{1}H NMR (300 MHz, CD_2Cl_2): δ 8.94 (s, 1H, ArH), 8.67 (s, 2H, ArH), 7.93 (dd, *J* = 7.9, 0.6 Hz, 1H, ArH), 7.87 – 7.83 (m, 1H, ArH), 7.83 – 7.79 (m, 2H, ArH), 7.56 (dd, *J* = 7.9, 1.7 Hz, 1H, ArH), 7.37 – 7.26 (m, 3H, ArH), 7.06 (dtd, *J* = 10.2, 7.5, 1.1 Hz, 3H, ArH), 6.86 (dd, *J* = 1.7, 0.6 Hz, 1H,

* This transition appears to be not very clear, occurring on a large range.
† In the light of the protons assignment of **2-5Pm-SBF**, we believe that 2 carbons are present at 128.40 ppm.

ArH), 6.68 – 6.60 (m, 3H, ArH); ^{13}C NMR (75 MHz, CD_2Cl_2): δ 157.8 (CH), 155.2 (CH), 150.7 (C), 149.7 (C), 148.8 (C), 143.2 (C), 142.4 (C), 141.4 (C), 134.53 (C), 134.45 (C), 129.0 (CH), 128.6 (CH), 128.5 (2xCH seen from HSQC), 127.3 (CH), 124.42 (CH), 124.35 (CH), 122.9 (CH), 121.6 (CH), 121.1 (CH), 120.8 (CH), 66.6 (Spiro C); HRMS calculated for $C_{29}H_{19}N_2$ 395.1548, found 395.1548 $[M+H]^+$; λ_{abs} [nm] (ε[10^4.L.mol^{-1}.cm^{-1}]) = 296 (2.5), 308 (2.5), 320 (1.8).

X-Ray :

Crystal was picked up with a cryoloop and then frozen at 150 K under a stream of dry N_2 on a APEX II Brucker AXS diffractometer for X-ray data collection (Mo Kα radiation, λ = 0.71073 Å). **4-Ph-SBF** structure was published previously.[44]

2-Ph-SBF (C_{62} H_{40})); *M* = 784.94. APEXII, Bruker-AXS diffractometer, Mo-Kα radiation (λ = 0.71073 Å), *T* = 150(2) K; triclinic *P-1* (I.T.2), a = 10.9027(4), b = 13.7902(6), c = 15.7771(5) Å, α = 102.1400(10), β = 97.4710(10), γ = 111.5900(10) °, *V* = 2099.47(14) Å^3.*Z* = 2, *d* = 1.242 g.cm^{-3}, μ = 0.07 mm^{-1}. The structure was solved by direct methods using the *SIR97* program,[65] and then refined with full-matrix least-square methods based on F^2 (*SHELXL-97*)[66] with the aid of the *WINGX*[67] program. All non-hydrogen atoms were refined with anisotropic atomic displacement parameters. H atoms were finally included in their calculated positions. A final refinement on F^2 with 9543 unique intensities and 559 parameters converged at ω*R*(F^2) = 0.1128 (*R*(*F*) = 0.0447) for 7649 observed reflections with *I* > 2σ(*I*).

2-5Pm-SBF (C_{29} H_{18} N_2, C H_4 O); *M* = 426.5. APEXII, Bruker-AXS diffractometer, Mo-Kα radiation (λ = 0.71073 Å), *T* = 150(2) K; orthorhombic *P c a b* (I.T.#61), a = 8.4342(3), b = 13.6588(5), c = 38.5506(13) Å, *V* = 4441.1(3) Å^3.*Z* = 8, *d* = 1.276 g.cm^{-3}, μ = 0.078 mm^{-1}. The structure was solved by direct methods using the *SIR97* program [1], and then refined with full-matrix least-square methods based on F^2 (*SHELXL-97*) [2] with the aid of the *WINGX* [3] program. All non-hydrogen atoms were refined with anisotropic atomic displacement parameters. H atoms were finally included in their calculated positions. A final refinement on F^2 with 5055 unique intensities and 300 parameters converged at ω*R*(F^2) = 0.1246 (*R*(*F*) = 0.0461) for 3820 observed reflections with *I* > 2σ(*I*).The figures were generated with Mercury software 3.3

Spectroscopic studies:

Cyclohexane (analytical grade, VWR) was used without further purification. Standard 1N solution of sulfuric acid was purcharsed from Alfa Aesar. UV-visible spectra were recorded using an UV-Visible spectrophotometer SHIMADZU UV-1605. The energy gap was calculated from the absorption edge of the UV-vis absorption spectra in solution in cyclohexane, using the formula ΔE^{opt} (eV) = hc/λ, λ being the absorption edge (in meter). With h = 6.6x10^{-34} J.s (1eV = 1.6x10^{-19} J) and c = 3.0x10^8 m.s^{-1}, this equation may be simplified as: ΔE^{opt} (eV) = 1237.5/λ (in nm). Triplet energy level E_T was calculated from the maximum of the first phosphorescence emission peak, and conversion in electron-volt was obtained with the previous formula. Emission spectra were recorded with a PTI spectrofluorimeter (PTI-814 PDS, MD 5020, LPS 220B) using a Xenon lamp. Quantum yields in solution ($ø_{sol}$) were calculated relative to quinine sulfate ($ø_{sol}$ = 0.546 in H_2SO_4 1N). $ø_{sol}$ was determined according to the following equation,

$$Øsol = Øref \times 100 \times \frac{(T_s \times A_r)}{(T_r \times A_s)} \times \left(\frac{n_s}{n_r}\right)^2$$

where, subscripts s and r refer respectively to the sample and reference. The integrated area of the emission peak in arbitrary units is given as T, n is the refracting index of the solvent (n_s = 1.426 for cyclohexane) and A is the absorbance. Three solutions of different concentration of the substrate (A<0.1) and three solutions of the reference (quinine sulfate) were prepared. The quinine sulfate concentration was chosen so as the absorption of the reference and the substrate were the same at the excitation wavelength. Three quantum yields were then calculated at this wavelength and the average value is reported. IR spectra were recorded on a Bruker Vertex 70 using a diamond crystal MIRacle ATR (Pike). Thin films were prepared by spin-coating 300 µL of solution of THF (10 g/L) on a sapphire plate (10 mm x 10 mm) at 2500 tr/min on a Süss MicroTech Labspin 6.

Fluorescence intensity decays were obtained by the time-correlated single-photon counting (TCSPC) method with femtosecond laser excitation using a Spectra-Physics set-up composed of a Titanium Sapphire Tsunami laser pumped by a doubled YAG laser Millennia. Light pulses at 990 nm (resp. 900 nm) were selected by optoacoustic crystals at a repetition rate of 4 MHz, and the third harmonics at 330 nm

(resp. 300 nm) was obtained through non-linear crystals. Fluorescence photons were detected through a monochromator by means of a Hamamatsu MCP R3809U photomultiplier. The time-to-amplitude converter was purchased from Tennelec. The fluorescence data were analyzed by a nonlinear least-squares global method using the Globals software package developed at the Laboratory for Fluorescence Dynamics at the University of Illinois, Urbana-Champaign.

Electrochemical studies. Electrochemical experiments were performed under argon atmosphere using a Pt disk electrode (diameter 1 mm), the counter electrode was a vitreous carbon rod and the reference electrode was a silver wire in a 0.1M $AgNO_3$ solution in CH_3CN. Ferrocene was added to the solution at the end of a series of experiments. The ferrocene/ferrocenium (Fc/Fc^+) couple served as internal standard. The three electrodes cell was connected to a PAR Model 273 potentiostat/galvanostat (PAR, EG&G, USA) monitored with the ECHEM Software. Activated Al_2O_3 was added in the electrolytic solution to remove excess moisture. For a further comparison of the electrochemical and optical properties, all potentials are referred to the SCE electrode that was calibrated at –0.405 V vs. Fc/Fc^+ system. Following the work of Jenekhe,[48] we estimated the electron affinity (EA) or lowest unoccupied molecular orbital (LUMO) and the ionisation potential (IP) or highest occupied molecular orbital (HOMO) from the redox data (tangent to the oxidation or reduction wave). The LUMO level was calculated from: LUMO (eV)= $-[E_{onset}^{red}$ (vs SCE) +4.4] and the HOMO level from: HOMO (eV) = $-[E_{onset}^{ox}$ (vs SCE) + 4.4], based on an SCE energy level of 4.4 eV relative to the vacuum. The electrochemical gap was calculated from: ΔE^{el} =|HOMO-LUMO| (in eV).

Theoretical modeling. Full geometry optimization with Density Functional Theory (DFT)[68 69] and Time-Dependent Density Functional Theory (TD-DFT) calculations were performed with the hybrid Becke-3 parameter exchange[70-72] functional and the Lee-Yang-Parr non-local correlation functional[73] (B3LYP) implemented in the Gaussian 09 (Revision B.01) program suite[74] using the 6-311G+(d,p) basis set and the default convergence criterion implemented in the program. The figures were generated with GaussView 5.0. The computed triplet adiabatic S_0 to T_1 excitation energies were calculated from the difference between the total energy of the molecule in their respective singlet and triplet states.

Thermal analysis:

Thermal Gravimetric Analysis (TGA) was carried out by using TA SDT Q600 instrument, at the "Ecole Nationale Supérieure de Chimie de Rennes" or at the "Institut des Sciences Analytiques" (UMR CNRS 5280) of Villeurbanne. TGA curves were measured at 10°C/min from 0 to 600°C under an azote atmosphere. Differential Scanning Calorimetry (DSC) was carried out by using NETZSCH DSC 200 F3 instrument equipped with an intracooler. DSC traces were measured at 10°C/min. Two heating/cooling cycles were succesively carried out and the glass transition Tg was determined from the 2nd heating cycle. Temperatures of the different transitions given are obtained with the tangent to the transition peak.

Device fabrication and characterisation:

OLEDs based on a multilayer structure have been fabricated onto patterned ITO coated glass substrates from XinYan Tech (thickness: 100 nm and sheet resistance: less of 20 W/m). The organic materials (from Aldrich and Lumtec) are deposited onto the ITO anode by sublimation under high vacuum (< 10^{-6} Torr) at a rate of 0.2 – 0.3 nm/s. The structure of the device is the following: ITO/CuPc(10 nm)/NPB (40 nm)/TCTA (10 nm)/Hosts:dopant (20 nm)/TPBi (40 nm)/LiF (1.2 nm)/Al (100 nm). In this device, ITO is used as the anode, CuPc (copper phtalocyanine) is the hole injecting layer, NPB (N,N'-di(1-naphtyl)-N,N'-diphenyl-[1,1'-biphenyl]-4,4'-diamine) is the hole-transporting layer, TCTA (4,4',4''-Tris(carbazol-9-yl)-triphenylamine) is the electron/exciton blocking layer, TPBI (1,3,5-Tris(1-phenyl-1H-benzimidazol-2-yl)benzene) is both the electron transporting layer and the hole blocking layer and a thin film of lithium fluoride over aluminum is the cathode. The entire device is fabricated in the same run without breaking the vacuum. In this study, the thicknesses of the different organic layers were kept constant for all the devices. The active area of the devices defined by the overlap of the ITO anode and the metallic cathode was 0.3 cm^2. The current-voltage-luminance (I-V-L) characteristics of the devices were measured with a regulated power supply (Laboratory Power Supply EA-PS 3032-10B) combined with a multimeter and a 1 cm^2 area silicon calibrated photodiode (Hamamatsu). The spectral emission was recorded with a SpectraScan PR650 spectrophotometer. All the measurements were performed at room temperature and at ambient atmosphere with no further encapsulation of devices.

REFERENCES

(1) Meng, Q.; Hu, W. *Phys. Chem. Chem. Phys.* **2012**, *14*, 14152–14164.
(2) Müllen, K.; Scherf, U. *Organic Light-Emitting Devices: Synthesis, Properties and Applications*; Wiley-VCH Verlag GMbH & Co. KGaA: Weinheim, 2006.
(3) Tang, C. W.; VanSlyke, S. A. *Appl. Phys. Lett.* **1987**, *51*, 913-915.
(4) Mishra, A.; Bäuerle, P. *Angew. Chem. Int. Ed.* **2012**, *51*, 2020–2067.
(5) Shaheen, S. E.; Ginley, D. S.; Jabbour, G. E. *Mat. Res. Soc. Bull.* **2005**, *30*, 10-19.
(6) Forrest, S. R.; Thompson, M. E. *Chem. Rev.* **2007**, *107*, 923-925.
(7) Grimsdale, A. C.; Müllen, K. *Macromol. Rapid Commun.* **2007**, *28*, 1676-1702.
(8) Special issue: π-Functional Materials; Bredas, J.-L.; Marder, S. R.; Reichmanis, E. *Chem. Mater.* **2011**, *23*.
(9) Shih, P.-I.; Chien, C.-H.; Chuang, C.-Y.; Shu, C.-F.; Yang, C.-H.; Chen, J.-H.; Chi, Y. *J. Mater. Chem.* **2007**, *17*, 1692-1698.
(10) Yeh, S.-J.; Wu, M.-F.; Chen, C.-T.; Song, Y.-H.; Chi, Y.; Ho, M.-H.; Hsu, S.-F.; Chen, C. H. *Adv. Mater.* **2005**, *17*, 285-289.
(11) Yook, K. S.; Lee, J. Y. L. *Adv. Mater.* **2012**, *24*, 3169–3190.
(12) Xie, J.-H.; Zhou, Q.-L. *Acc. Chem. Res.* **2008**, *41*, 581-594.
(13) Poriel, C.; Ferrand, Y.; Le Maux, P.; Rault-Berthelot, J.; Simonneaux, G. *Synth. Met.* **2008**, *158*, 796-801.
(14) Poriel, C.; Ferrand, Y.; Le Maux, P.; Rault-Berthelot, J.; Simonneaux, G. *Chem. Commun.* **2003**, 1104-1105.
(15) Poriel, C.; Ferrand, Y.; Le Maux, P.; Rault-Berthelot, J.; Simonneaux, G. *Inorg. Chem.* **2004**, *43*, 5086-5095.
(16) Ferrand, Y.; Poriel, C.; Le Maux, P.; Rault-Berthelot, J.; Simonneaux, G. *Tet. Asym.* **2005**, *16*, 1463-1472.
(17) Poriel, C.; Ferrand, Y.; Le Maux, P.; Paul-Roth, C.; Simonneaux, G.; Rault-Berthelot, J. *J. Electroanal. Chem.* **2005**, *583*, 92-103.
(18) Schneider, D.; Rabe, T.; Riedl, T.; Dobbertin, T.; Kröger, M.; Becker, E.; H.-H., J.; Kowalski, W.; Weimann, T.; Wang, J.; Hinze, P.; Gerhard, A.; Stössel, P.; Vestweber, H. *Adv. Mater.* **2005**, *17*, 31-34.
(19) Kim, Y. S.; Lee, M.; Boo, B. H. *J. Chem. Phys.* **1998**, *109*, 2593.
(20) Moreau, F.; Audebrand, N.; Poriel, C.; Moizan-Baslé, V.; Ouvry, J. *J. Mater. Chem.* **2011**, *21*, 18715-18722.
(21) Saragi, T. P. I.; Spehr, T.; Siebert, A.; Fuhrmann-Lieker, T.; Salbeck, J. *Chem. Rev.* **2007**, *107*, 1011-1065.
(22) Romain, M.; Tondelier, D.; Vanel, J.-C.; Geffroy, B.; Jeannin, O.; Rault-Berthelot, J.; Métivier, R.; Poriel, C. *Angew. Chem. Int. Ed.* **2013**, *52*, 14147–14151.
(23) Thirion, D.; Romain, M.; Rault-Berthelot, J.; Poriel, C. *J. Mater. Chem.* **2012**, *22*, 7149-7157.
(24) Tao, Y.; Ao, L.; Wang, Q.; Zhong, C.; Yang, C.; Qin, J.; Ma, D. *Chem. Asian J.* **2010**, *5*, 278-284.
(25) Jeon, S. O.; Yook, K. S.; Lee, J. Y. *Thin Solid Films* **2010**, *519*, 890-893.
(26) Jahng, Y.; Rahman, A. F. M. M. *Bull. Chem. Soc. Jpn.* **2010**, *83*, 672-677.
(27) Ying, L.; Zou, J.; Yang, W.; Zhang, A.; Wu, Z.; Zhao, W.; Cao, Y. *Dyes and Pigments* **2009**, *82*, 251-257.
(28) Wu, P.-T.; Kim, F. S.; Champion, R. D.; Jenekhe, S. A. *Macromol.* **2008**, *41*, 7021 - 7028.
(29) Hughes, G.; Bryce, M. R. *J. Mater. Chem.* **2005**, *15*, 94-107.
(30) Hughes, G.; Wang, C.; Batsanov, A. S.; Fern, M.; Frank, S.; Bryce, M. R.; Perepichka, I. F.; Monkman, A. P.; Lyons, B. P. *Org. Biomol. Chem.* **2003**, *1*, 3069-3077.
(31) Montilla, F.; Mallavia, R. *Adv. Funct. Mater.* **2007**, *17*, 71-78.
(32) Poriel, C.; Rault-Berthelot, J.; Thirion, D.; Barrière, F.; Vignau, L. *Chem. -Eur. J.* **2011**, *17*, 14031-14046.
(33) Grimsdale, A. C. *Curr. Org. Chem.* **2010**, *14*, 2196-2217.
(34) Farrar, S. R.; Contoret, A. E. A.; O'Neill, M.; Nicholls, J. E.; Eastwood, A. J.; Richards, G. J.; Vlachos, P.; Kelly, S. M. *Appl. Surf. Sc.* **2002**, *186*, 435-440.
(35) Wu, C.-C.; Lin, Y.-T.; Chiang, H.-H.; Cho, T. Y.; Chen, C. W.; Wong, K.-T.; Liao, Y.-L.; Lee, G. H.; Peng, S. M. *App. Phys. Lett.* **2002**, *81*, 577-579.
(36) Lee, R.-H.; Huang, Y.-W.; Wang, Y.-Y.; Chang, H.-Y. *Thin Solid Films* **2008**, *516*, 5062-5068.
(37) Jiang, Z.; Yao, H.; Zhang, Z.; Yang, C.; Liu, Z.; Tao, Y.; Qin, J.; Ma, D. *Org. Lett.* **2009**, *11*, 2607–2610.
(38) Fan, C.; Chen, Y.; Gan, P.; Yang, C.; Zhong, C.; Qin, J.; Ma, D. *Org. Lett.* **2010**, *12*, 5648–5651.
(39) Jang, S. E.; Joo, C. W.; Ok, J. S.; Soo, Y. K.; Lee, J. Y. *Org. Elec.* **2010**, *11*, 1059-1065.
(40) Lee, K. H.; Kim, S. O.; Yook, K. S.; Jeon, S. O.; Lee, J. Y.; Yoon, S. S. *Synt. Met.* **2011**, *161*, 2024-2030.
(41) Dong, S.-C.; Gao, C.-H.; Zhang, Z.-H.; Jiang, Z.-Q.; Lee, S.-T.; Liao, L.-S. *Phys. Chem. Chem. Phys.* **2012**, *14*, 14224-14228.
(42) Dong, S.-C.; Gao, C.-H.; Yuan, X.-D.; Cui, L.-S.; Jiang, Z.-Q.; Lee, S.-T.; Liao, L.-S. *Org. Elec.* **2013**, *14*, 902-908.
(43) Poriel, C.; Métivier, R.; Rault-Berthelot, J.; Thirion, D.; Barrière, F.; Jeannin, O. *Chem. Commun.* **2011**, *47*, 11703-11705.
(44) Thiery, S.; Tondelier, D.; Declairieux, C.; Seo, G.; Geffroy, B.; Jeannin, O.; Rault-Berthelot, J.; Métivier, R.; Poriel, C. *J. Mater. Chem. C* **2014**, **2014**, 2, 4156-4166
(45) Pei, J.; Ni, J.; Zhou, X.-H.; Cao, X.-Y.; Lai, Y.-H. *J. Org. Chem.* **2002**, *67*, 4924-4936.
(46) Demers, E.; Maris, T.; Wiest, J. D. W. *Cryst. Growth Des.* **2005**, *5*, 1227-1235.
(47) Wong, K.-T.; Liao, Y.-L.; Peng, Y.-C.; Wang, C.-C.; Lin, S.-Y.; Yang, C.-H.; Tseng, S.-M.; Lee, G.-H.; Peng, S.-M. *Cryst. Growth Des.* **2005**, *5*, 667–671.
(48) Kulkarni, A. P.; Tonzola, C. J.; Babel, A.; Jenekhe, S. A. *Chem. Mater.* **2004**, *16*, 4556–4573.
(49) Poriel, C.; Liang, J.-J.; Rault-Berthelot, J.; Barrière, F.; Cocherel, N.; Slawin, A. M. Z.; Horhant, D.; Virboul, M.; Alcaraz, G.; Audebrand, N.; Vignau, L.; Huby, N.; Wantz, G.; Hirsch, L. *Chem. -Eur. J.* **2007**, *13*, 10055-10069.
(50) Aizawa, N.; Pu, Y.-J.; Sasabe, H.; Kido, J. *Org. Electron.* **2012**, *13*, 2235-2242.

(51) Tsai, M.-H.; Hong, Y.-H.; Chang, C.-H.; Su, H.-C.; Wu, C.-C.; Matoliukstyte, A.; Simokaitiene, J.; Grigalevicius, S.; Grazulevicius, J. V.; Hsu, C.-P. *Adv. Mater.* **2007**, *19*, 862-866.
(52) Belletête, M.; Ranger, M.; Beaupré, S.; Leclerc, M.; Durocher, G. *Chem. Phys. Lett.* **2000**, *316*, 101-107.
(53) Wang, J.-F.; Feng, J.-K.; Ren, A.-M.; Yang, L. *Chin. J. Chem.* **2005**, *23*, 1618-1624.
(54) Thirion, D.; Poriel, C.; Métivier, R.; Rault-Berthelot, J.; Barrière, F.; Jeannin, O. *Chem. -Eur. J.* **2011**, *17*, 10272-10287.
(55) Thirion, D.; Poriel, C.; Barrière, F.; Métivier, R.; Jeannin, O.; Rault-Berthelot, J. *Org. Lett.* **2009**, *11*, 4794-4797.
(56) Ooyama, Y.; Ito, G.; Kushimoto, K.; Komaguchi, K.; Imae, I.; Harima, Y. *Org. Biomol. Chem.* **2010**, *8*, 2756-2770.
(57) Chi, C.-C.; Chiang, C.-L.; Liu, S.-W.; Yueh, H.; Chen, C.-T.; Chen, C.-T. *J. Mater. Chem.* **2009**, *19*, 5561-5571.
(58) Adachi, C.; Kwong, R. C.; Djurovich, P.; Adamovich, V.; Baldo, M. A.; Thompson, M. E.; Forrest, S. R. *Appl. Phys. Lett.* **2001**, *79*, 2082.
(59) Wong, K.-T.; Chen, Y.-M.; Lin, Y.-T.; Su, H.-C.; Wu, C.-C. *Org.Lett.* **2005**, *7*, 5361-5364.
(60) Seo, J. H.; Han, N. S.; Shim, H. S.; Kwon, J. H.; Song, J. K. *Bull. Korean Chem. Soc.* **2011**, *32*, 1415.
(61) Chi, L.-C.; Hung, W.-Y.; Chiu, H.-C.; Wong, K.-T. *Chem. Commun.* **2009**, 3892-3894.
(62) Han, N. S.; Sohn, S. H.; Park, S. M.; Song, J. K. *Bull. Korean Chem. Soc.* **2013**, *34*, 1547-1550.
(63) Winter-Werner, B.; Diederich, F.; Gramlich, V. *Helv. Chim. Acta* **1996**, *79*, 1338–1360.
(64) Jeon, S. O.; Yook, K. S.; Joo, C. W.; Son, H. S.; Lee, J. Y. *Thin Solid Films* **2010**, *518*, 3716-3720.
(65) Altomare, A.; Burla, M. C.; Camalli, M.; Cascarano, C.; Giacovazzo, A.; Guagliardi, A.; Moliterni, A. G. G.; Polidori, G.; Spagna, R. *J. Appl. Cryst.* **1999**, *32*, 115-119.
(66) Sheldrick, G. M. *Acta Crystallogr.* **2008**, *A64*, 112-122.
(67) Farrugia, L. J. *J. Appl. Cryst.* **2012**, *45*, 849-854.
(68) Hohenberg, P.; Kohn, W. *Phys. Rev.* **1964**, *136*, B864-B871.
(69) Calais, J.-L. *Int. J. Quantum Chem.* **1993**, *47*, 101.
(70) Becke, A. D. *Phys. Rev. A* **1988**, *38*, 3098-3100.
(71) Becke, A. D. *J. Chem. Phys.* **1993**, *98*, 5648 –5652.
(72) Becke, A. D. *J. Chem. Phys.* **1993**, *98*, 1372-1377.
(73) Lee, C.; Yang, W.; Parr, R. G. *Phys. Rev. B* **1988**, *37*, 785-789.
(74) Frisch, M. J.; Trucks, G. W.; Schlegel, H. B.; Scuseria, G. E.; Robb, M. A.; Cheeseman, J. R.; Scalmani, G.; Barone, V.; Mennucci, B.; Petersson, G. A.; Nakatsuji, H.; Caricato, M.; Li, X.; Hratchian, H. P.; Izmaylov, A. F.; Bloino, J.; Zheng, G.; Sonnenberg, J. L.; Hada, M.; Ehara, M.; Toyota, K.; Fukuda, R.; Hasegawa, J.; Ishida, M.; Nakajima, T.; Honda, Y.; Kitao, O.; Nakai, H.; Vreven, T.; Montgomery, J. A. J.; Peralta, J. E.; Ogliaro, F.; Bearpark, M.; Heyd, J. J.; Brothers, E.; Kudin, K. N.; Staroverov, V. N.; Keith, T.; Kobayashi, R.; Normand, J.; Raghavachari, K.; Rendell, A.; Burant, J. C.; Iyengar, S. S.; Tomasi, J.; Cossi, M.; Rega, N.; Millam, J. M.; Klene, M.; Knox, J. E.; Cross, J. B.; Bakken, V.; Adamo, C.; Jaramillo, J.; Gomperts, R.; Stratmann, R. E.; Yazyev, O.; Austin, A. J.; Cammi, R.; Pomelli, C.; Ochterski, J. W.; Martin, R. L.; Morokuma, K.; Zakrzewski, V. G.; Voth, G. A.; Salvador, P.; Dannenberg, J. J.; Dapprich, S.; Daniels, A. D.; Farkas, O.; Foresman, J. B.; Ortiz, J. V.; Cioslowski, J.; Fox, D. J., *Gaussian 09, Revision B.01, Gaussian, Inc., Wallingford CT, 2010.*

Supplementary Materials for

2-substituted vs 4-substituted-9,9'-spirobifluorene host materials for green and blue phosphorescent OLEDs: A Structure-Property Relationship Study

*Sébastien Thiery,[a] Céline Declairieux,[c] Denis Tondelier,[c] Gijun Seo,[c] Bernard Geffroy,[c,d] Olivier Jeannin,[a] Rémi Métivier,[b] Joëlle Rault-Berthelot,[*a] Cyril Poriel[*a]*

a. Université de Rennes 1-UMR CNRS 6226, "Institut des Sciences Chimiques de Rennes" MaCSE group. Bat 10C, Campus de Beaulieu, 35042 Rennes, France

b. PPSM, Institut d'Alembert, ENS Cachan, UMR CNRS 8531, 61 Avenue du Président Wilson, 94235 Cachan, France

c. LPICM, Ecole Polytechnique, UMR CNRS 7647, Route de Saclay, 91128, Palaiseau

d. LICSEN, CEA Saclay, IRAMIS/NIMBE, 91191 Gif sur Yvette

Summary

X-RAY DIFFRACTION

Table 1 Crystal data and structure refinement for **2-Ph-SBF**

Identification code	2-Ph-SBF
Empirical formula	C_{62} H_{40}
Formula weight	784.94
Temperature	150(2) K
Wavelength	0.71073 Å
Crystal system	Triclinic
Space group	P-1
Unit cell dimensions	a = 10.9027(4) Å α= 102.1400(10)°.
	b = 13.7902(6) Å β= 97.4710(10)°.
	c = 15.7771(5) Å γ = 111.5900(10)°.
Volume	2099.47(14) $Å^3$
Z	2
Density (calculated)	1.242 g/cm^3
Absorption coefficient	0.070 mm^{-1}
F(000)	824
Crystal size	0.26 x 0.24 x 0.09 mm^3
Theta range for data collection	1.36 to 27.50°.
Index ranges	-14<=h<=13, -17<=k<=17, -20<=l<=20
Reflections collected	20625
Independent reflections	9543 [R(int) = 0.0307]
Completeness to theta = 27.50°	98.9 %
Absorption correction	Semi-empirical from equivalents
Max. and min. transmission	0.994 and 0.982
Refinement method	Full-matrix least-squares on F^2
Data / restraints / parameters	9543 / 0 / 559
Goodness-of-fit on F^2	1.074
Final R indices [I>2sigma(I)]	R1 = 0.0447, wR2 = 0.1128
R indices (all data)	R1 = 0.0583, wR2 = 0.1272
Largest diff. peak and hole	0.261 and -0.269 $e.Å^{-3}$

Table 2 Crystal data and structure refinement for **2-5Pm-SBF**

Identification code	**2-5Pm-SBF**
Empirical formula	$C_{30}\ H_{22}\ N_2\ O$
Formula weight	426.5
Temperature	150(2) *K*
Wavelength	0.71073 Å
Crystal system	orthorhombic
space group	*P c a b*
Unit cell dimensions	a = 8.4342(3) Å, α = 90 ° b = 13.6588(5) Å, β = 90 ° c = 38.5506(13) Å, γ = 90 °
Volume	4441.1(3) $Å^3$
Z	8
Calculated density	1.276 ($g.cm^{-3}$)
Absorption coefficient	0.078 mm^{-1}
F(000)	1792
Crystal size	0.36 x 0.31 x 0.05 mm
Theta range for data collection	1.06 to 27.46 °
h_min, h_max	-10, 9
k_min, k_max	-17, 16
l_min, l_max	-45, 50
Reflections collected / unique	21000 / 5055 [R(int)[a] = 0.0327]
Reflections [I>2σ]	3820
Completeness to theta_max	0.994
Absorption correction type	multi-scan
Refinement method	Full-matrix least-squares on F^2
Data / restraints / parameters	5055 / 0 / 300
Goodness-of-fit	1.124
Final *R* indices [I>2σ]	$R1^c$ = 0.0461, $wR2^d$ = 0.1246
R indices (all data)	$R1^c$ = 0.0711, $wR2^d$ = 0.1511
Largest diff. peak and hole	0.36 and -0.315 $e^-.Å^{-3}$

2-Ph-SBF

2-Ph-SBF MOLECULE 1

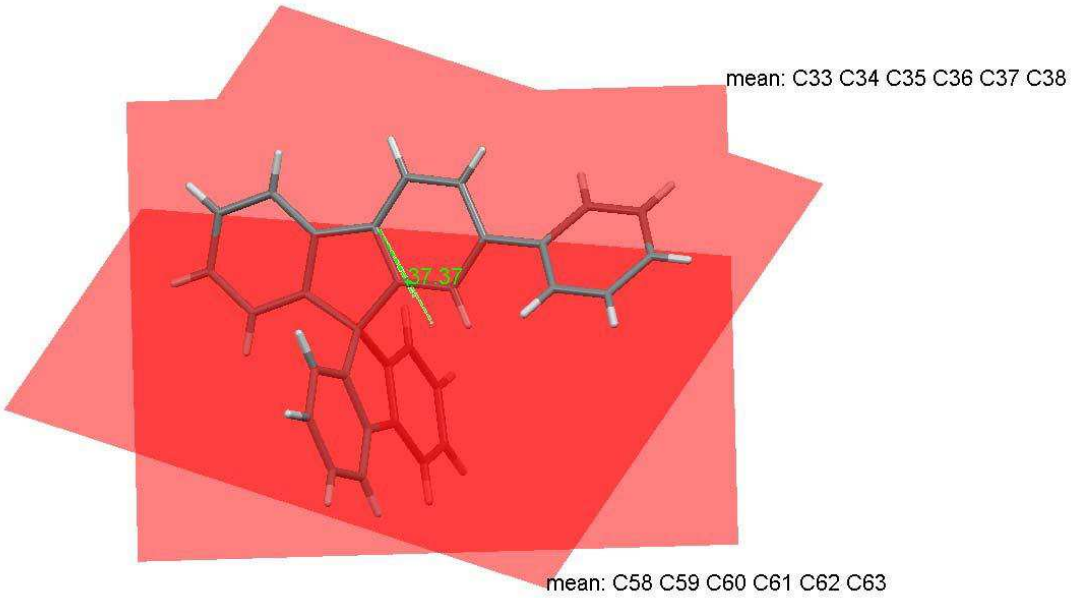

S 1 Top: Angle between the mean plane of the pendant phenyl ring and that of its attached phenyl ring of the fluorene : 37.37° ; **Bottom:** Angle between the two mean planes of each fluorene: 7.08°

2-Ph-SBF MOLECULE 2

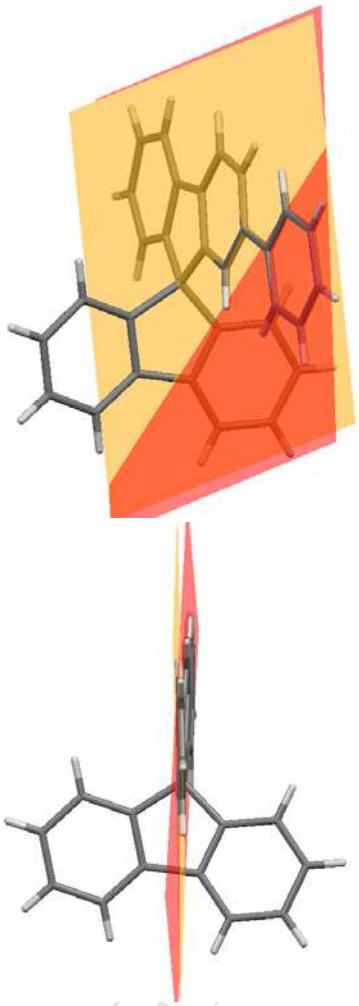

S 2 Angle between the mean plane of the pendant phenyl ring and that of its attached phenyl ring of the fluorene: 4.58°

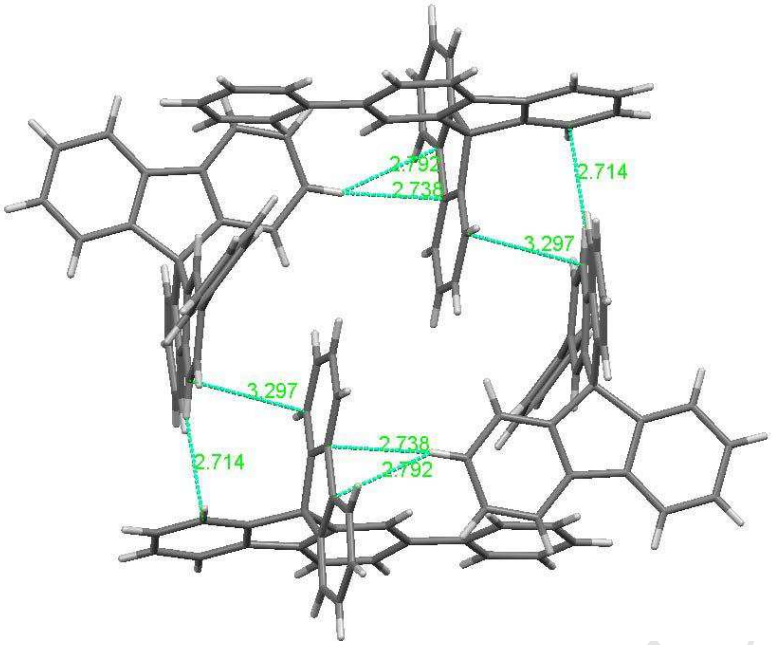

S 3 Short contacts (CH and C-C, distance < (sum of r_{vdw}-0.1) detected in crystal packing of **2-Ph-SBF**.

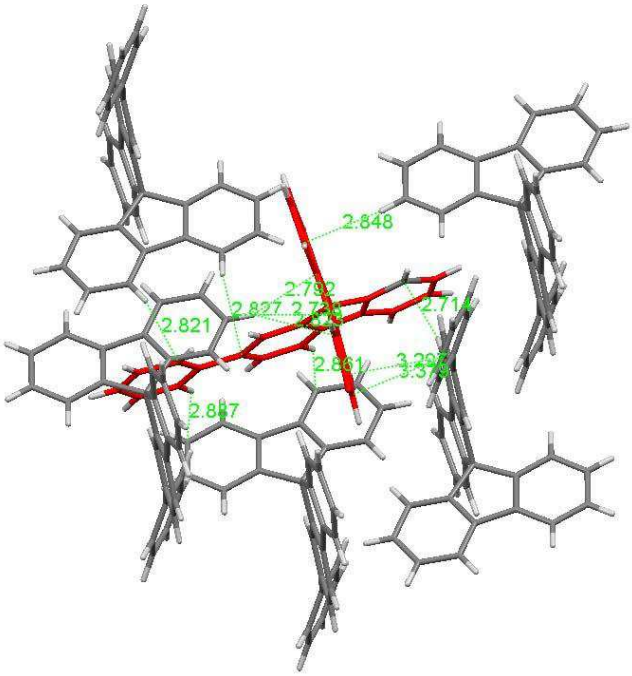

S 4 Short contacts (CH and C-C, distance < (sum of r_{vdw}) detected for the **2-Ph-SBF** molecule 2 (in red above)

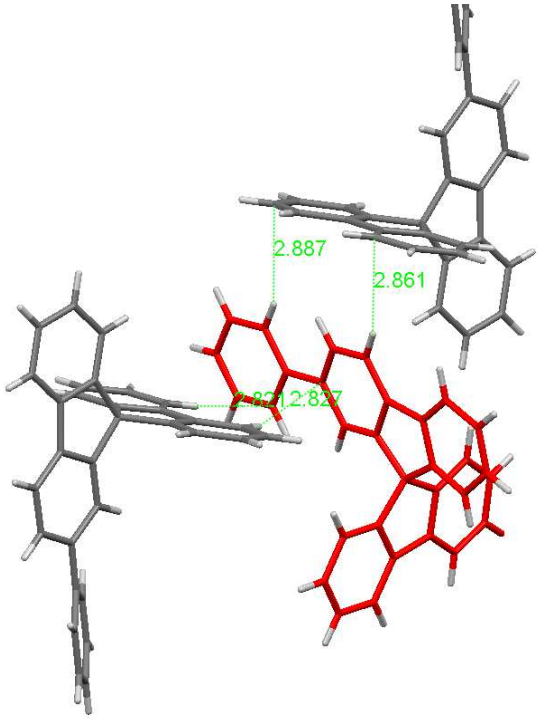

S 5 Short contacts (CH and C-C, distance < (sum of r_{vdw}) detected for the pendant phenyl unit of **2-Ph-SBF**molecule 2 (in red above)

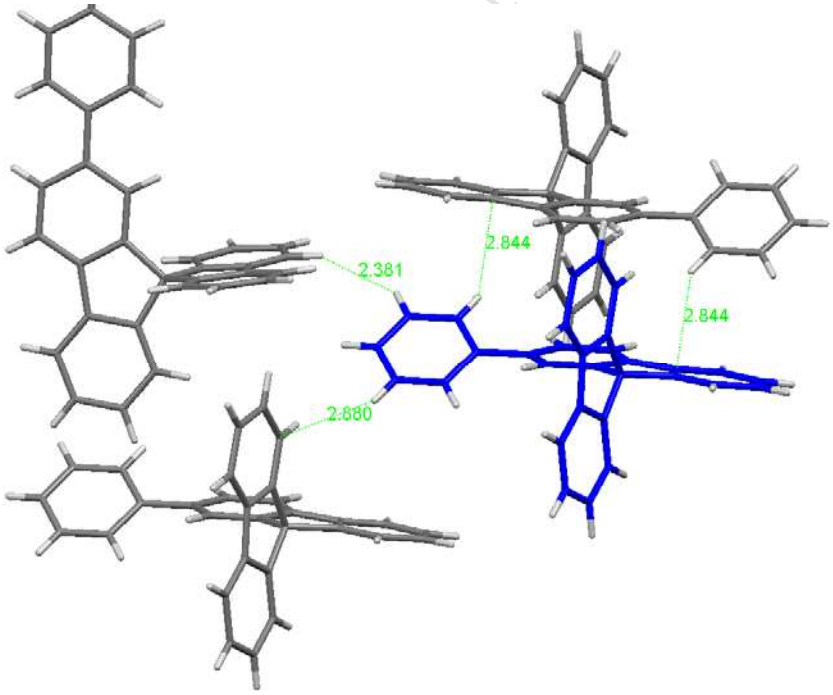

S 6 Short contacts (CH and C-C, distance < (sum of r_{vdw}) detected for the pendant phenyl unit of **2-Ph-SBF** molecule 1 (in blue above)

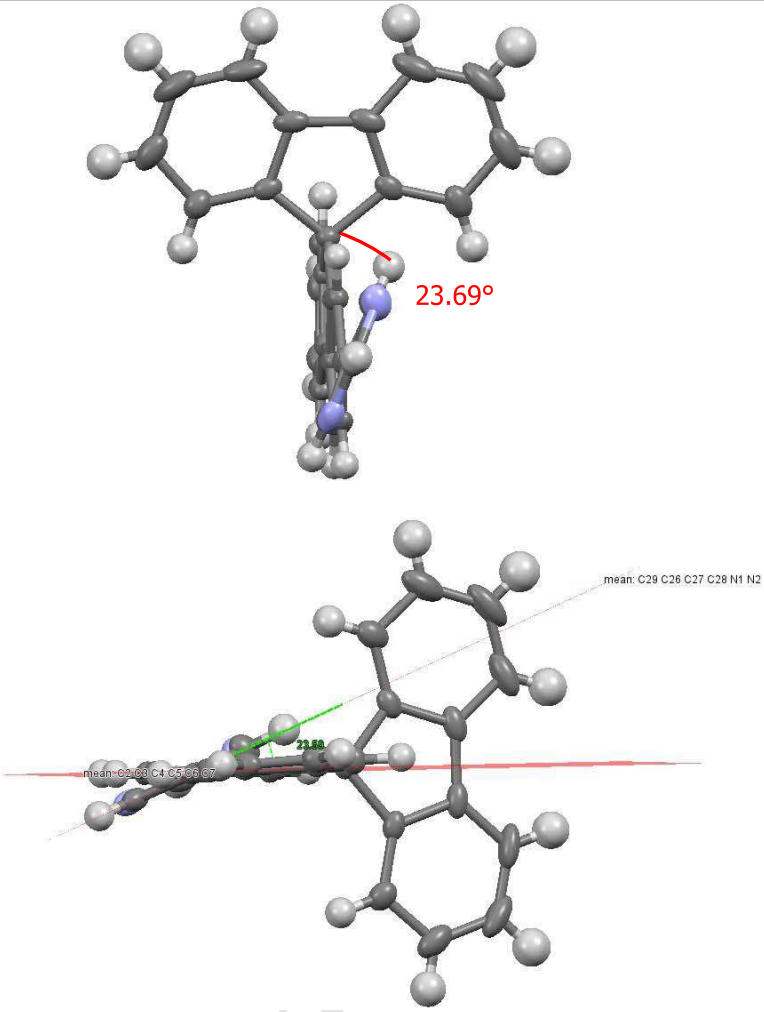

S 7 **2-5Pm-SBF** :Angle between the mean plane of the pyrimidine plane and that of its attached phenyl ring: 23.69°

Photophysical properties

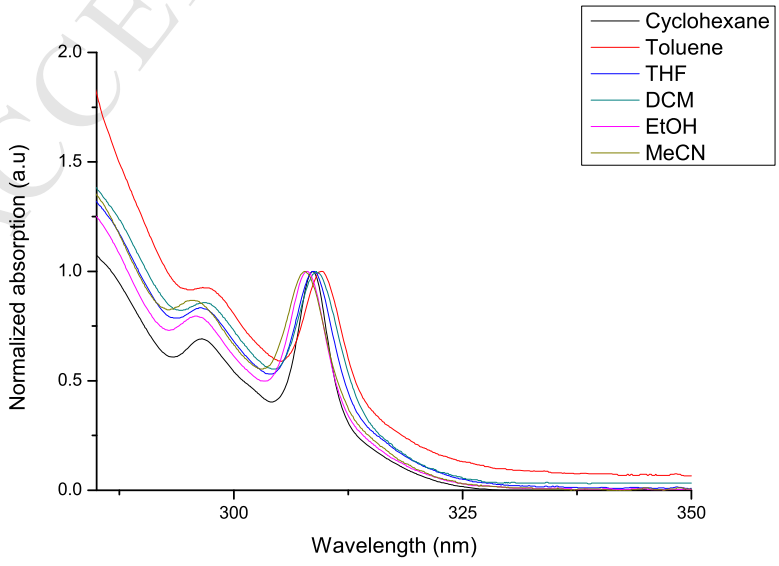

S 8 UV-Vis absorption spectrum of **4-Ph-SBF** in various solvents

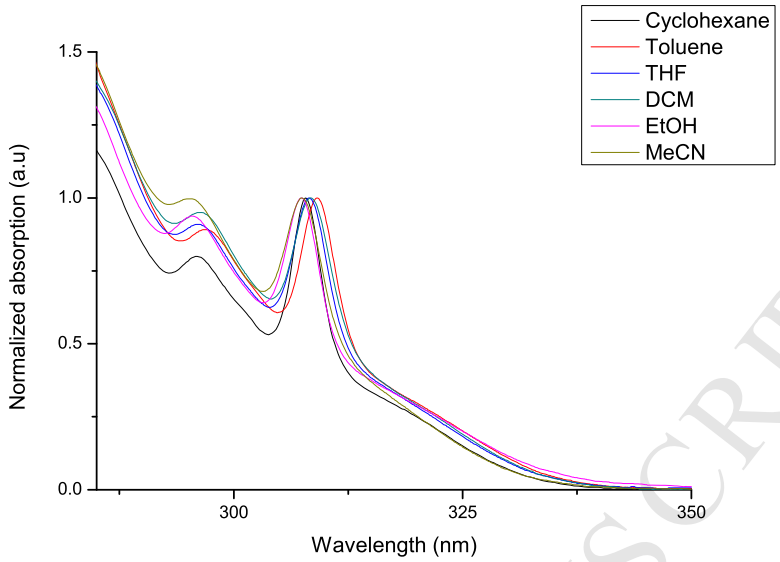

S 9 UV-Vis absorption spectrum of **4-5Pm-SBF** in various solvents

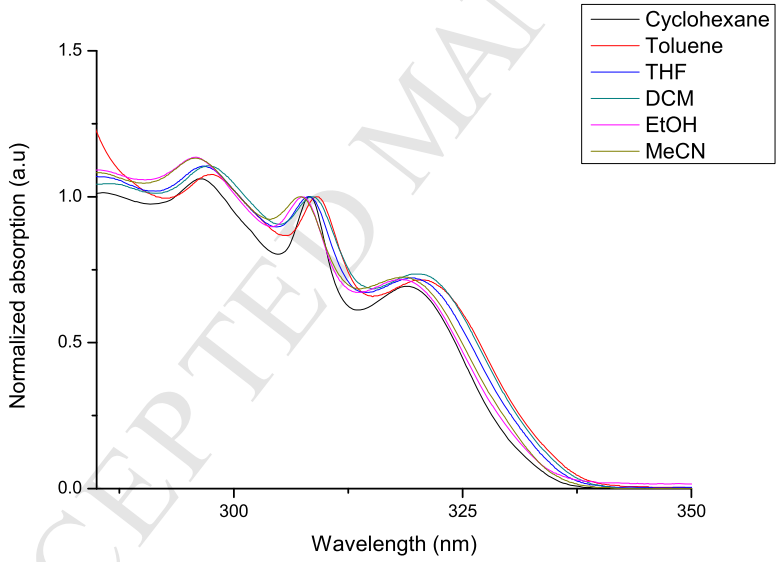

S 10 UV-Vis absorption spectrum of **2-Ph-SBF** in various solvents

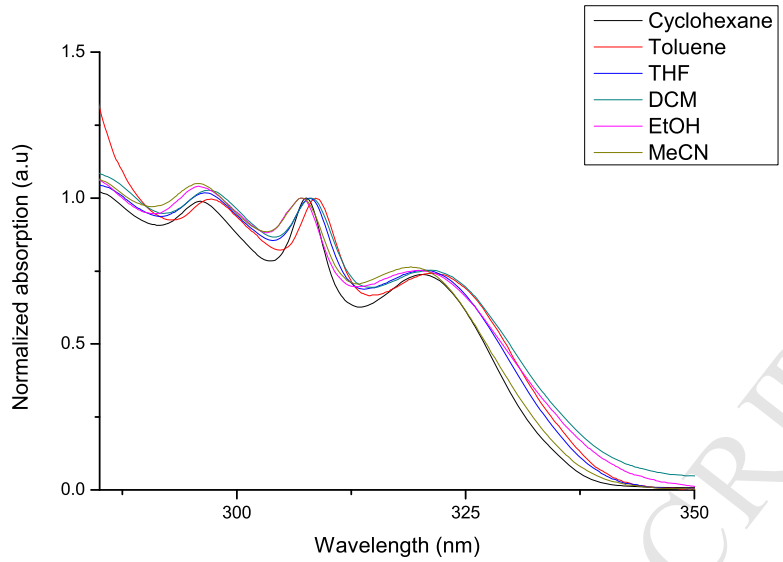

S 11 UV-Vis absorption spectrum of **2-5Pm-SBF** in various solvents

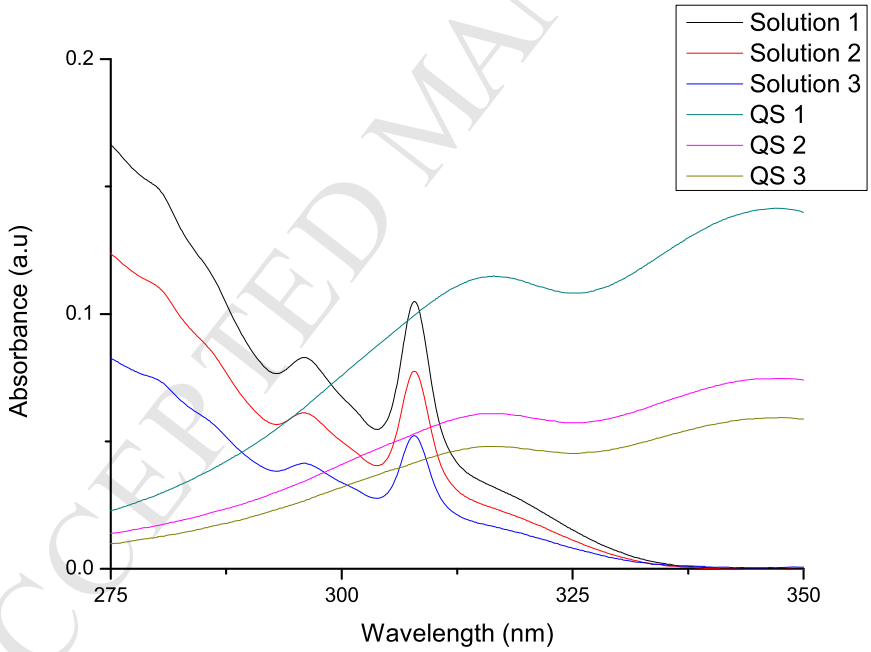

S 12 Quantum yield measurements: Absorption of solutions of **4-5Pm-SBF** in cyclohexane and quinine sulfate (QS) in H_2SO_4 1N

Table 2 Quantum yield calculation of **4-5Pm-SBF**

Solution	λ (nm)	A	T_S	T_{QS}	n_D^{25} (cyclohexane)	n_D^{25} (H_2SO_4 1N)	φ
1	308.5	0.1011	14134.4	238032	1.42662	1.3325	4%
	299	0.0721	7610.04	120670	1.42662	1.3325	4%
2	309.5	0.0569	10314.6	150249	1.42662	1.3325	4%
	302	0.0442	6316.68	89861.1	1.42662	1.3325	4%
3	309	0.0435	8040.89	122287	1.42662	1.3325	4%
	300.5	0.0328	4539.62	67376.1	1.42662	1.3325	4%

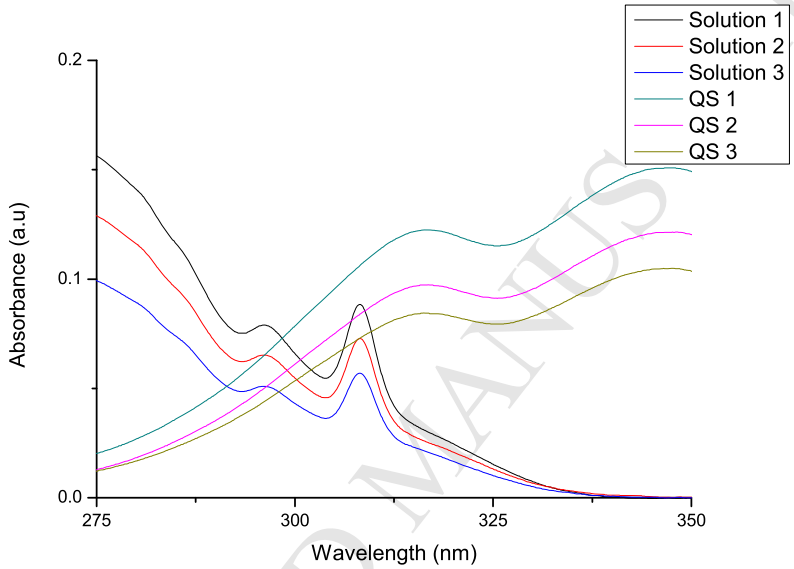

S 13 Quantum yield measurements: Absorption of solutions of **4-5Pm-SBF** in tetrahydrofurane and quinine sulfate (QS) in H_2SO_4 1N

Table 3 Quantum yield calculation of **4-5Pm-SBF**

Solution	λ (nm)	A	T_S	T_{QS}	n_D^{25} (cyclohexane)	n_D^{25} (H_2SO_4 1N)	φ
1	299	0,073	5032,56	60164,3	1,42662	1,3325	5%
2	299	0,058	4262,56	52110,2	1,42662	1,3325	5%
3	298	0,049	5132,74	43404,5	1,42662	1,3325	7%

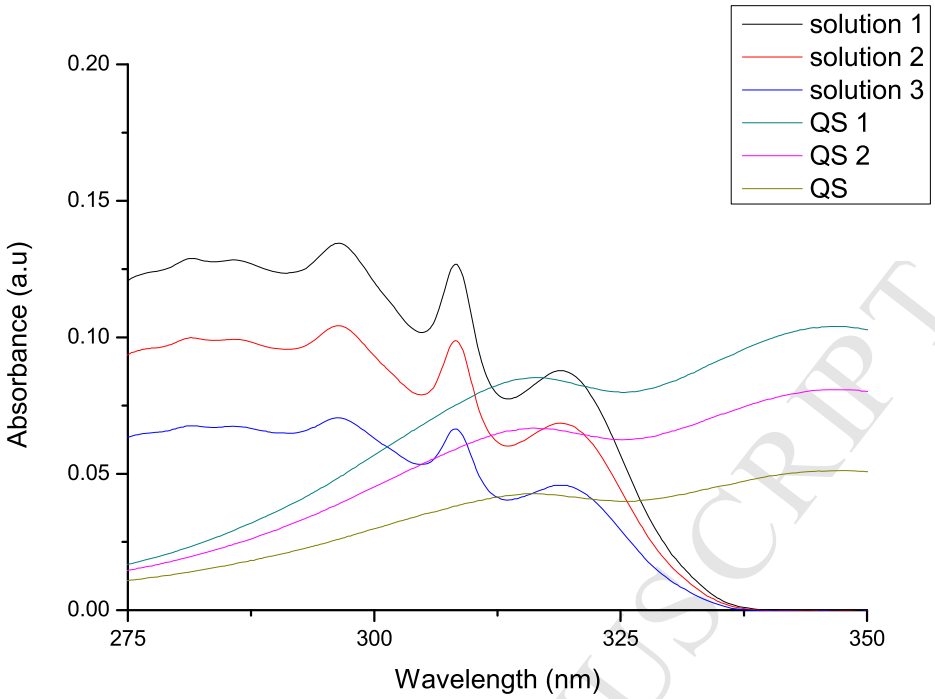

S 14 Quantum yield measurements: Absorption of solutions of **2-Ph-SBF** in cyclohexane and quinine sulfate (QS) in H_2SO_4 1N

Table 4 Quantum yield calculation of **2-Ph-SBF**

Solution	λ (nm)	A	T_S	T_{QS}	n_D^{25} (cyclohexane)	n_D^{25} (H_2SO_4 1N)	φ
1	312	0.0815	65759.6	48449.5	1.42662	1.3325	85%
2	312	0.064	51316.1	37356.8	1.42662	1.3325	86%
3	312.5	0.0413	36521.4	25376.8	1.42662	1.3325	90%

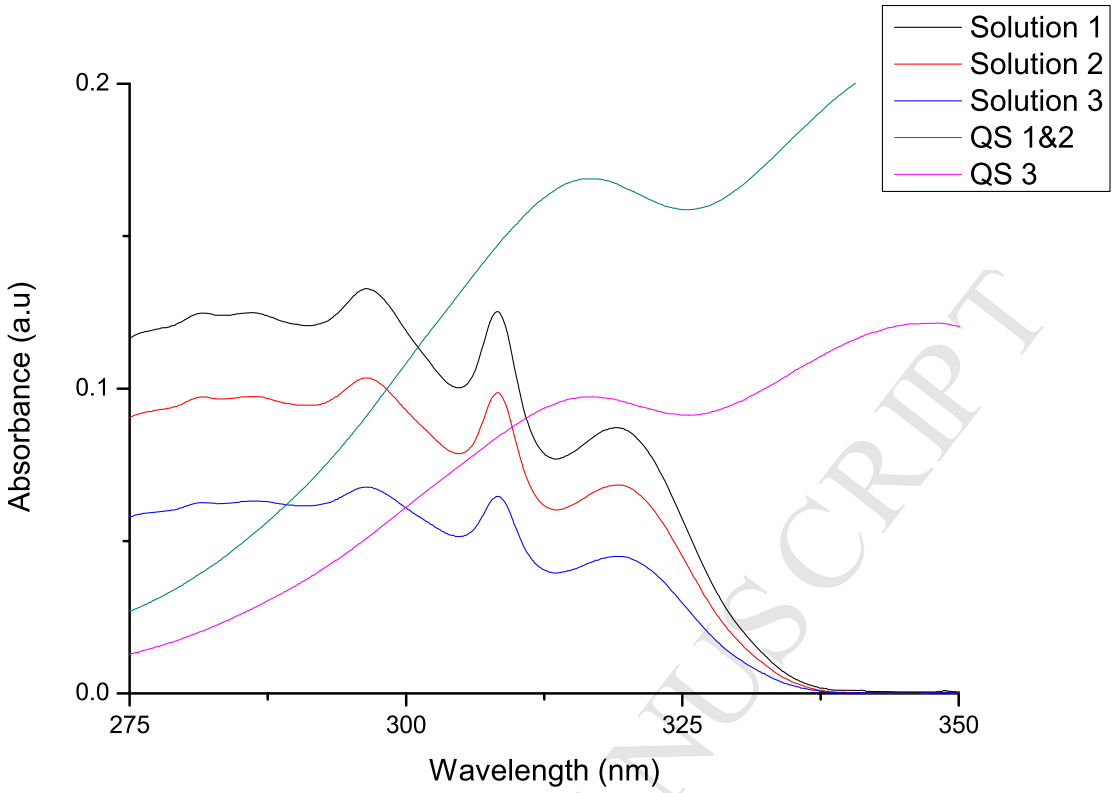

S 15 Quantum yield measurements: Absorption of solutions of **2-Ph-SBF** in cyclohexane and quinine sulfate (QS) in H_2SO_4 1N

Table 5: Quantum yield calculation of **2-Ph-SBF**

Solution	λ (nm)	A	T_S	T_{QS}	n_D^{25} (cyclohexane)	n_D^{25} (H_2SO_4 1N)	φ
1	301	0.113	119399	95186.3	1.42662	1.3325	79%
2	299	0.100	96821.3	77070.8	1.42662	1.3325	79%
3	300	0.061	73910.6	57692.5	1.42662	1.3325	80%

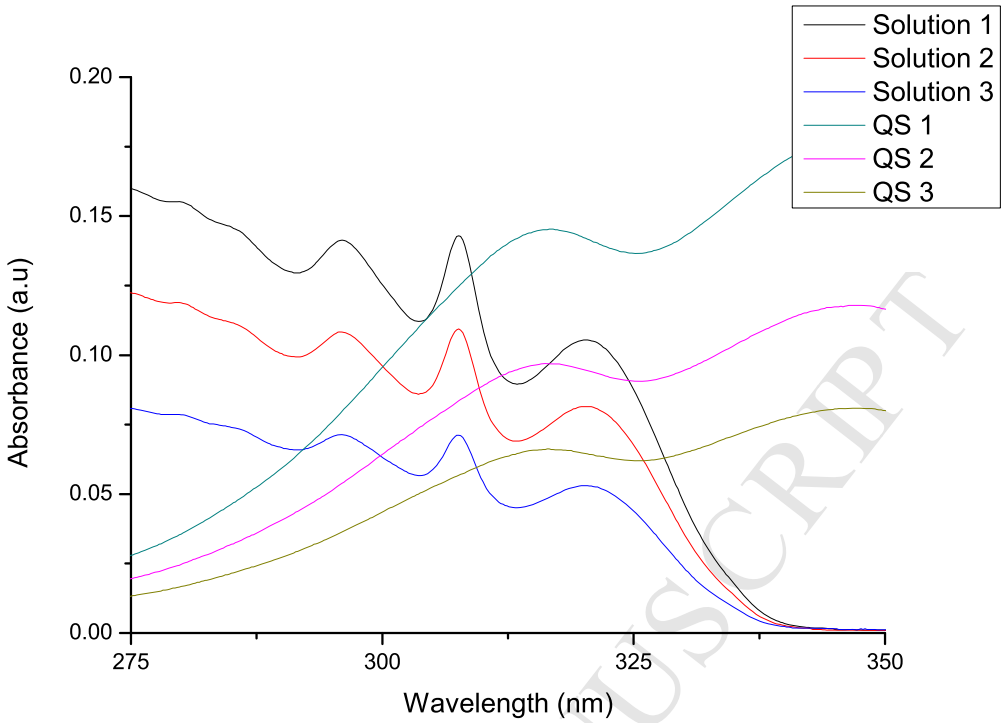

S 16 Quantum yield measurements: Absorption of solutions of **2-5Pm-SBF** in cyclohexane and quinine sulfate (QS) in H_2SO_4 1N

Table 6 Quantum yield calculation of **2-5Pm-SBF**

Solution	λ (nm)	A	T_S	T_{QS}	n_D^{25} (cyclohexane)	n_D^{25} (H_2SO_4 1N)	φ
1	309	0.129	10082.1	240980	1.42662	1.3325	3%
2	309.5	0.0881	6580.11	176643	1.42662	1.3325	2%
3	309.5	0.0593	5162.04	134942	1.42662	1.3325	2%

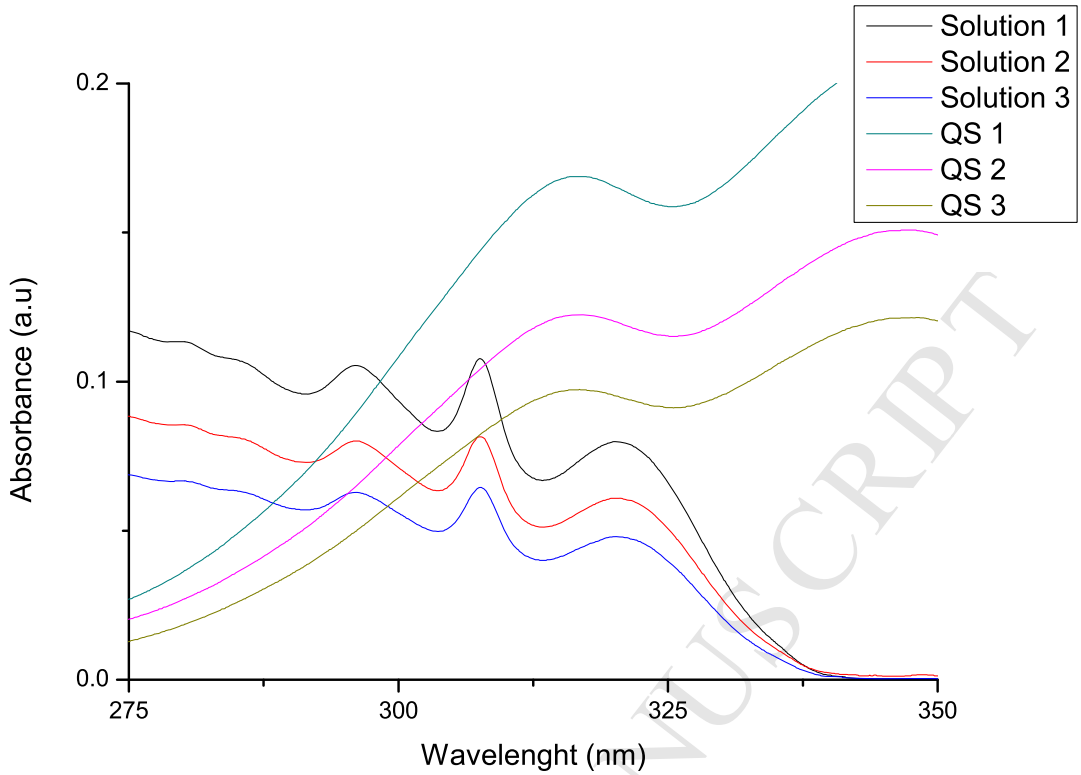

S 1 Quantum yield measurements: Absorption of solutions of **2-5Pm-SBF** in cyclohexane and quinine sulfate (QS) in H_2SO_4 1N

Table 7 Quantum yield calculation of **2-5Pm-SBF**

Solution	λ (nm)	A	T_S	T_{QS}	n_D^{25} (cyclohexane)	n_D^{25} (H_2SO_4 1N)	φ
1	299	0.100	2965.74	77070.8	1.42662	1.3325	2%
2	299	0.074	2565.15	63262.2	1.42662	1.3325	3%
3	299	0.058	2084.54	52110.2	1.42662	1.3325	3%

THEORETICAL MODELING

Predicted UV-vis Spectra from TD-DFT energy calculations

SBF

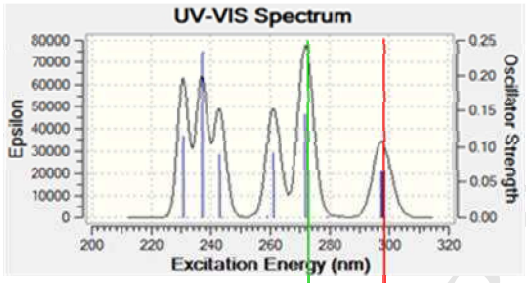

4-Ph-SBF

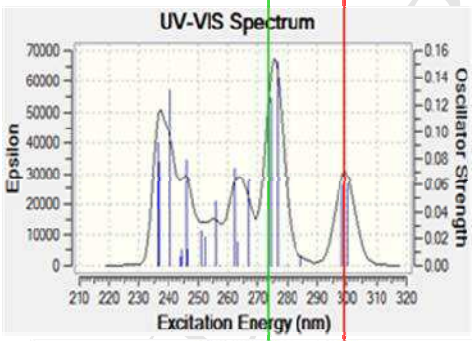

4-5Pm-SBF

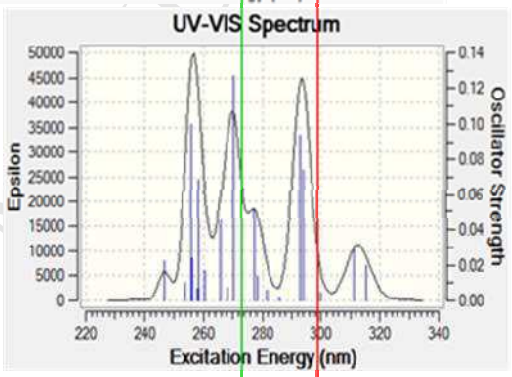

2-5Pm-SBF

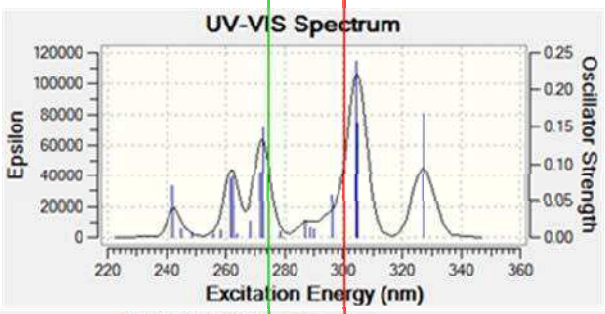

2-Ph-SBF

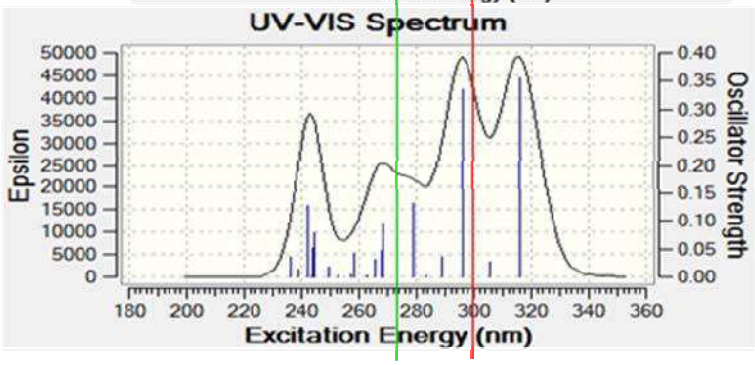

S 2 Predicted UV-Vis spectra from TD-DFT energy calculations

SBF

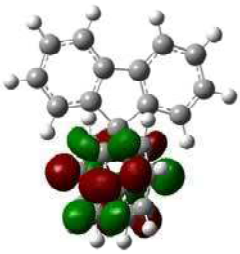

LUMO+1: -1.25 eV

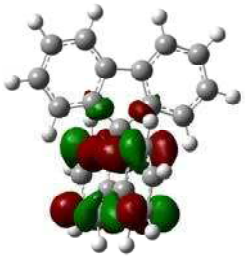

LUMO+2: -0.84 eV

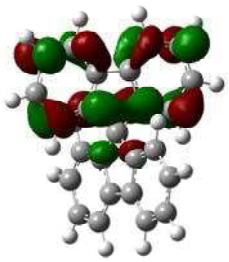

LUMO+3: -0.84 eV

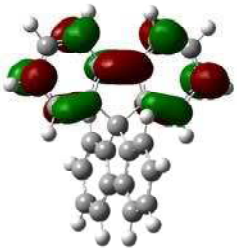

LUMO: -1.25 eV

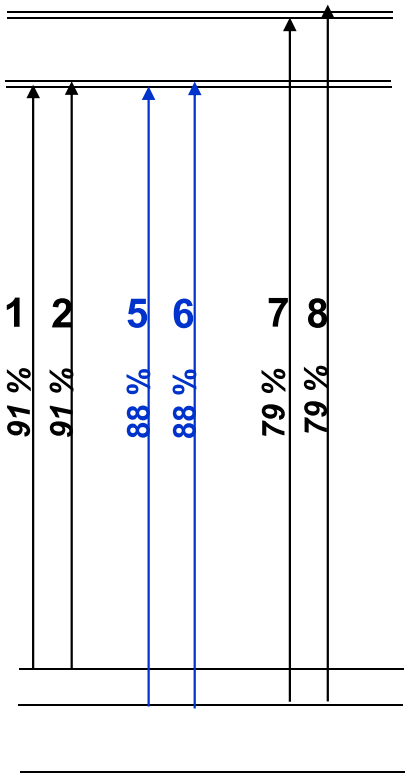

Excited state 1
λ: 297.6 nm
f: 0.064
Excited state 2
λ: 297.59nm
f: 0.064
Excited states 3 and 4
f: 0
Excited state 5
λ : 271.95 nm
f: 0.1449
Excited state 6
λ : 271.95 nm
f: 0.1449
Excited state 7
λ : 261.09 nm
f: 0.0905
Excited state 8
λ: 261.09 nm
f: 0.0906

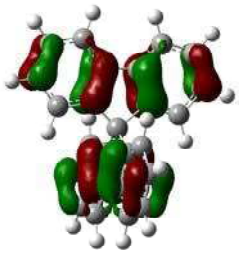

HOMO: -5.99 eV

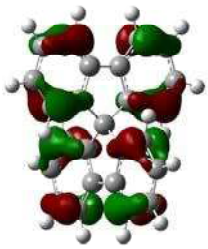

HOMO-2: -6.79 eV

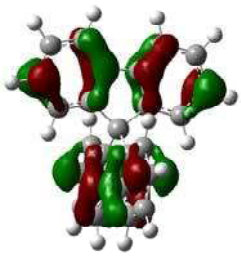

HOMO-1: -6.26 eV

S 3 Calculated frontier molecular orbitals by DFT and the 6th first calculated electronic transitions by TD-DFT of **SBF**, after geometry optimization with DFT B3LYP/6-311G+(d,p), show with an isovalue of 0.04

4-Ph-SBF

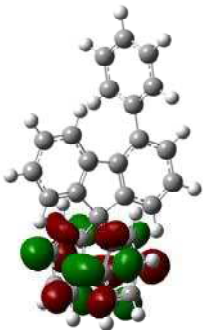

LUMO+1: -1.24 eV

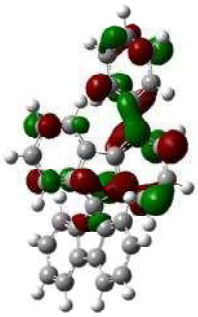

LUMO+2: -0.94 eV

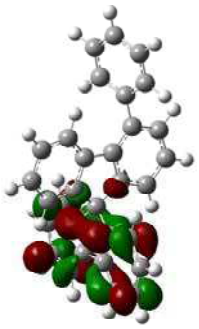

LUMO+3: -0.84 eV

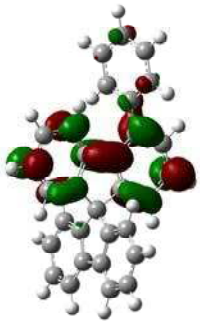

LUMO: -1.27eV

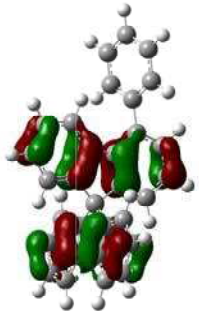

HOMO: -5.97 eV

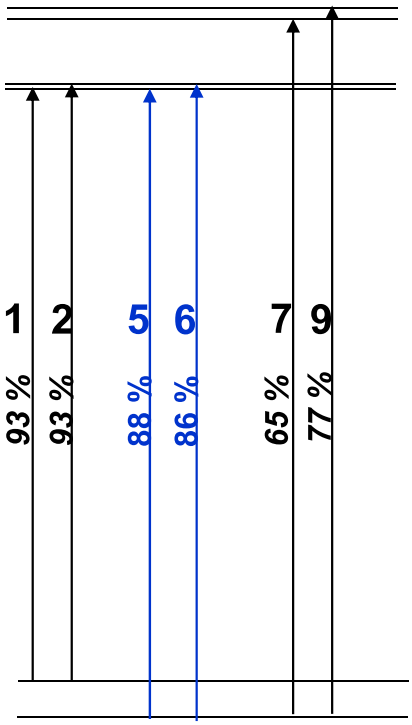

Excited state 1
λ: 300.25 nm
f: 0.06
Excited state 2
λ: 298.49nm
f: 0.059
Excited states 3 and 4
f: 0
Excited state 5
λ : 276.78 nm
f: 0.1519
Excited state 6
λ : 274.41 nm
f: 0.1249
Excited state 7
λ : 266.68 nm
f: 0.06
Excited state 8
f: 0
Excited state 9
λ: 263.08 nm
f: 0.01

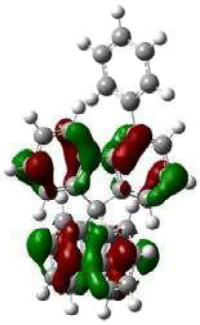

HOMO-1: -6.25 eV

S 4 Calculated frontier molecular orbitals by DFT and the 6th first calculated electronic transitions by TD-DFT of **4-Ph-SBF**, after geometry optimization with DFT B3LYP/6-311G+(d,p), show with an isovalue of 0.04

4-5Pm-SBF

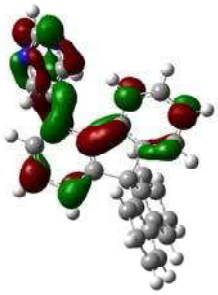

LUMO+1: -1.645 eV

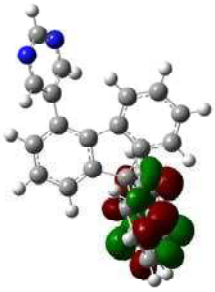

LUMO+2: -1.38 eV

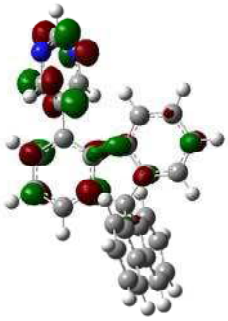

LUMO+3: -1.18 eV

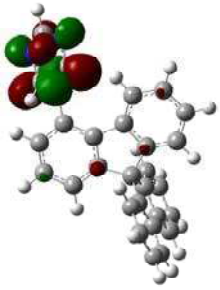

LUMO: -1.65 eV

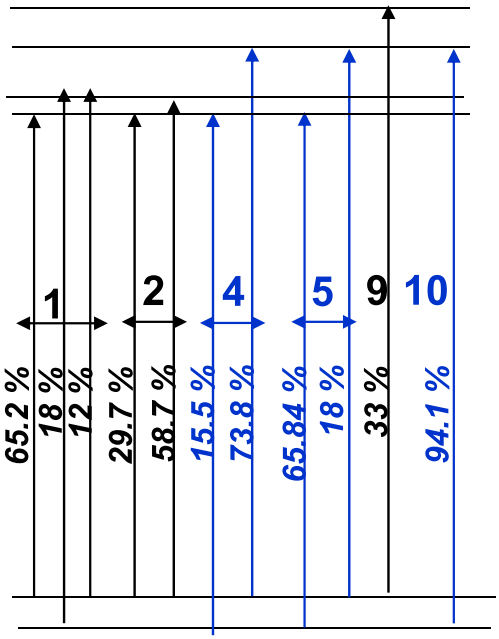

Excited state 1
λ: 315.225 nm
f: 0.0198
Excited state 2
λ: 311.07 nm
f: 0.0303
Excited state 4
λ : 293.96 nm
f: 0.0744
Excited state 5
λ : 292.97 nm
f: 0.0937
Excited state 9
λ : 277.29 nm
f: 0.0513
Excited state 10
λ : 270.34 nm
f: 0.1271

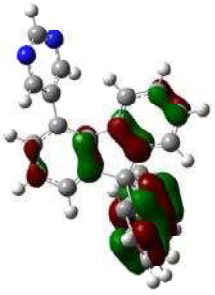

HOMO: -6.16 eV

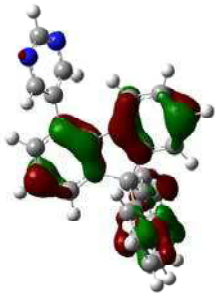

HOMO-1: -6.25 eV

S 5 Calculated frontier molecular orbitals by DFT and the 6th first calculated electronic transitions by TD-DFT of **4-5Pm-SBF**, after geometry optimization with DFT B3LYP/6-311G+(d,p), show with an isovalue of 0.04

2-Ph-SBF

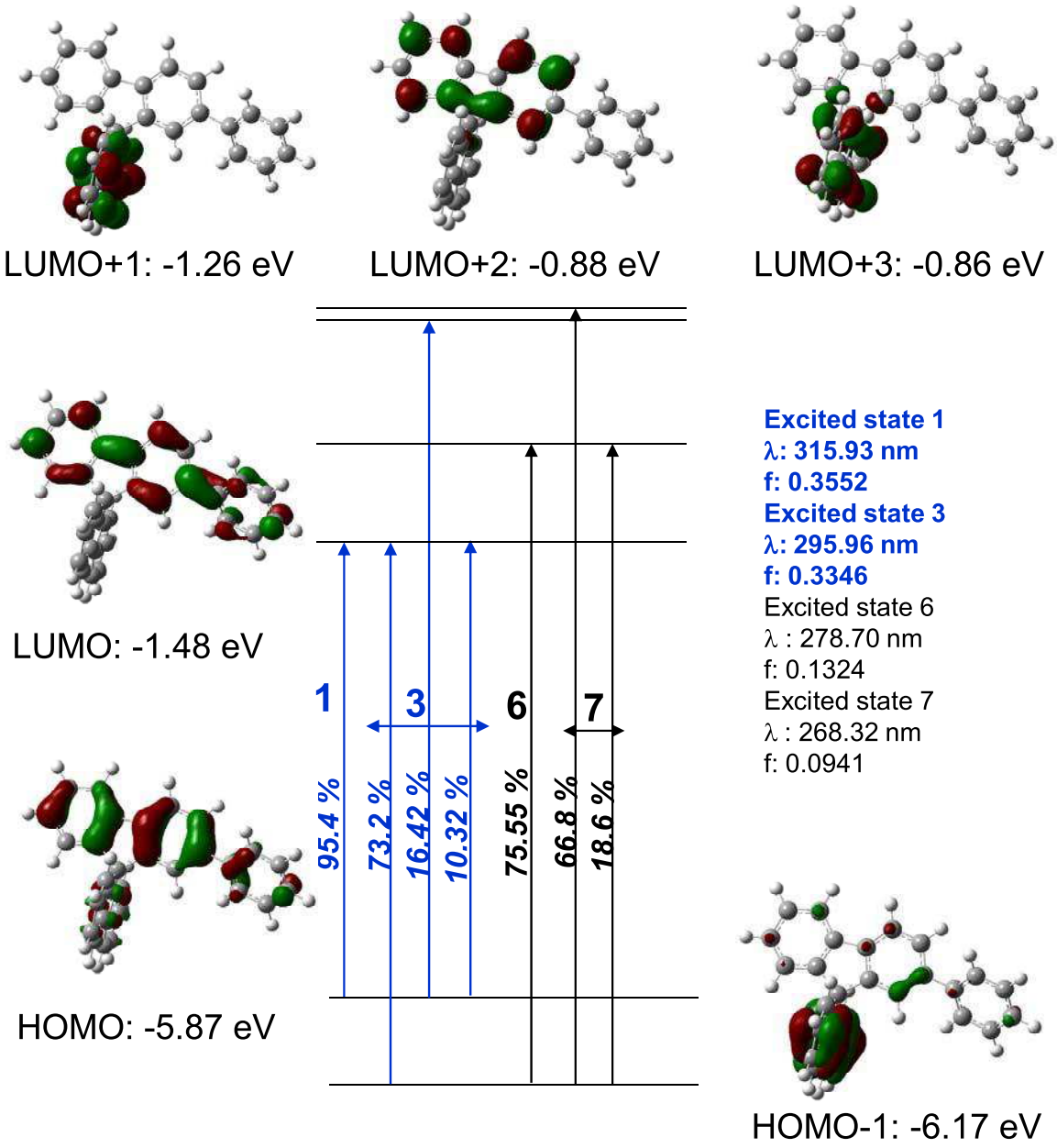

S 22 Calculated frontier molecular orbitals by DFT and the 6th first calculated electronic transitions by TD-DFT of **2-Ph-SBF**, after geometry optimization with DFT B3LYP/6-311G+(d,p), show with an isovalue of 0.04

2-5Pm-SBF

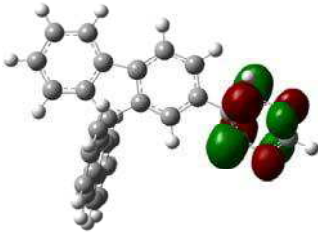

LUMO+1: -1.50 eV

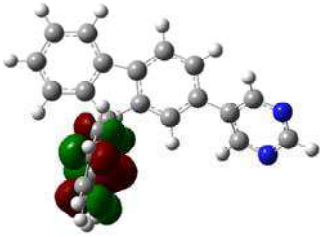

LUMO+2: -1.38 eV

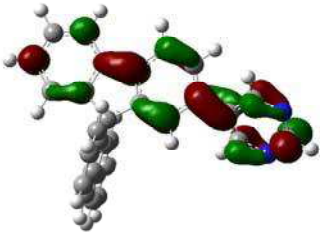

LUMO: -1.85 eV

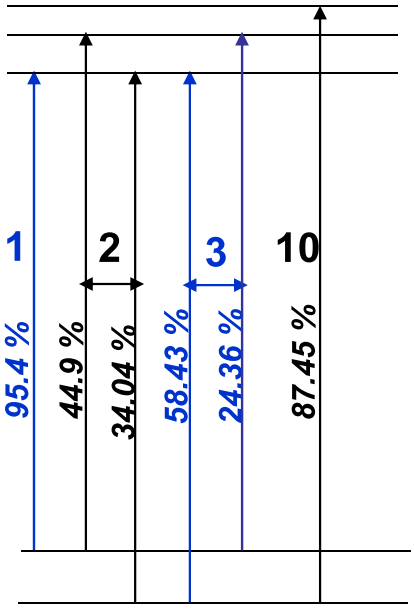

Excited state 1
λ: 327.18 nm
f: 0.1677
Excited state 2
λ: 304.91 nm
f: 0.1553
Excited state 3
λ : 304.41 nm
f: 0.239
Excited state 10
λ : 272.97 nm
f: 0.1497

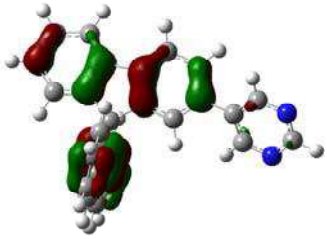

HOMO: -6.13 eV

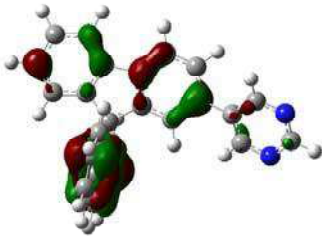

HOMO-1: -6.37 eV

S 23 Calculated frontier molecular orbitals by DFT and the 6th first calculated electronic transitions by TD-DFT of **2-5Pm-SBF**, after geometry optimization with DFT B3LYP/6-311G+(d,p), show with an isovalue of 0.04

THERMAL PROPERTIES

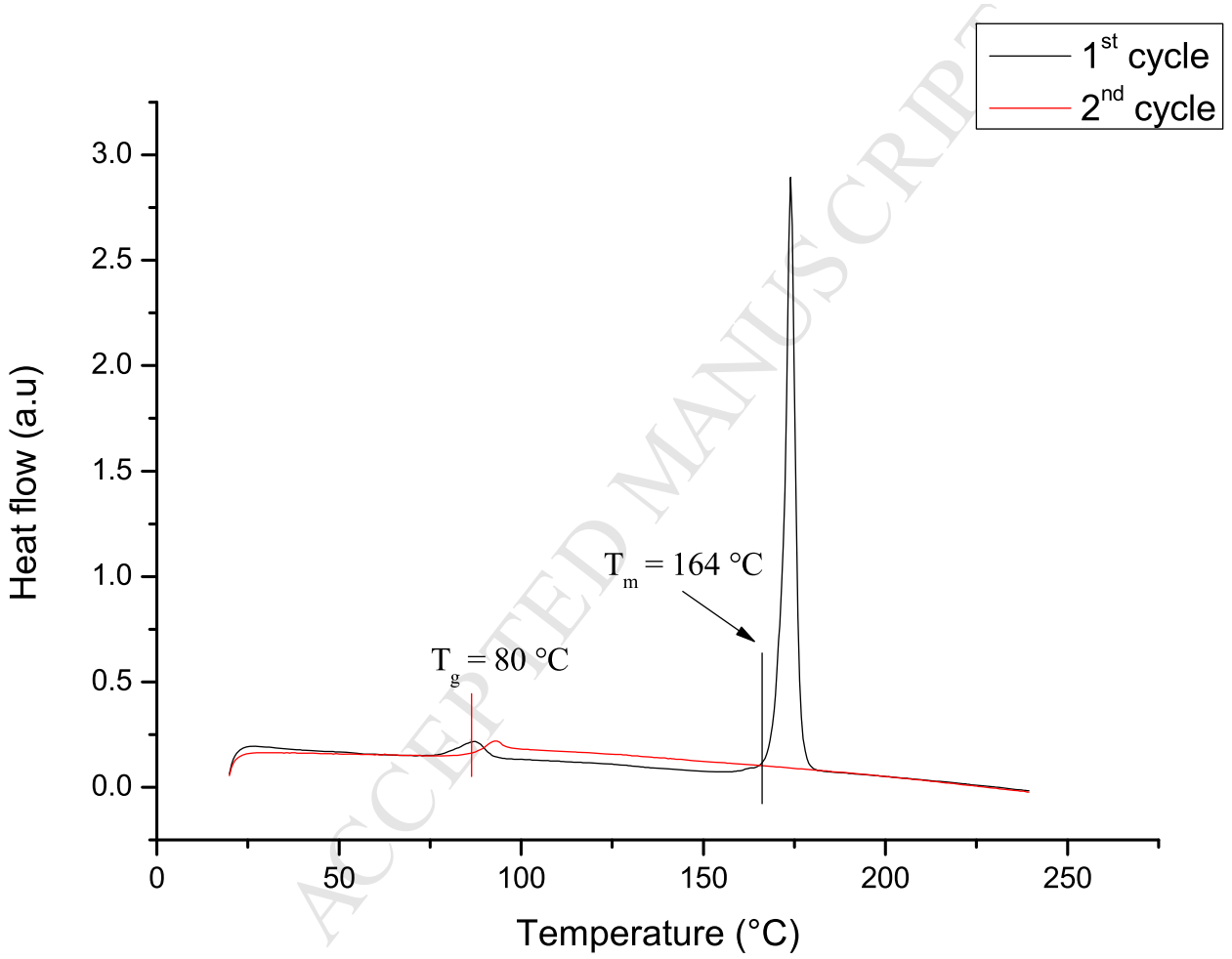

S 24 DSC curves of **4-5Pm-SBF**

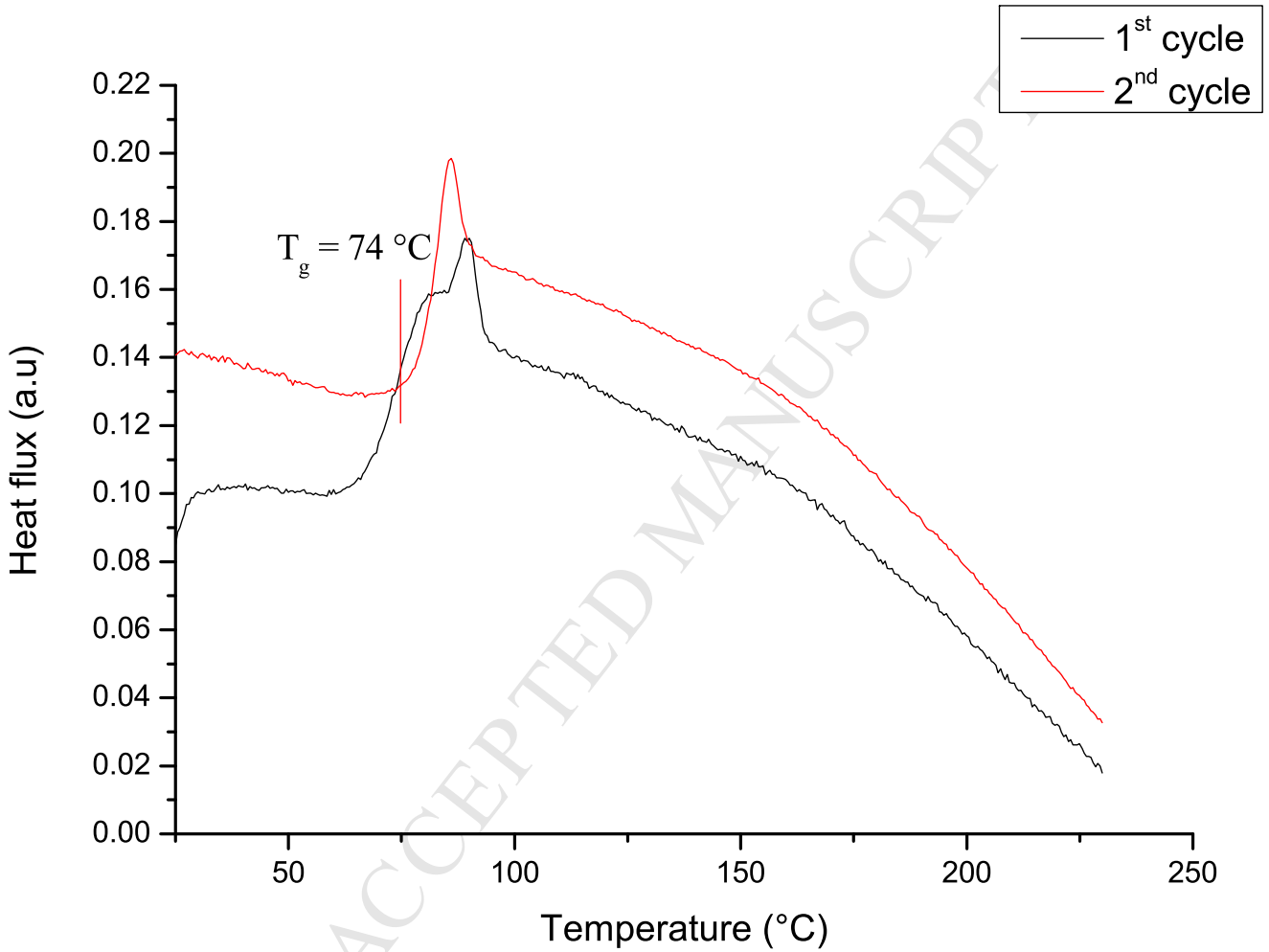

S 25 DSC curves of **2-Ph-SBF**

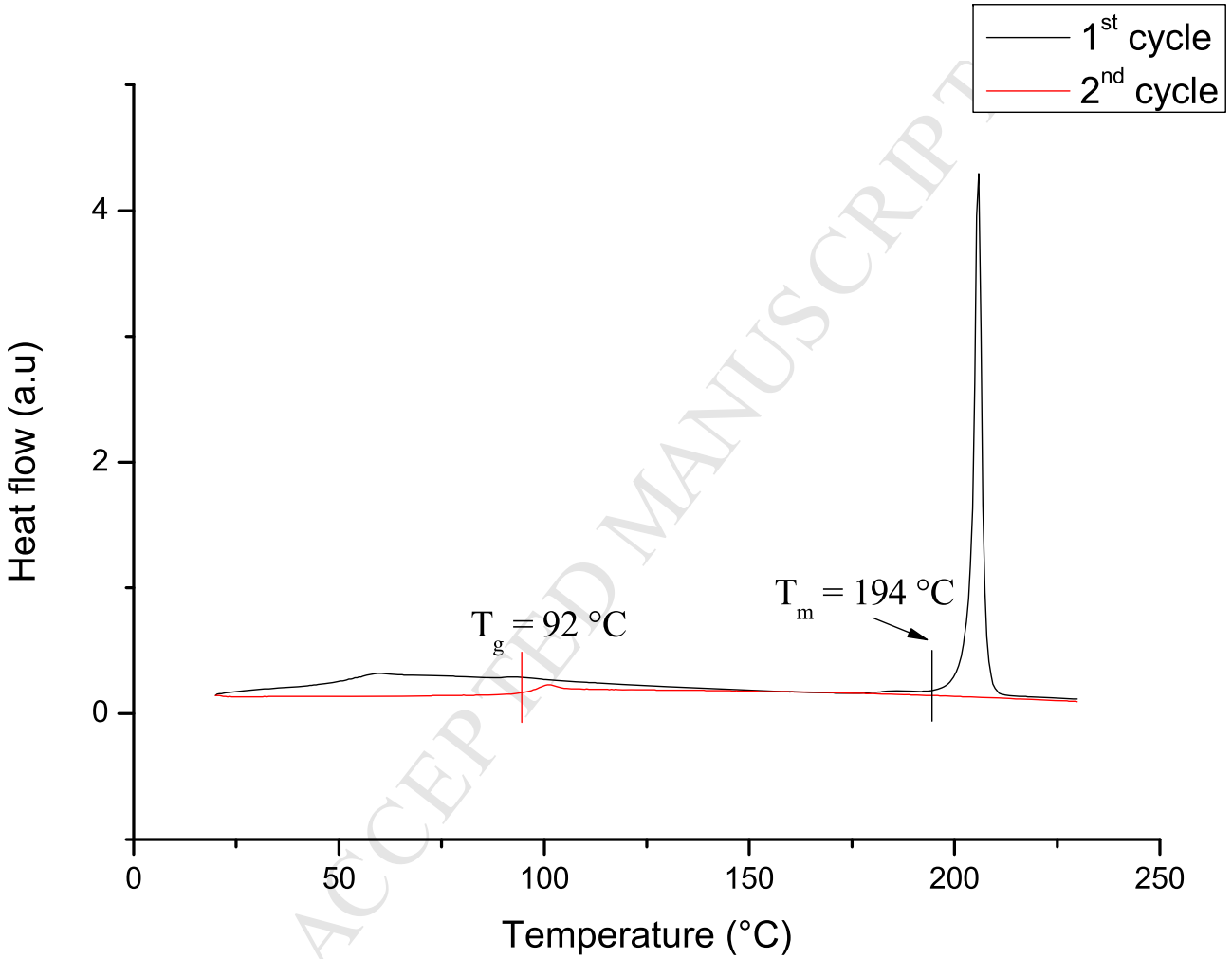

S 26 DSC curves of **2-5Pm-SBF**

ELECTROCHEMICAL PROPERTIES

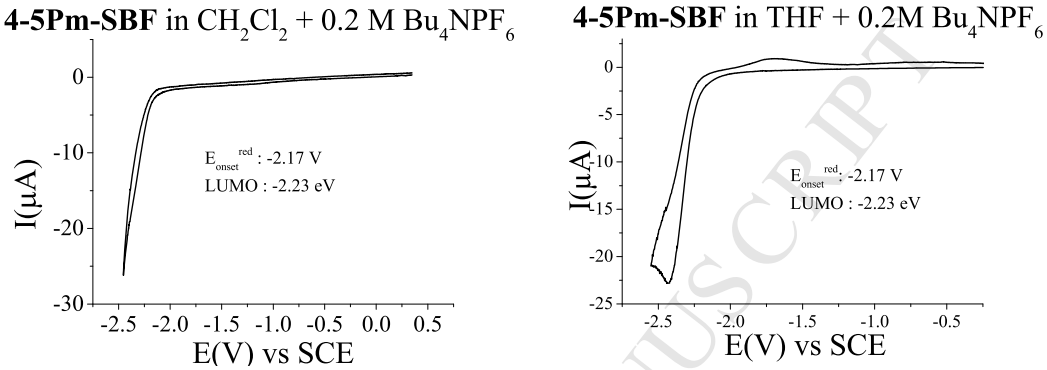

S 6 Cyclic voltammetry of **4-5Pm-SBF** 5 10^{-3} M in CH_2Cl_2 (**left**) or THF (**right**) + Bu_4NPF_6 0.2 M, sweep-rate 100 $mV.s^{-1}$, platinum disk (Ø: 1mm) working electrode.

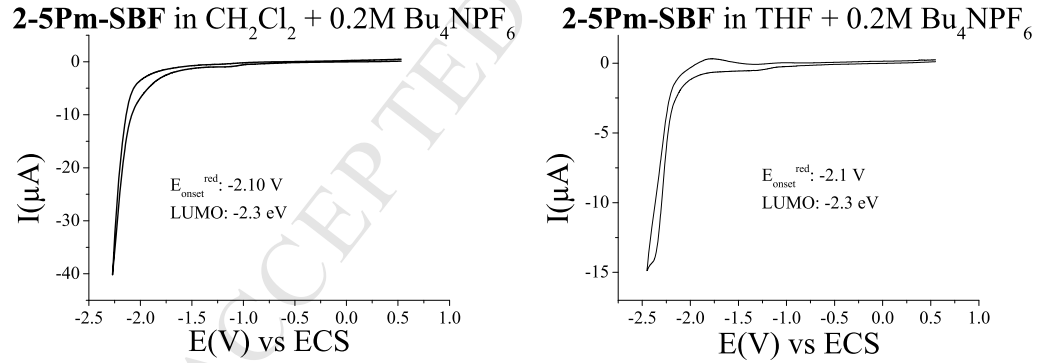

S 7 Cyclic voltammetry of **2-5Pm-SBF** 2 10^{-3} M in CH_2Cl_2 (**left**) or THF (**right**) + Bu_4NPF_6 0.2 M, sweep-rate 100 $mV.s^{-1}$, platinum disk (Ø: 1mm) working electrode.

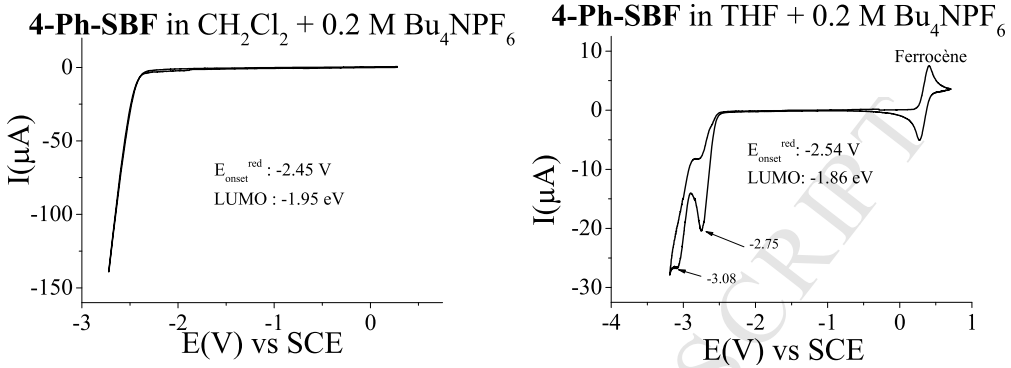

S 8 Cyclic voltammetry of **4-Ph-SBF** 5 10^{-3} M in CH_2Cl_2 (**left**) or THF (**right**) + Bu_4NPF_6 0.2 M, sweep-rate 100 mV.s^{-1}, platinum disk (Ø: 1mm) working electrode.

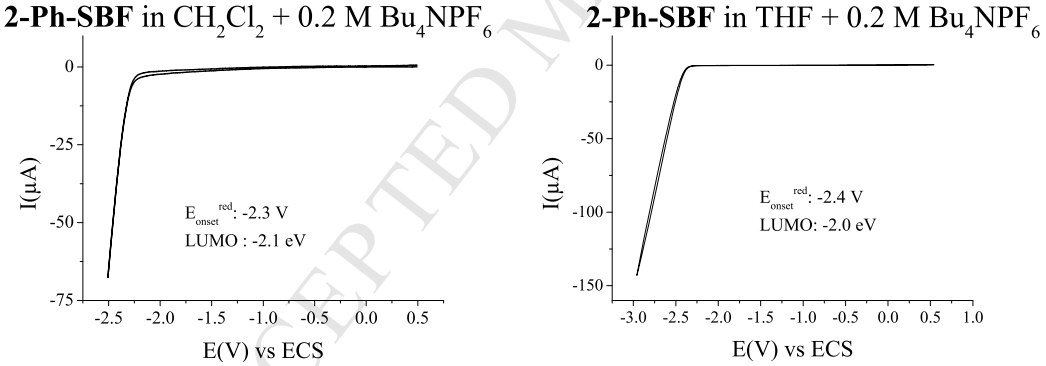

S 30 Cyclic voltammetry of **2-Ph-SBF** 5 10^{-3} M in CH_2Cl_2 (**left**) or THF (**right**) + Bu_4NPF_6 0.2 M, sweep-rate 100 mV.s^{-1}, platinum disk (Ø: 1mm) working electrode.

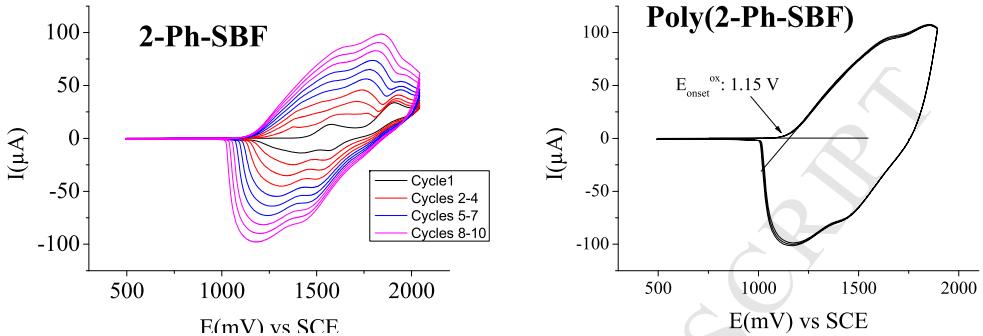

S 31 Left: Cyclic voltammetry of **2-Ph-SBF** 5 10^{-3} M in CH_2Cl_2 + Bu_4NPF_6 0.2 M, 10 repeated cycles between 495 and 2045 mV, sweep-rate 100 mV.s^{-1}, platinum disk (Ø: 1mm) working electrode. **Right**: Cyclic voltammetry in CH_2Cl_2 + Bu_4NPF_6 0.2 M, 3 repeated cycles between 580 and 1895 mV, sweep-rate 100 mV.s^{-1}, platinum disk (Ø: 1mm) covered previously in left with **poly(2-Ph-SBF)** working electrode.

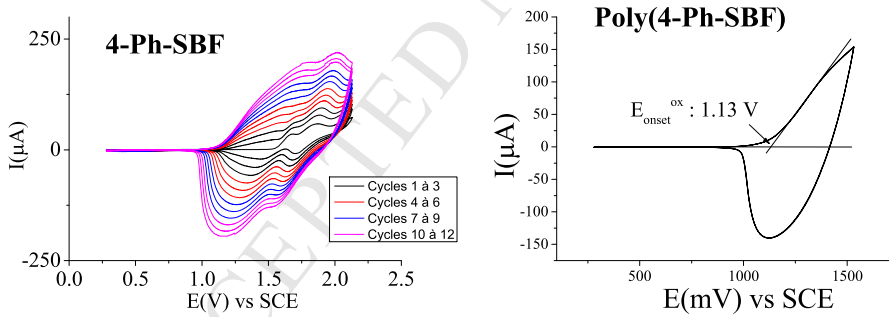

S 32 Left: Cyclic voltammetry of **4-Ph-SBF** 5 10^{-3} M in CH_2Cl_2 + Bu_4NPF_6 0.2 M, 12 repeated cycles between 0.28 and 2.13 V, sweep-rate 100 mV.s^{-1}, platinum disk (Ø: 1mm) working electrode. **Right**: Cyclic voltammetry in CH_2Cl_2 + Bu_4NPF_6 0.2 M, 3 repeated cycles between 280 and 1530 mV, sweep-rate 100 mV.s^{-1}, platinum disk (Ø: 1mm) covered previously in left with **poly(4-Ph-SBF)** working electrode.

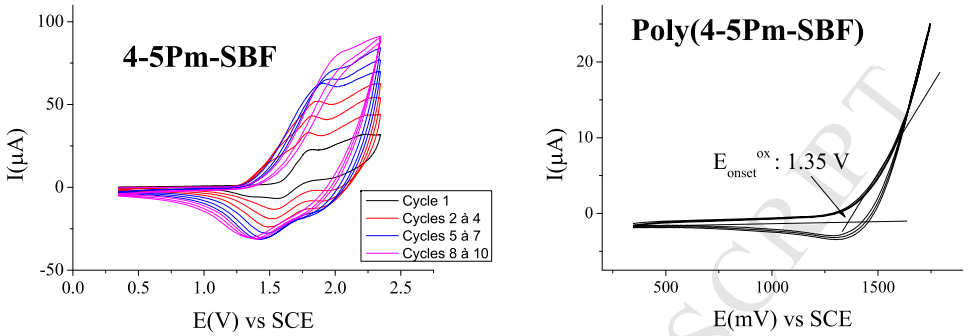

S 33 Left: Cyclic voltammetry of **4-5Pm-SBF** 5 10^{-3} M in CH_2Cl_2 + Bu_4NPF_6 0.2 M, 10 repeated cycles between 0.35 and 2.35 V, sweep-rate 100 $mV.s^{-1}$, platinum disk (Ø: 1mm) working electrode. **Right**: Cyclic voltammetry in CH_2Cl_2 + Bu_4NPF_6 0.2 M, 3 repeated cycles between 350and 1750 mV, sweep-rate 100 $mV.s^{-1}$, platinum disk (Ø: 1mm) covered previously in left with **poly(4-5Pm-SBF)** working electrode.

2D NMR STUDIES

4-5Pm-SBF-COSY-CD_2Cl_2

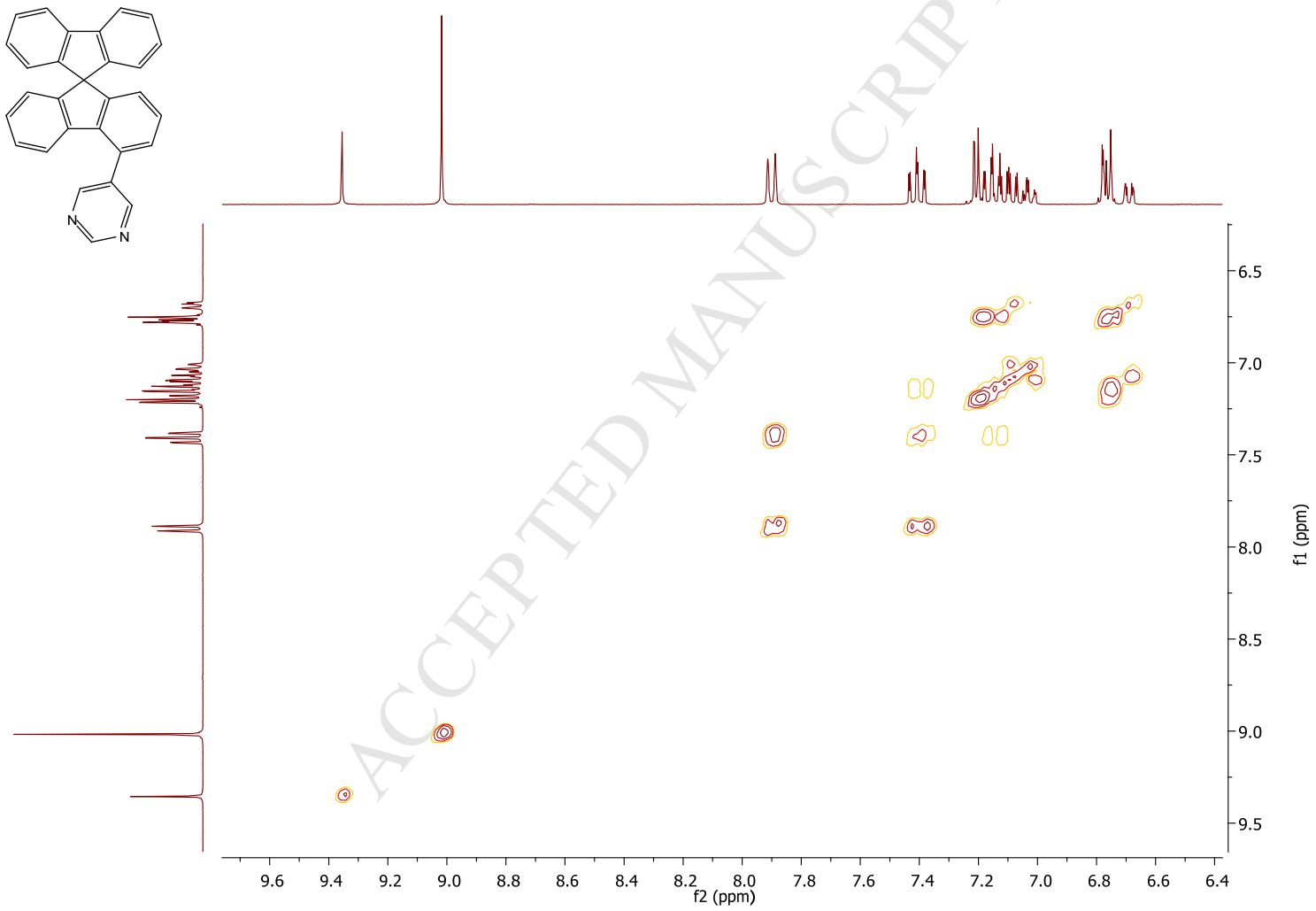

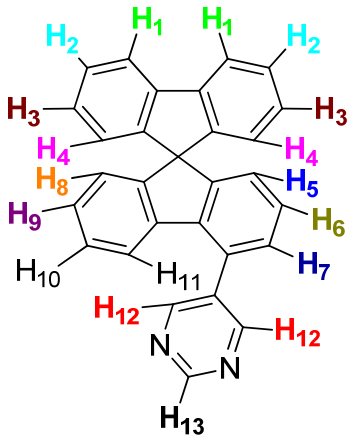

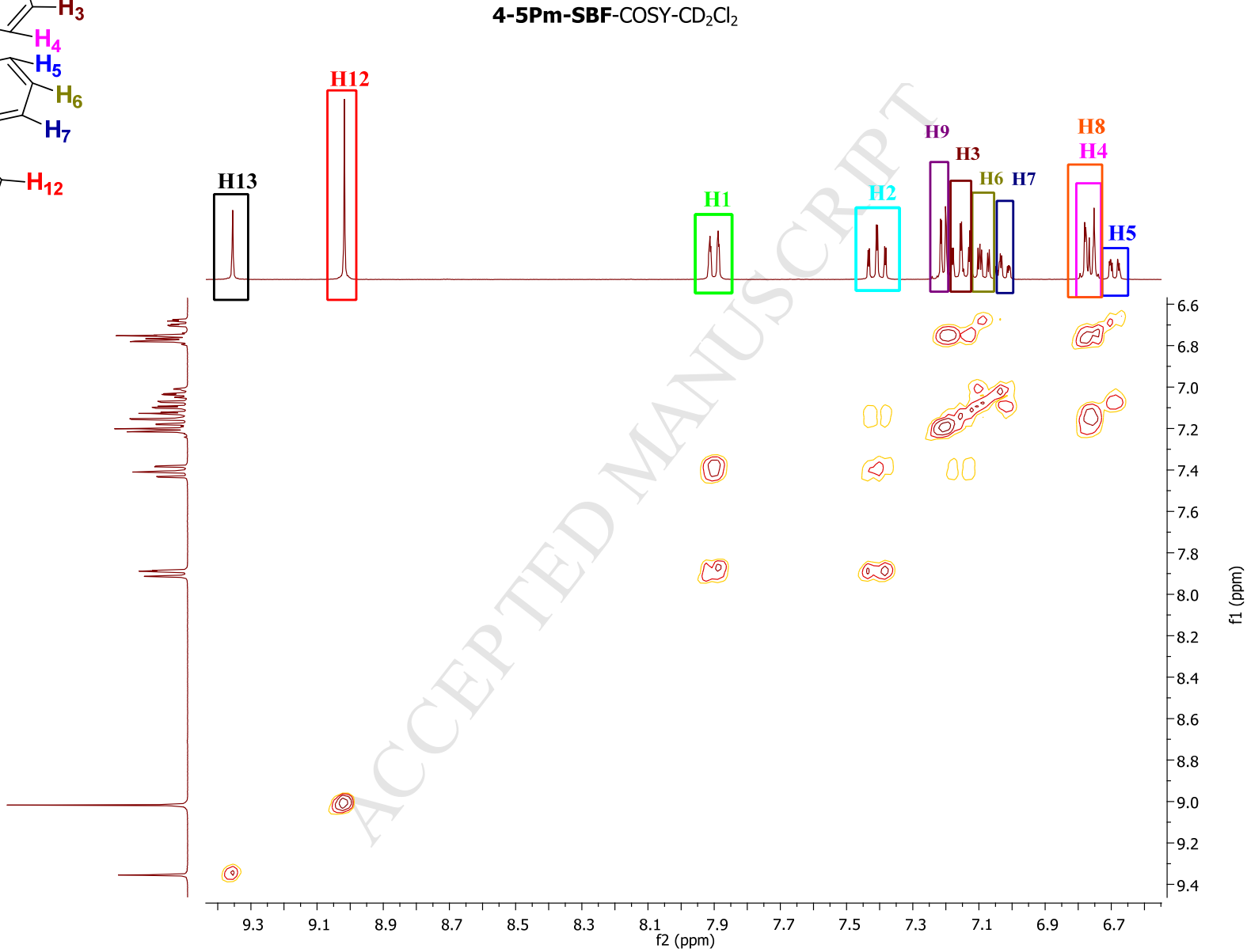

4-5Pm-SBF-HSQC-CD_2Cl_2

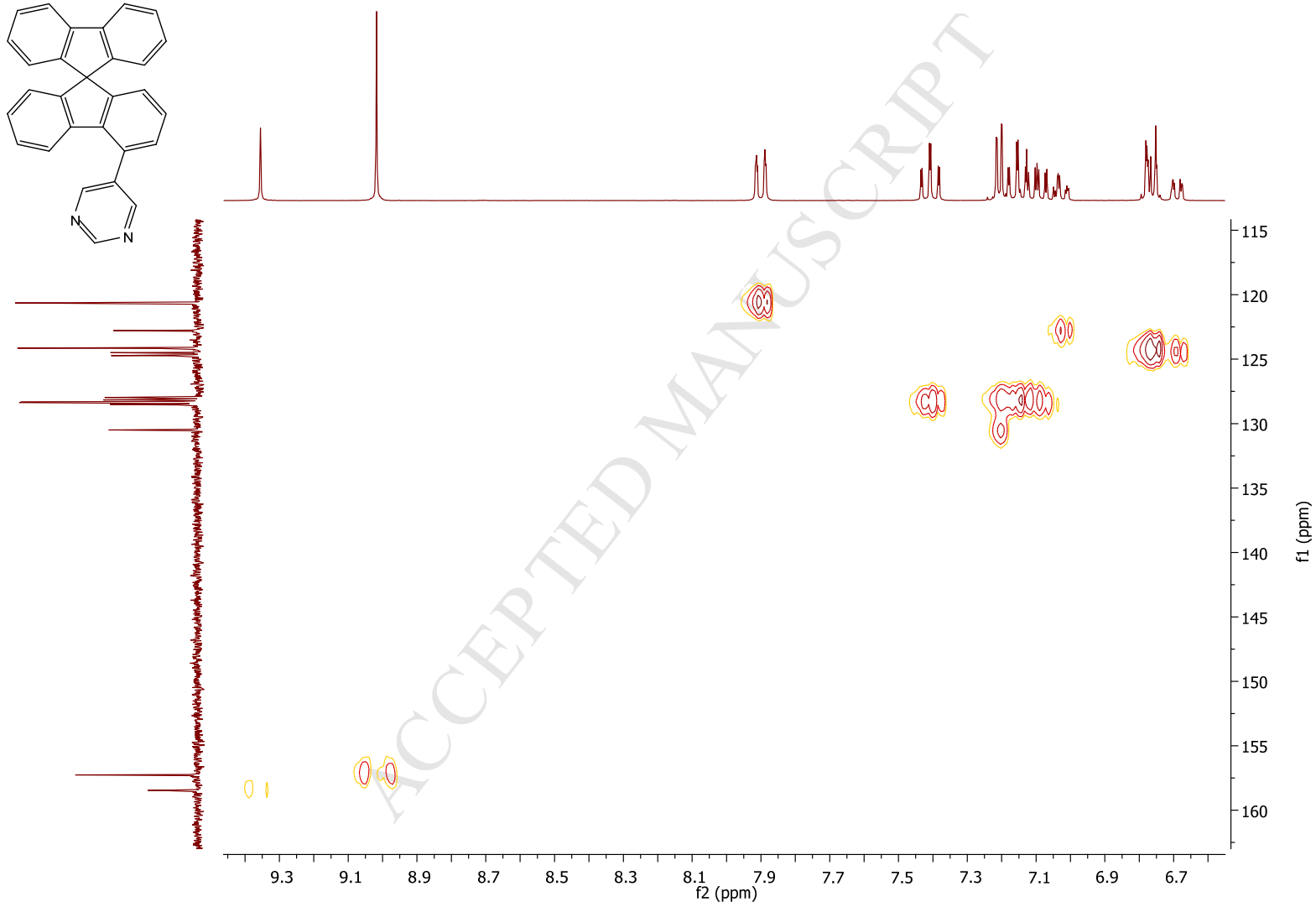

4-5Pm-SBF-HSQC (Zoom)-CD_2Cl_2

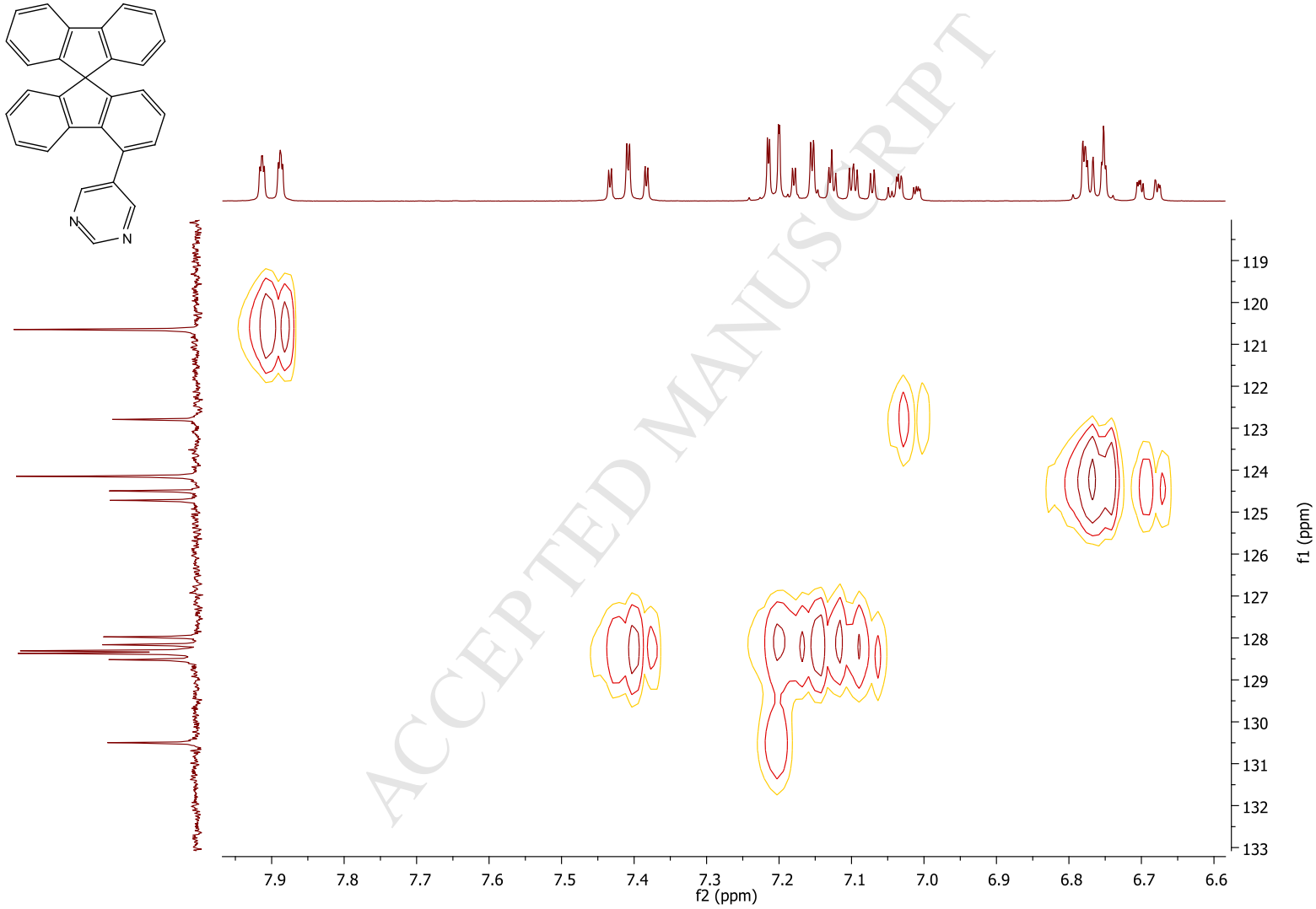

4-5Pm-SBF-HMBC-CD_2Cl_2

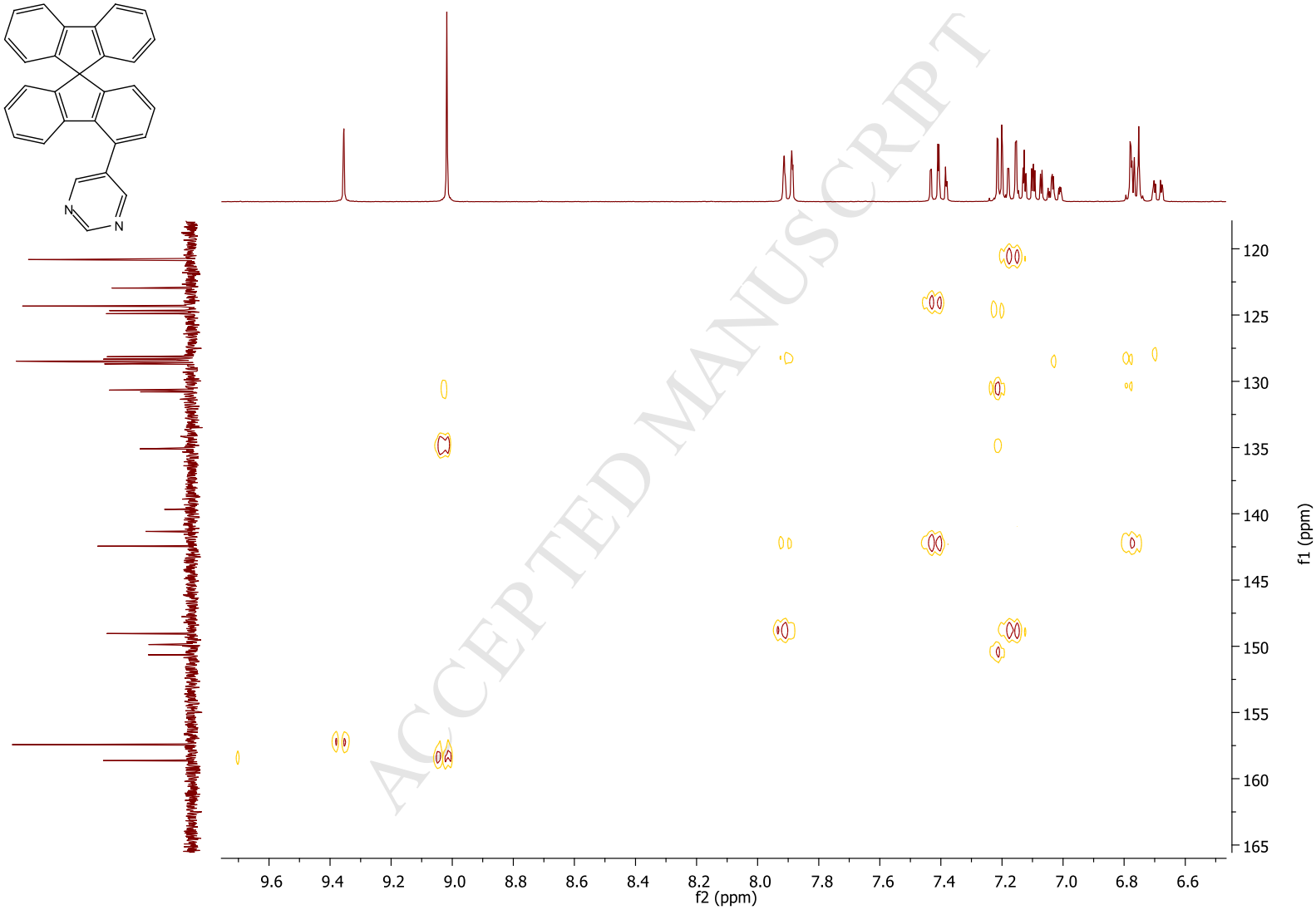

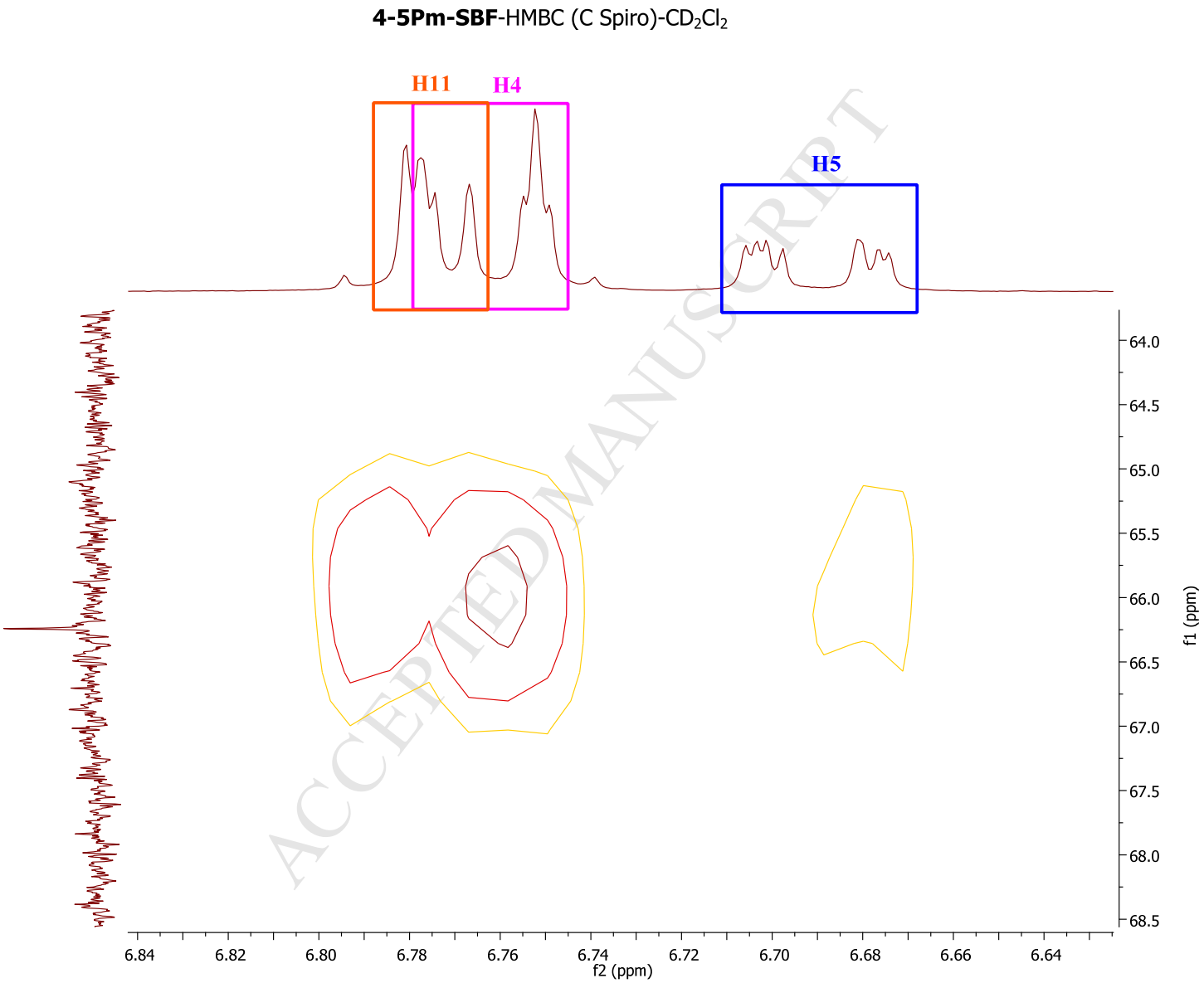

2-Ph-SBF-COSY-CD_2Cl_2

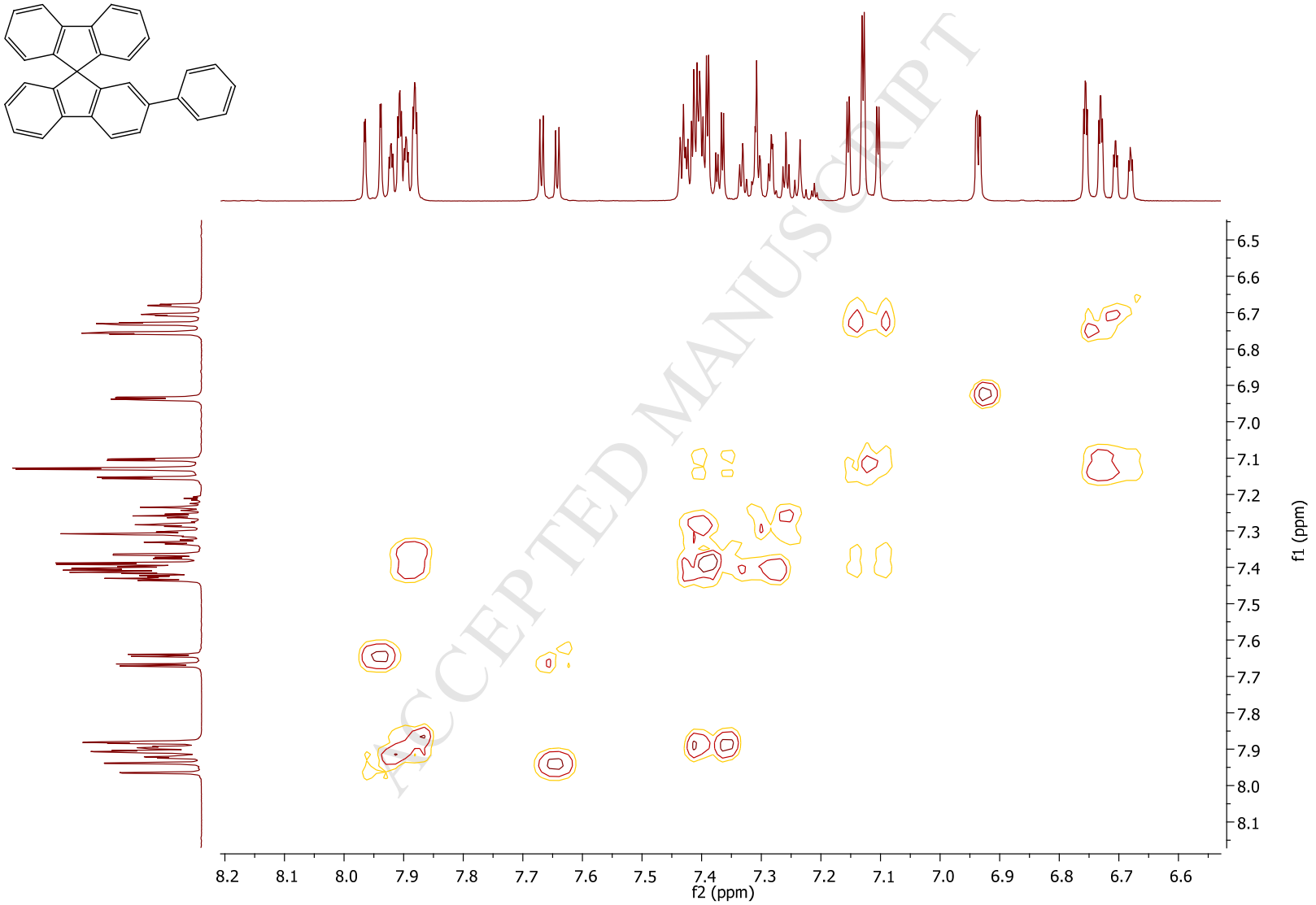

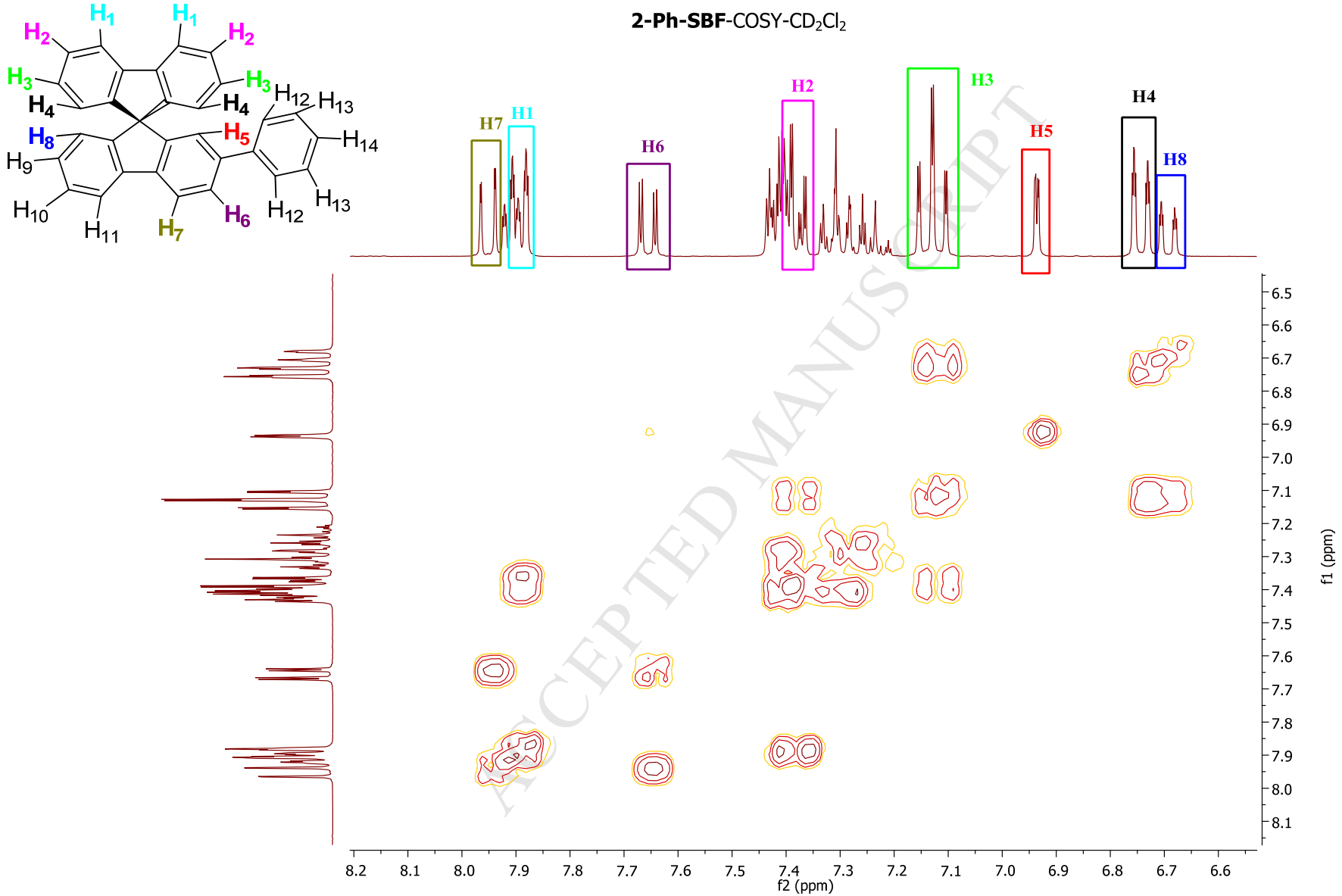

2-Ph-SBF-HSQC-CD_2Cl_2

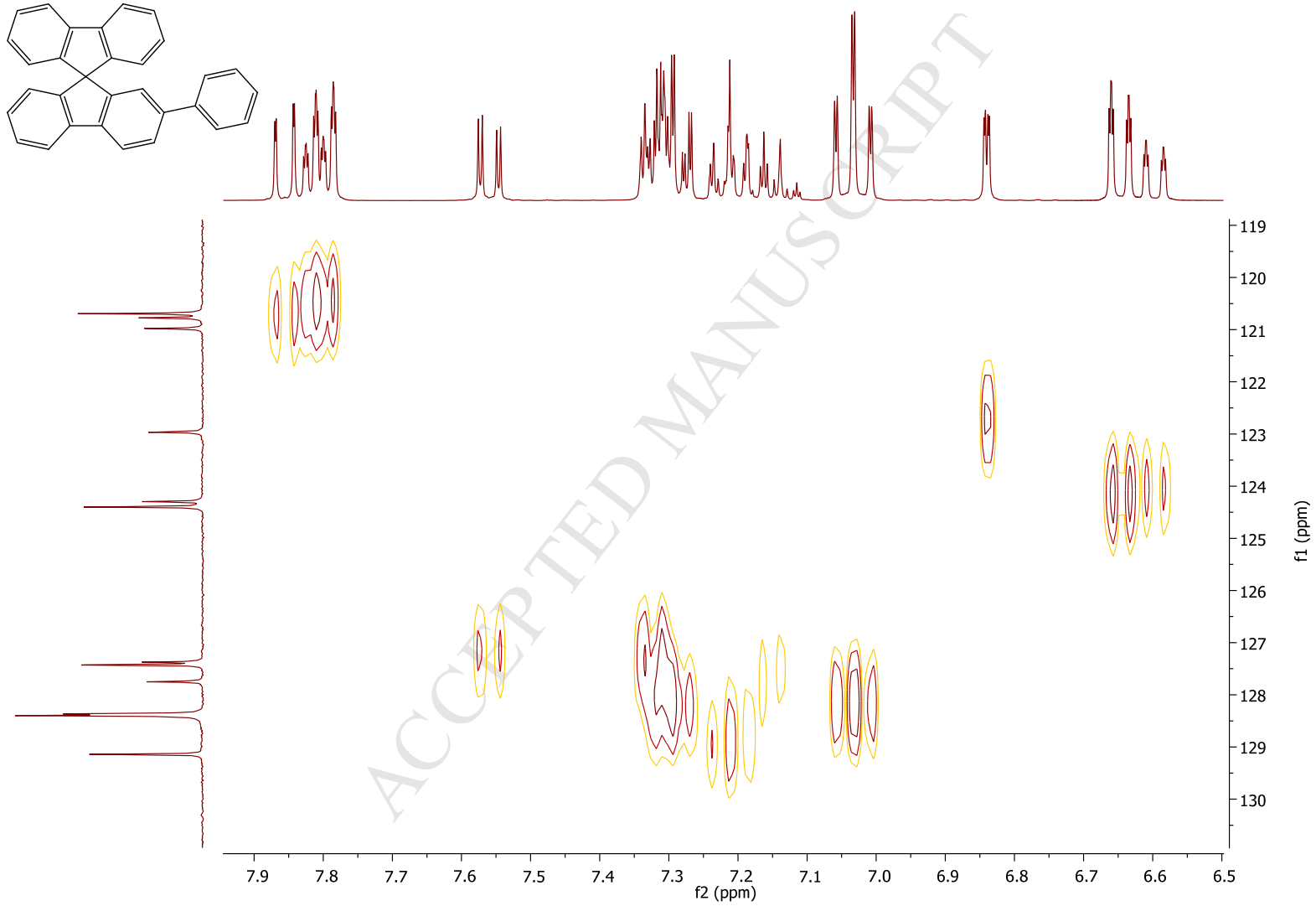

2-Ph-SBF-HSQC (Zoom)-CD_2Cl_2

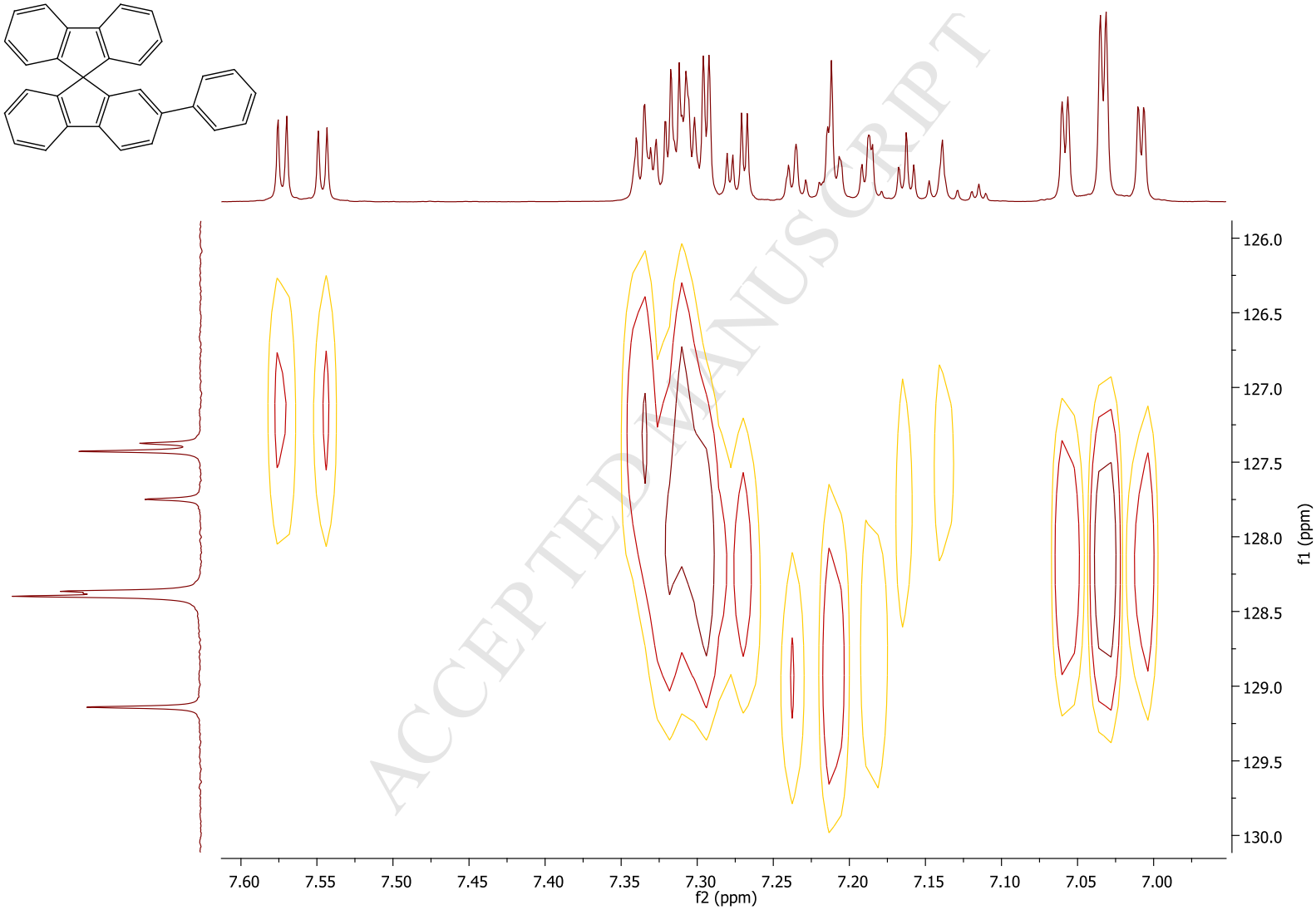

2-Ph-SBF-HMQC-CD_2Cl_2

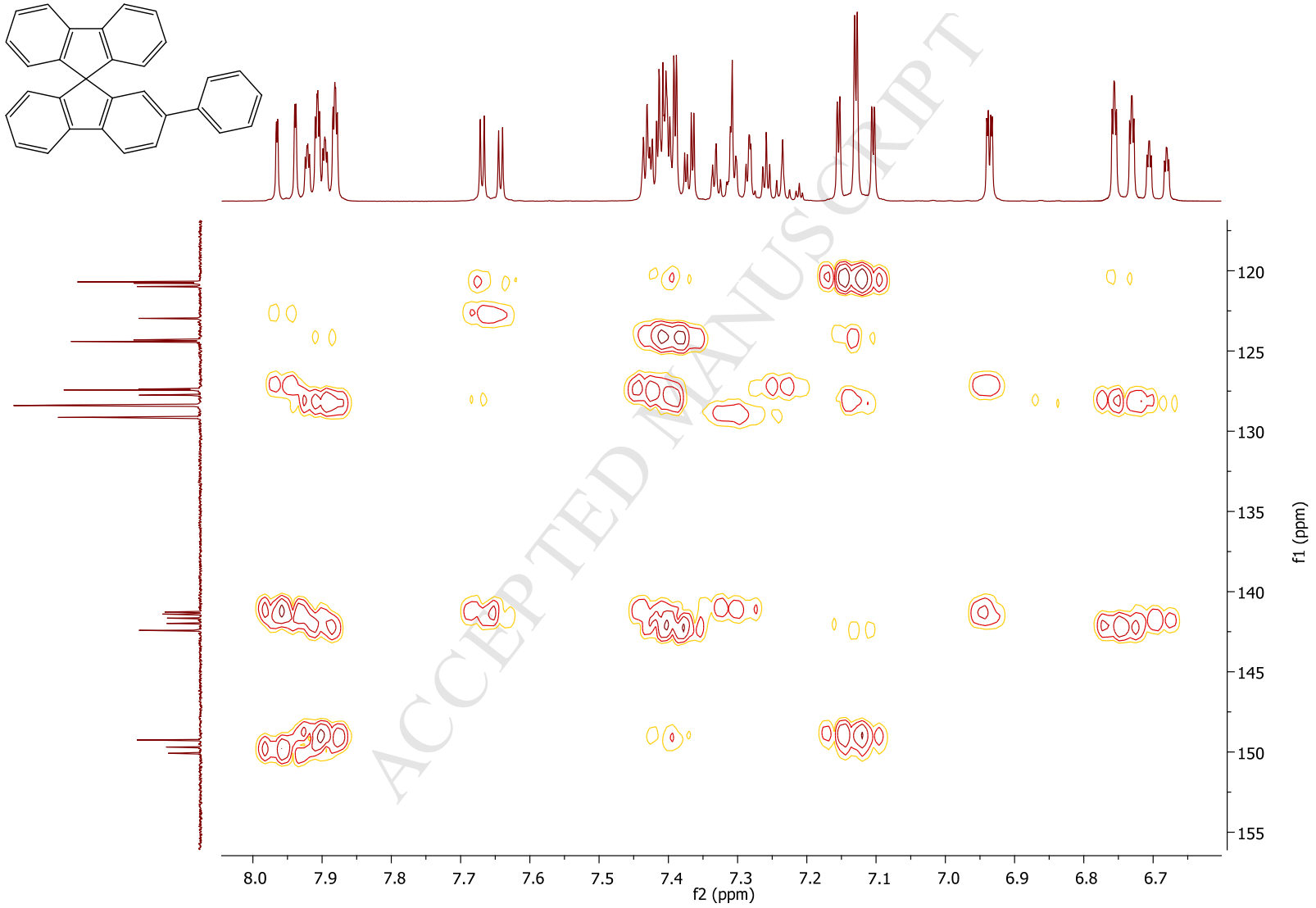

2-Ph-SBF-HMBC (C Spiro)-CD_2Cl_2

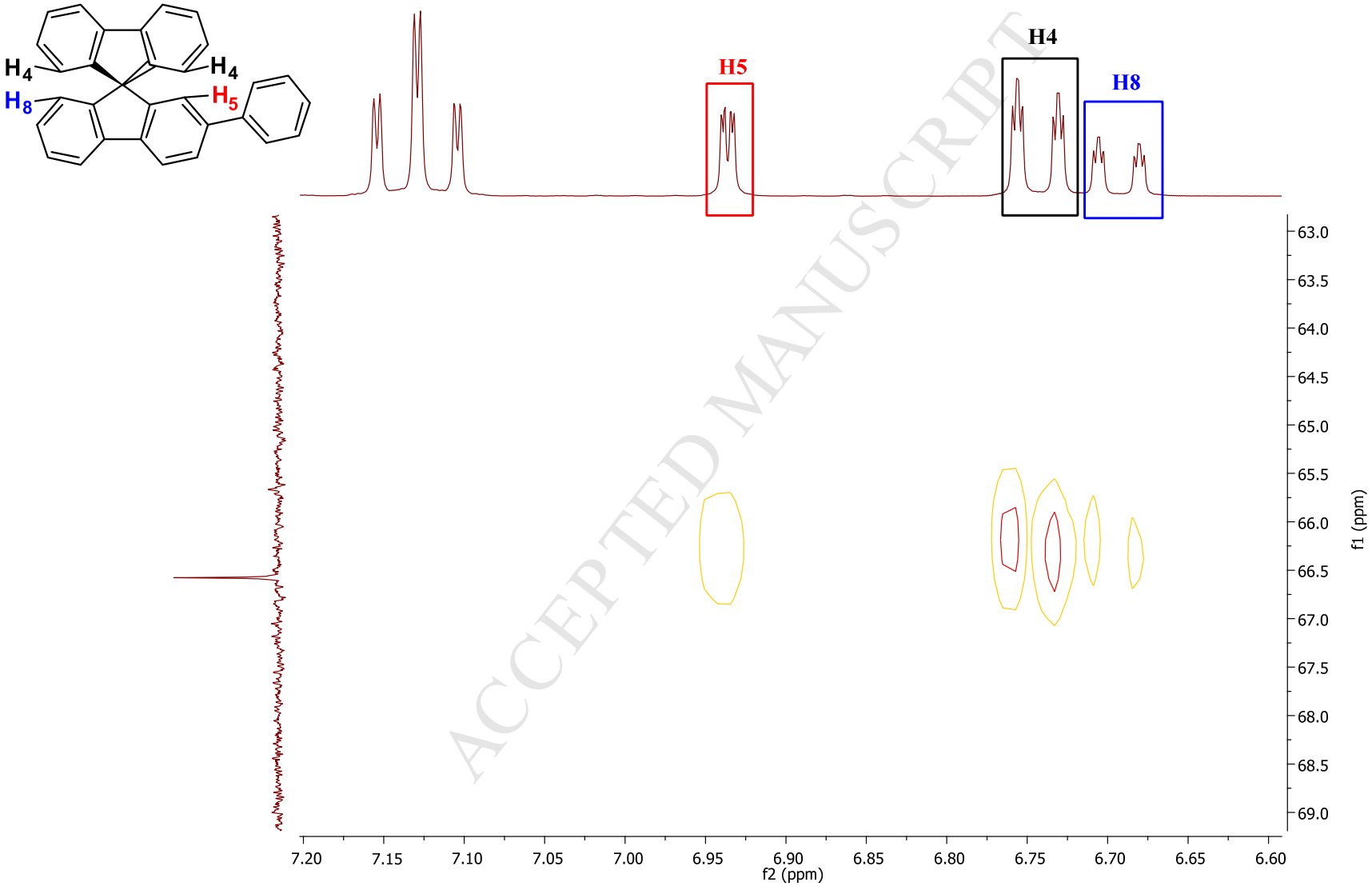

2-5Pm-SBF-COSY-CD_2Cl_2

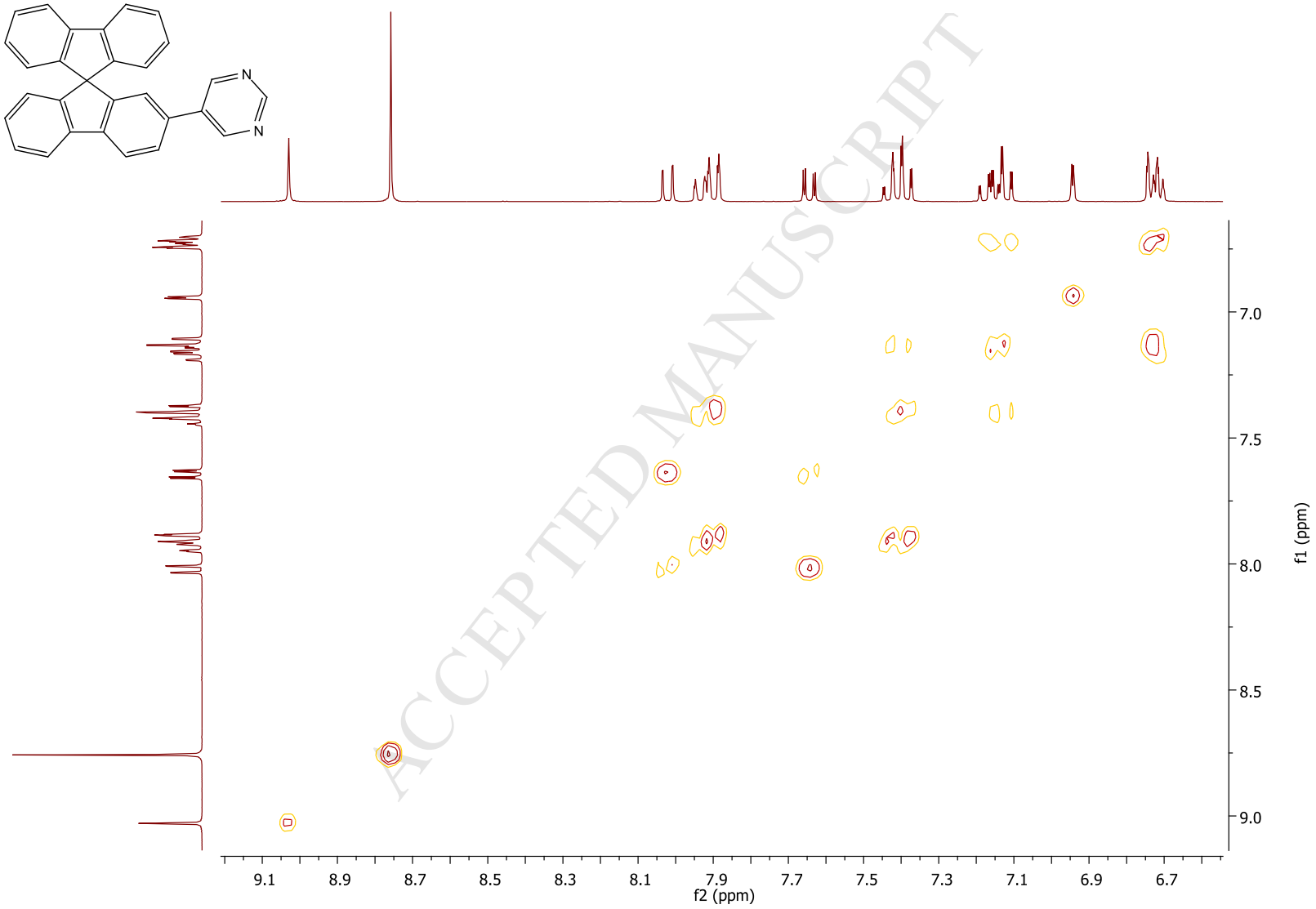

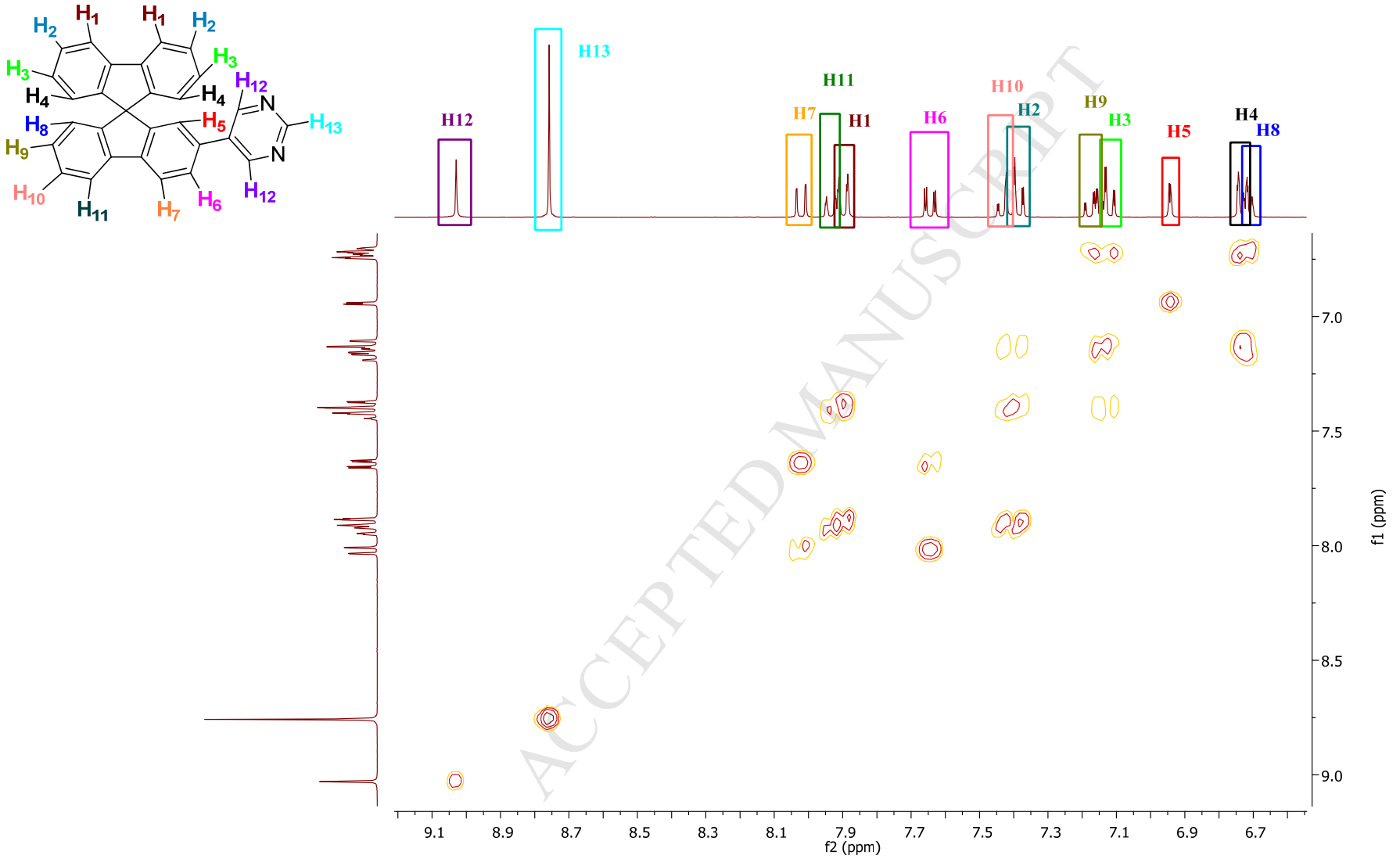

2-5Pm-SBF-HSQC-CD_2Cl_2

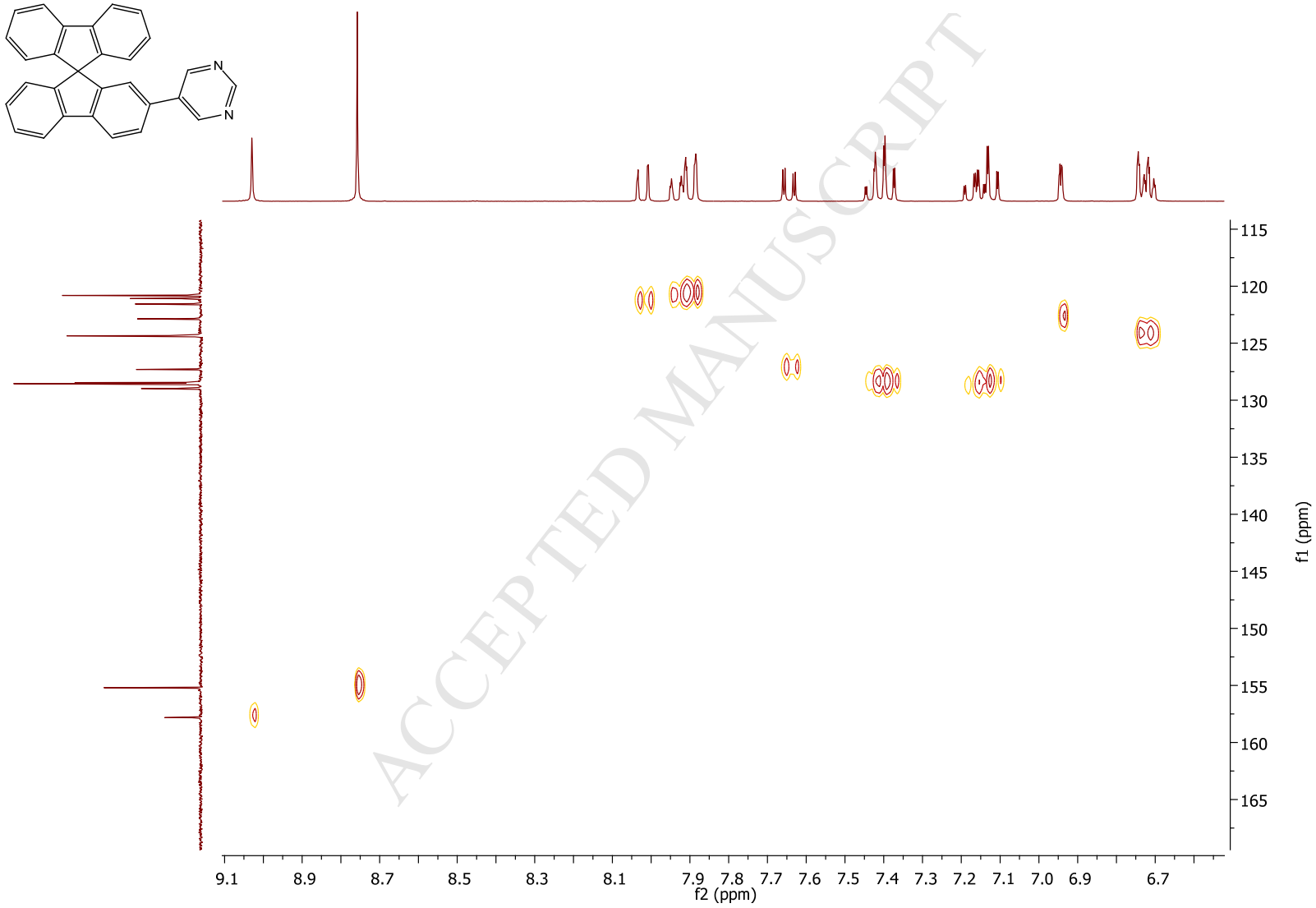

2-5Pm-SBF-HSQC (Zoom)-CD_2Cl_2

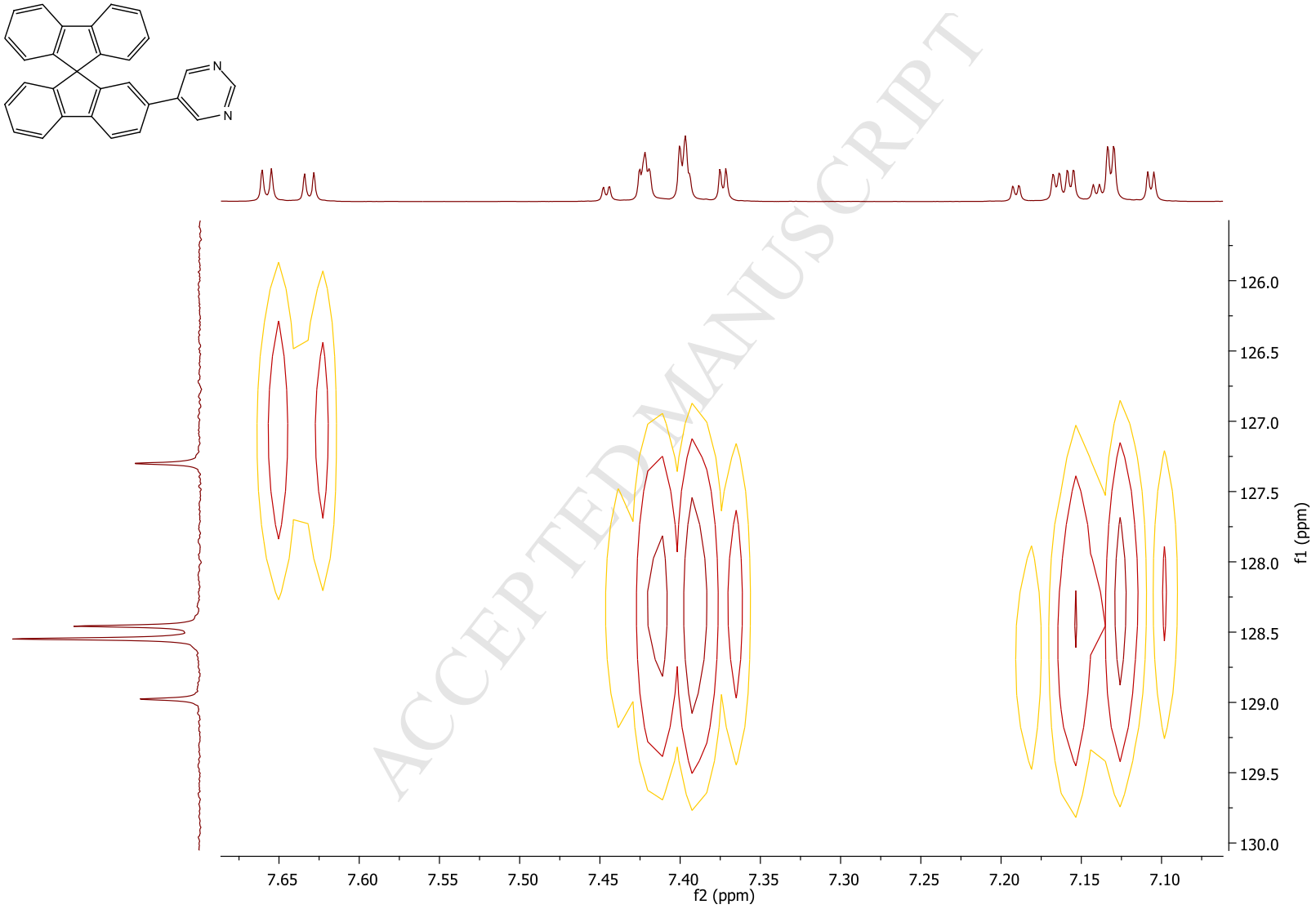

2-5Pm-SBF-HMBC-CD_2Cl_2

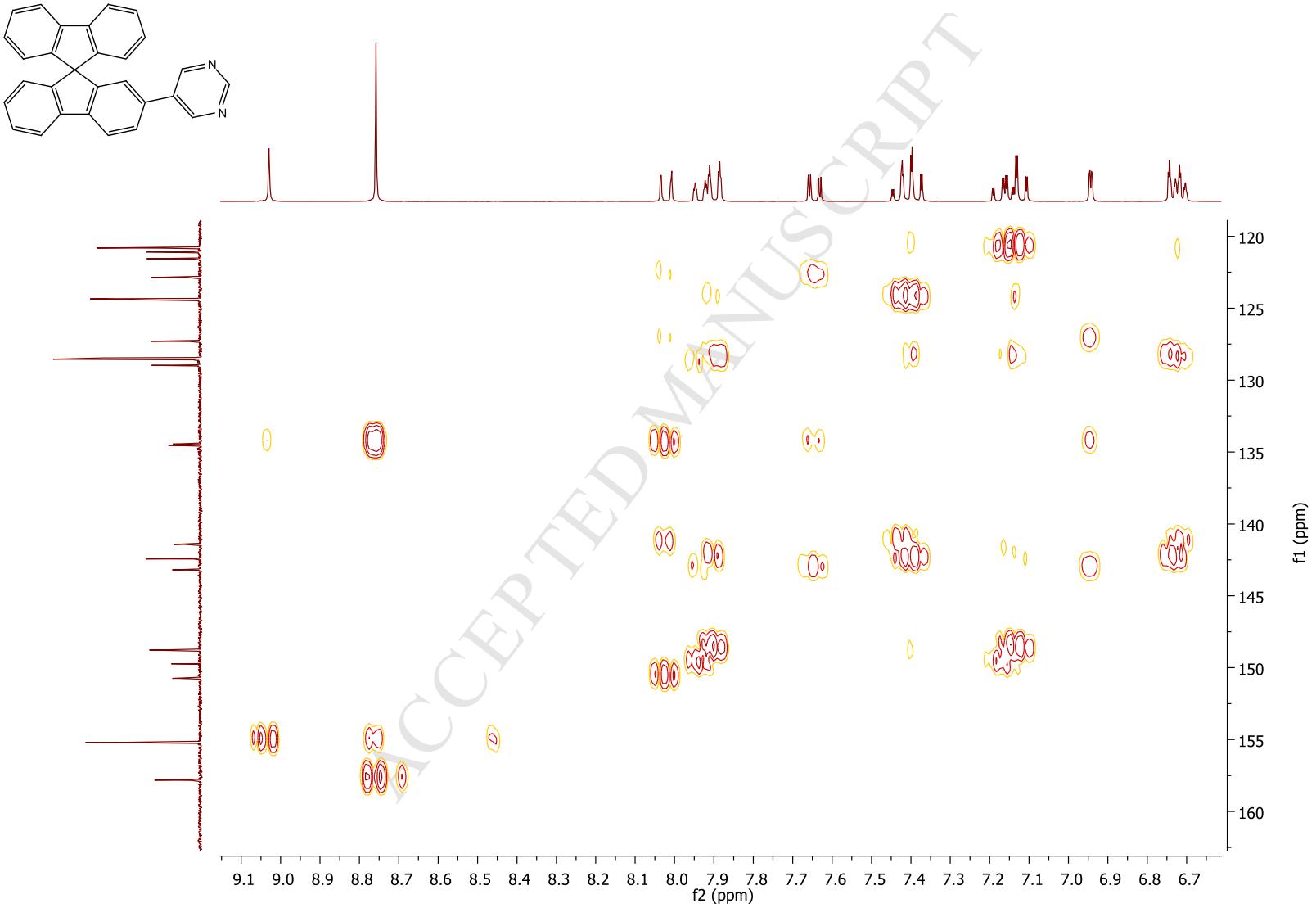

2-5Pm-SBF-HMBC (C Spiro)-CD_2Cl_2

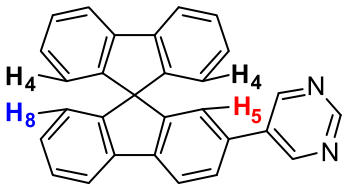

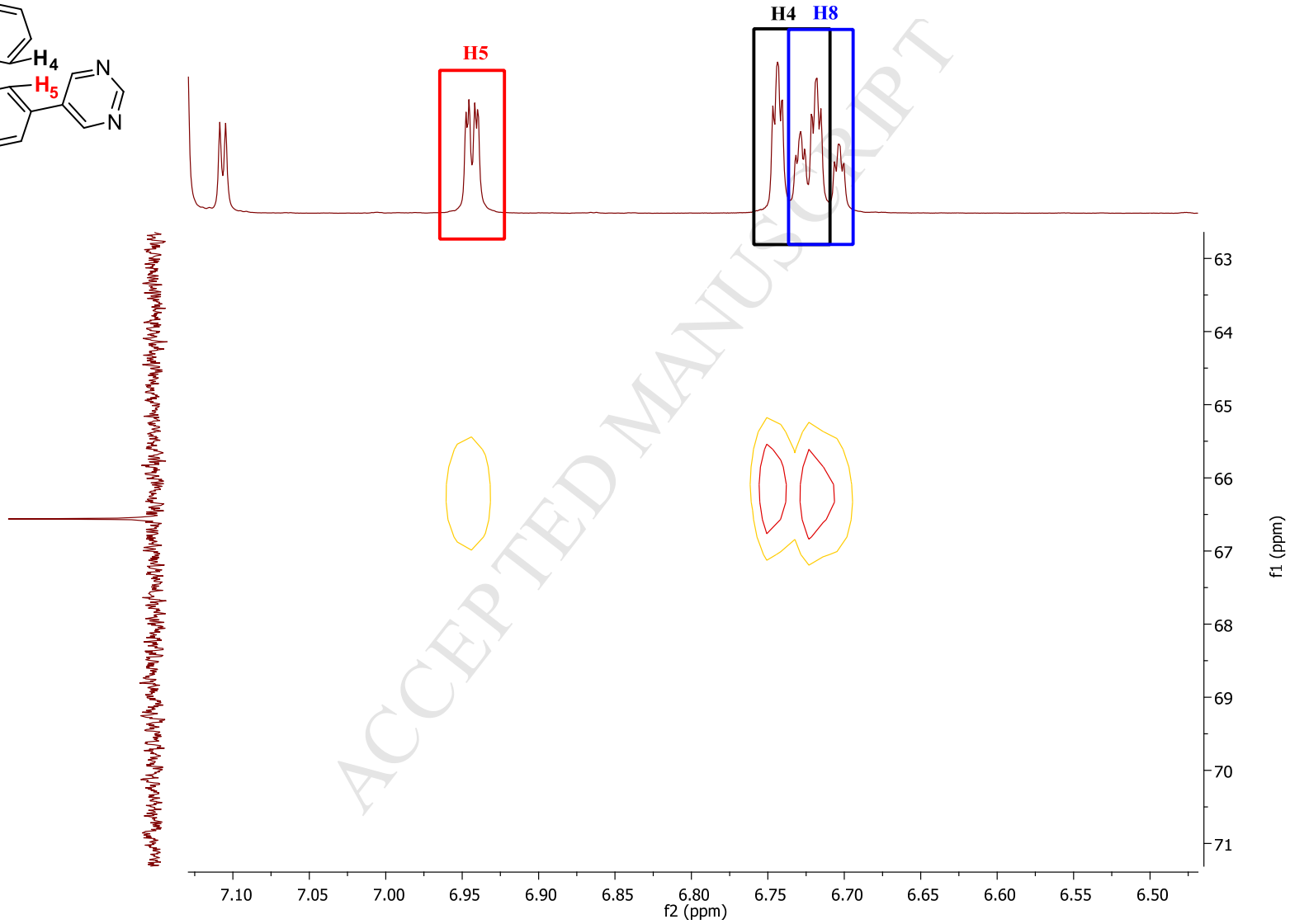

COPY OF NMR SPECTRA

2-^{1}H-CD_2Cl_2

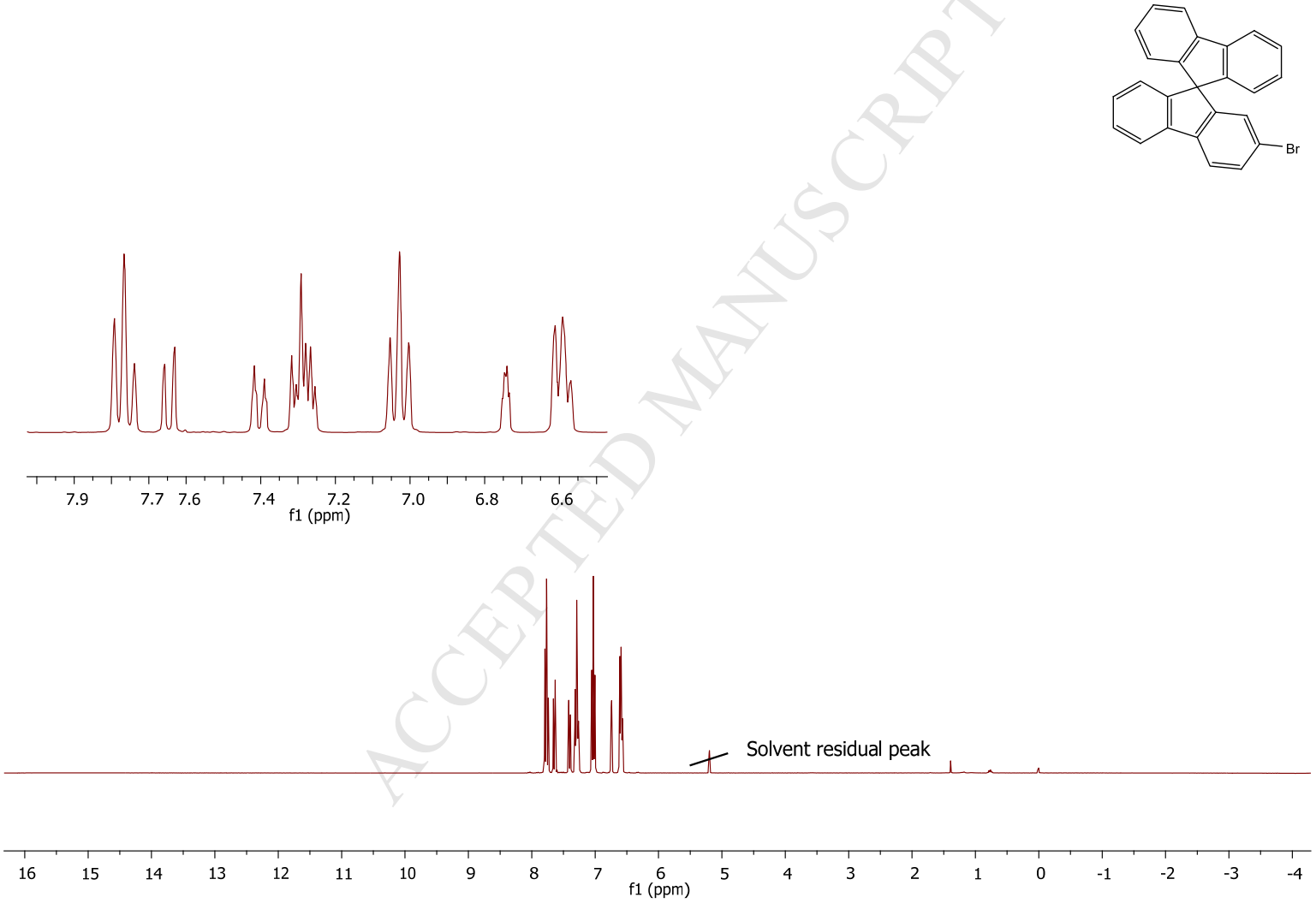

2-^{13}C-CD_2Cl_2

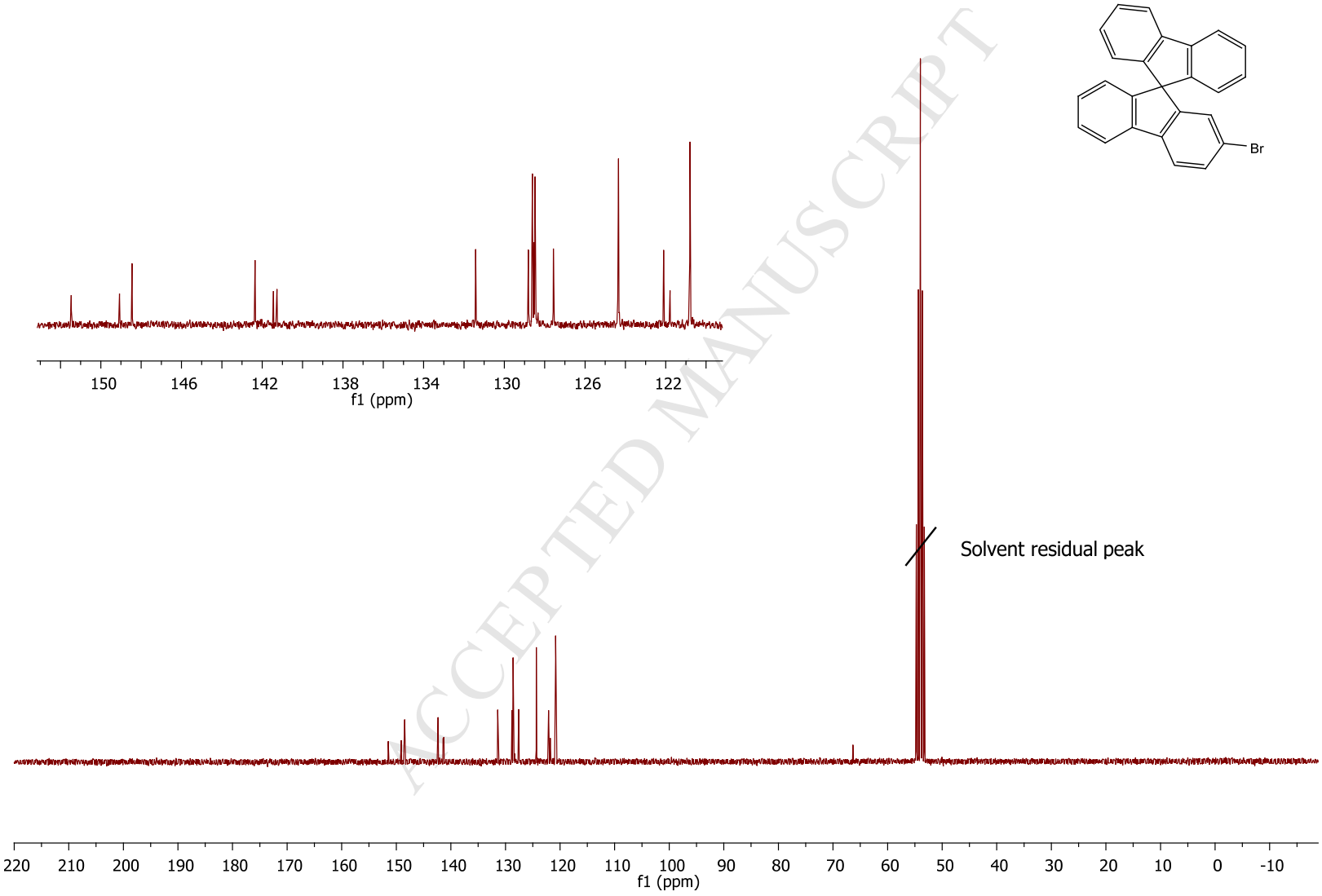

2-DEPT-CD_2Cl_2

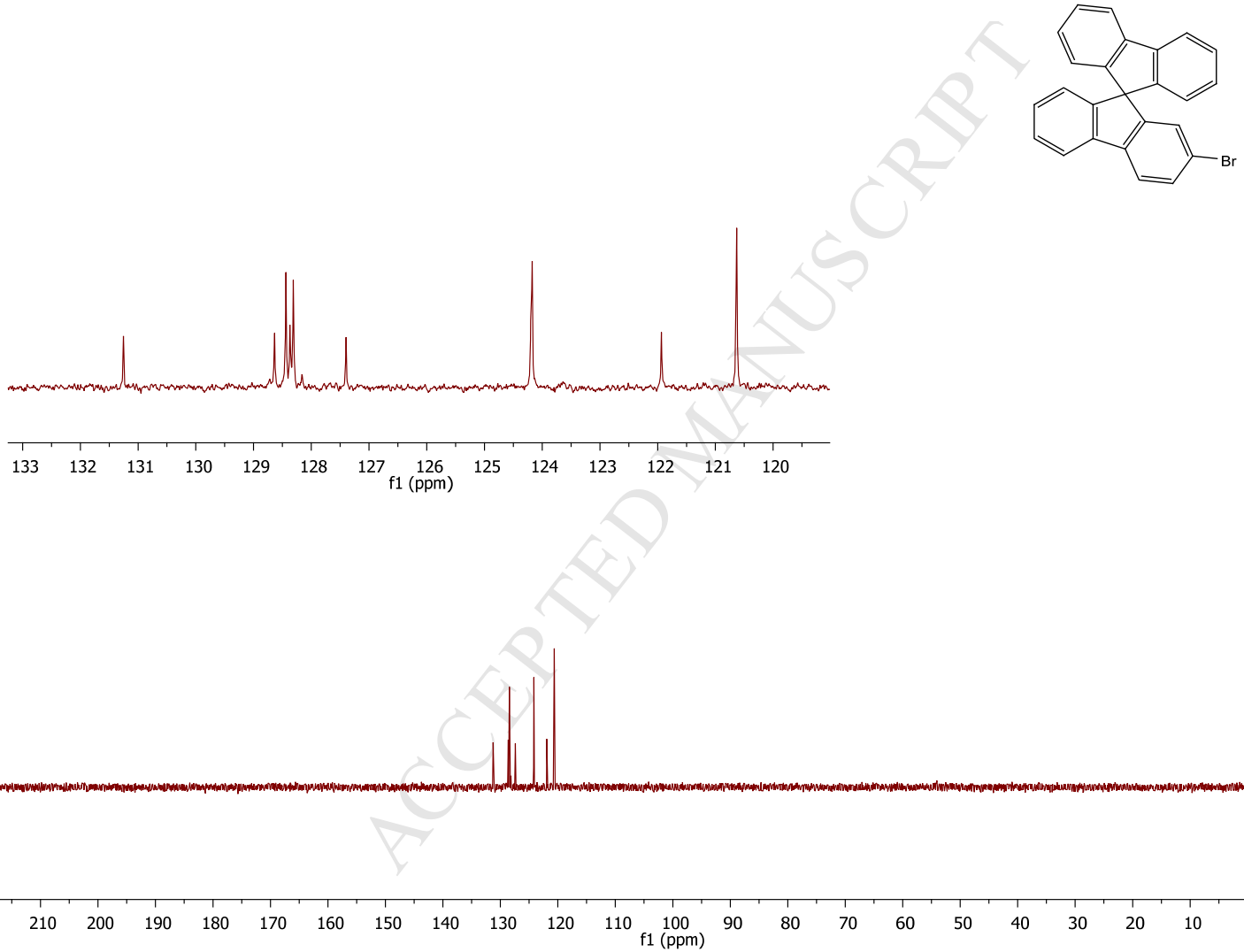

4-5Pm-SBF-^{1}H-CD_2Cl_2

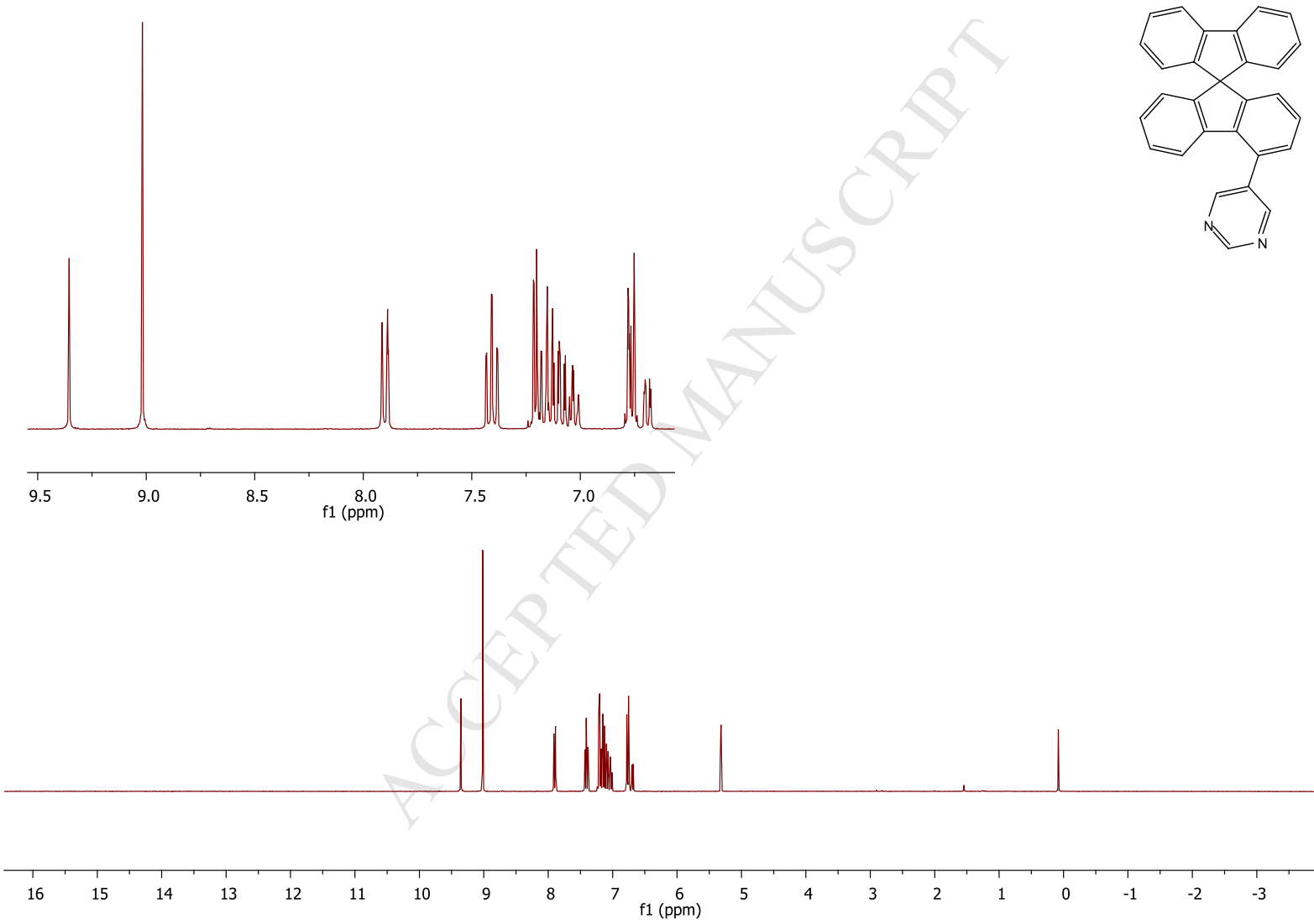

4-5Pm-SBF-^{13}C-CD_2Cl_2

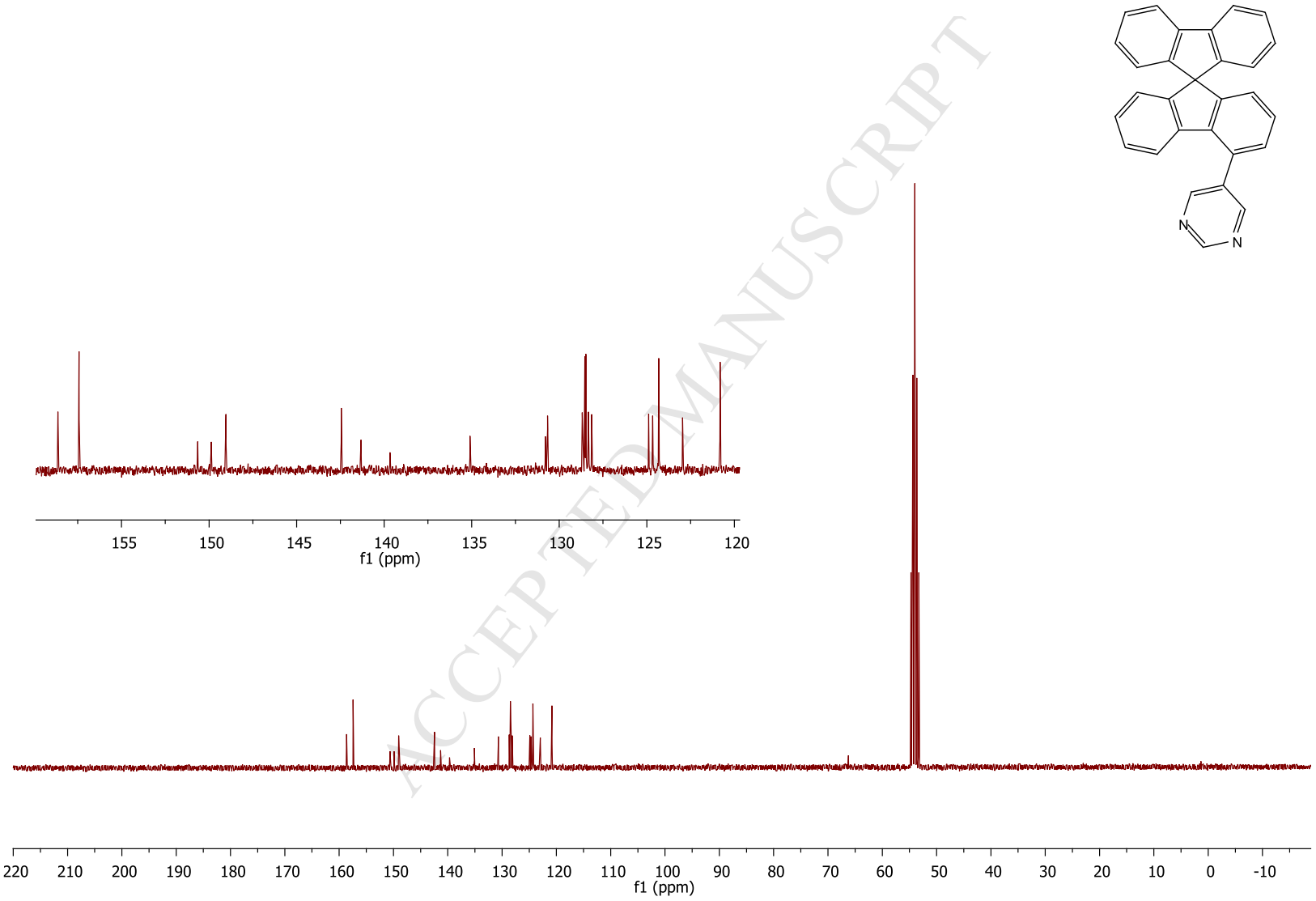

4-5Pm-SBF-DEPT-CD_2Cl_2

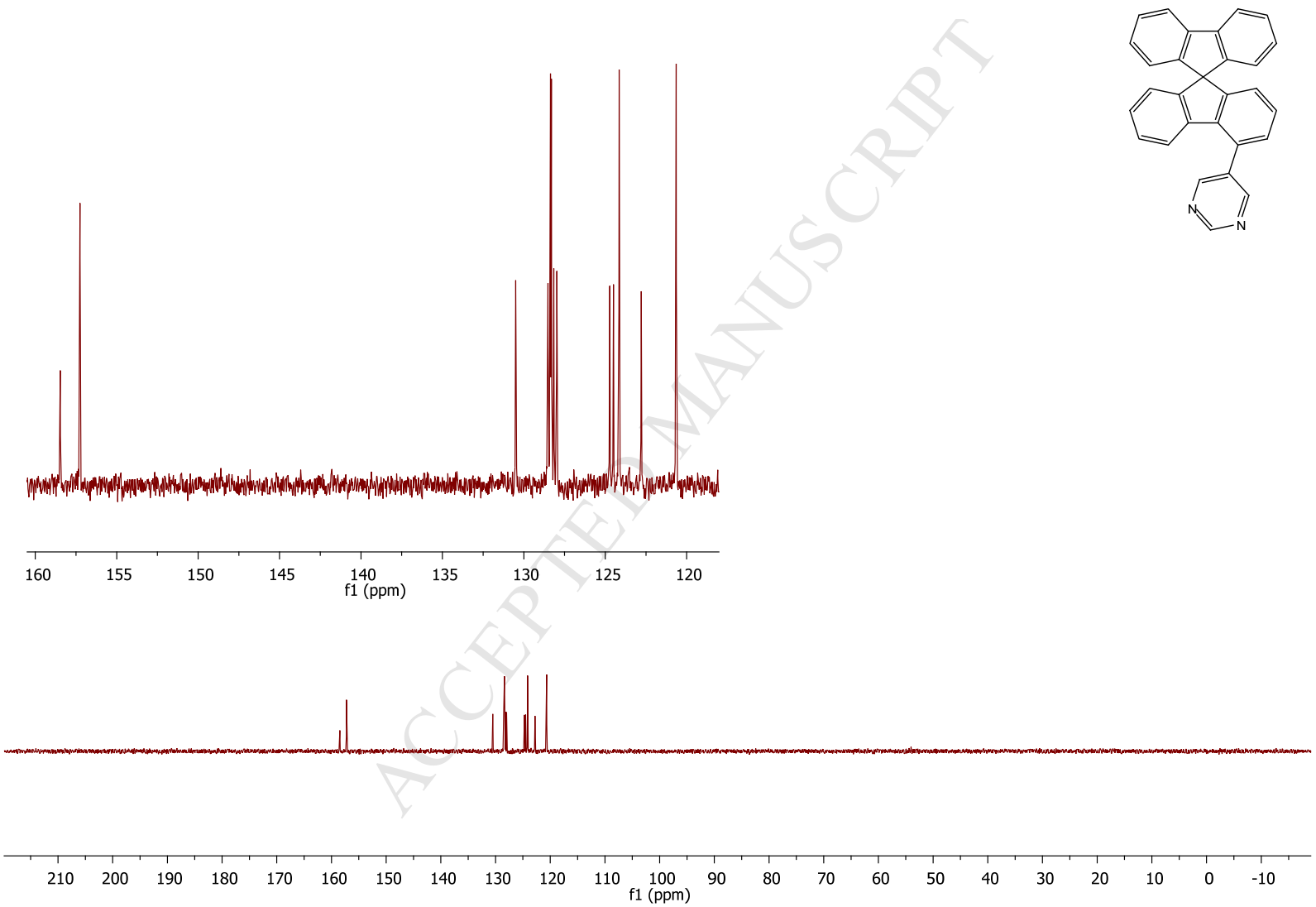

2-Ph-SBF-^{1}H-CD_2Cl_2

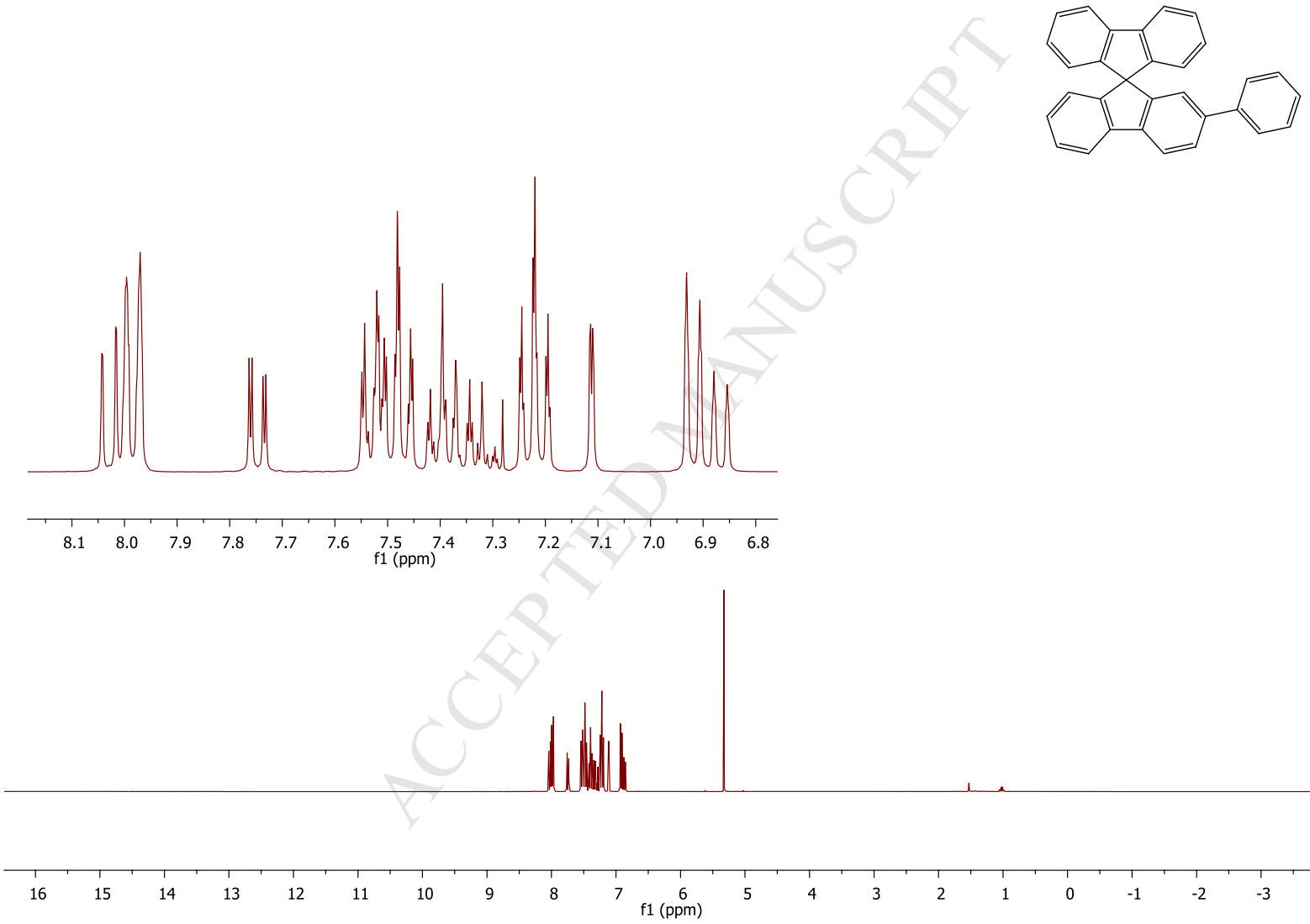

2-Ph-SBF-^{13}C-CD_2Cl_2

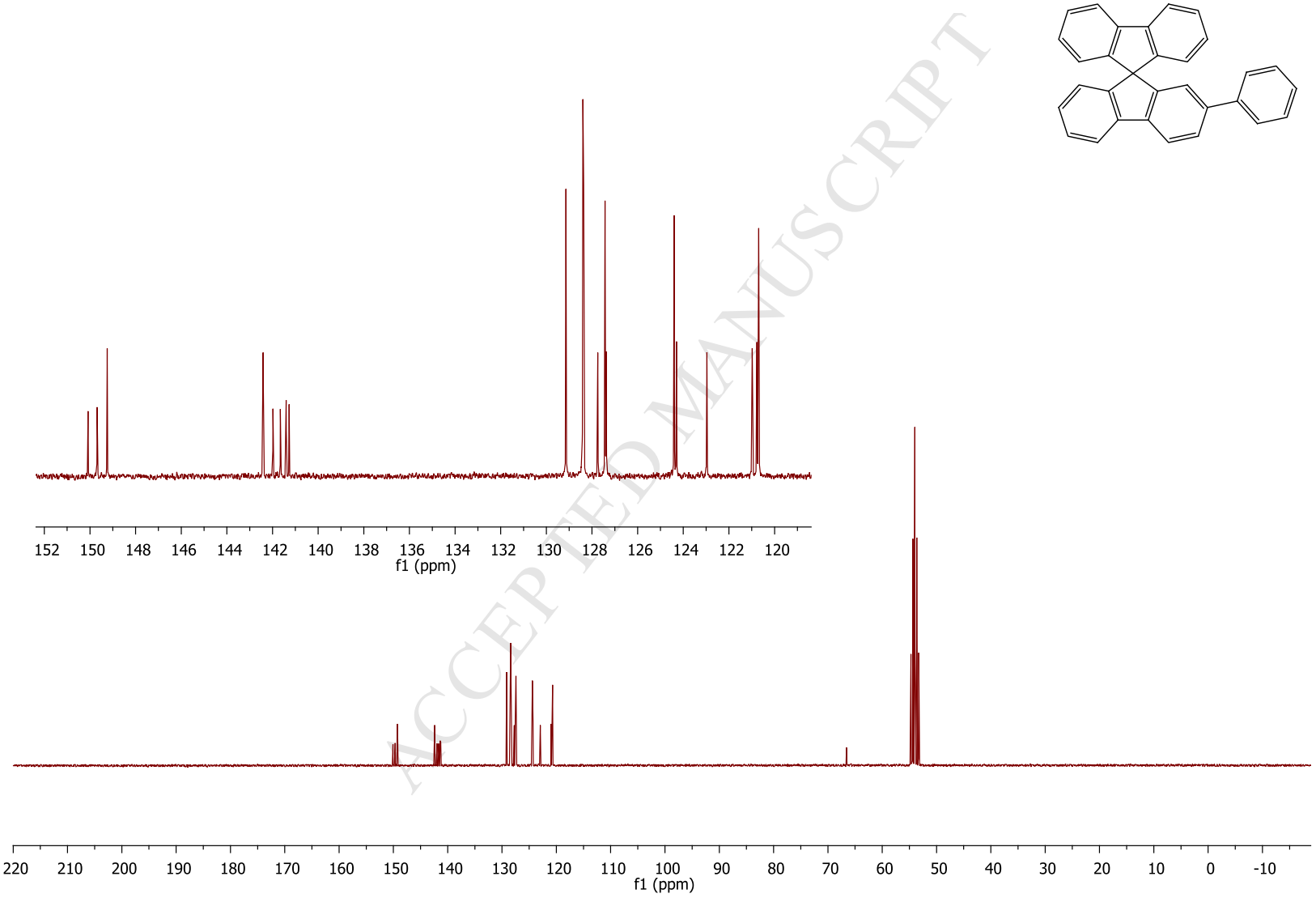

2-Ph-SBF-DEPT-CD_2Cl_2

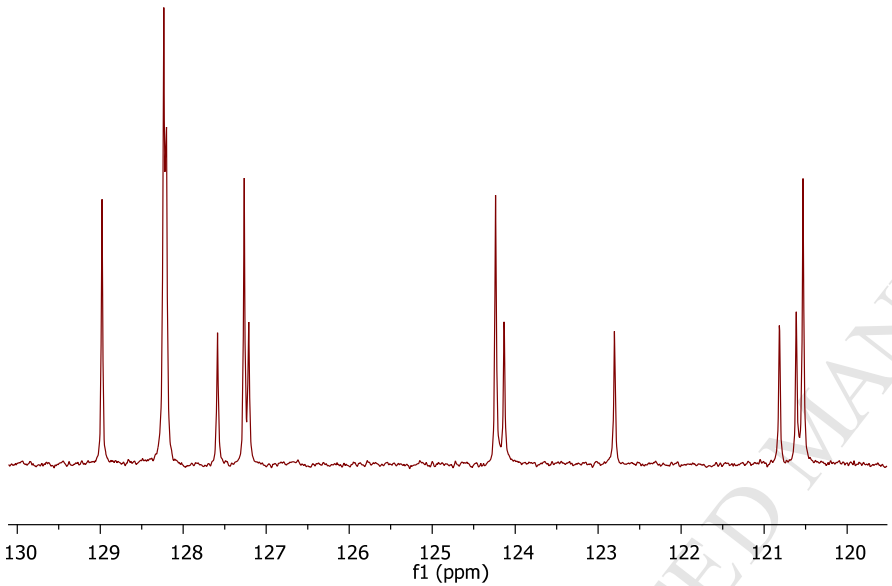

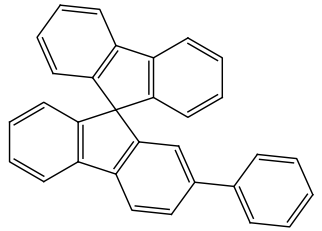

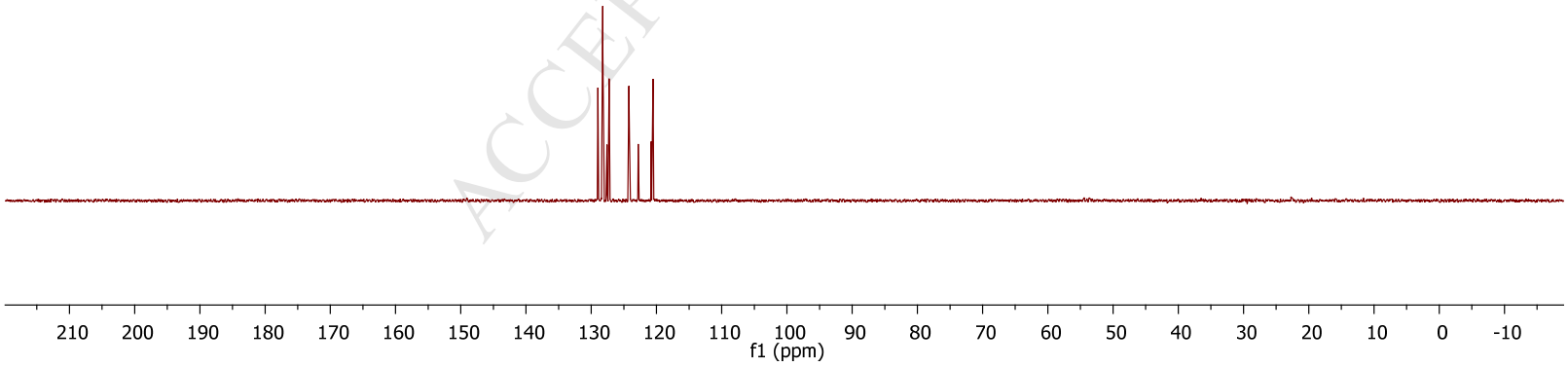

2-5Pm-SBF-^{1}H-CD_2Cl_2

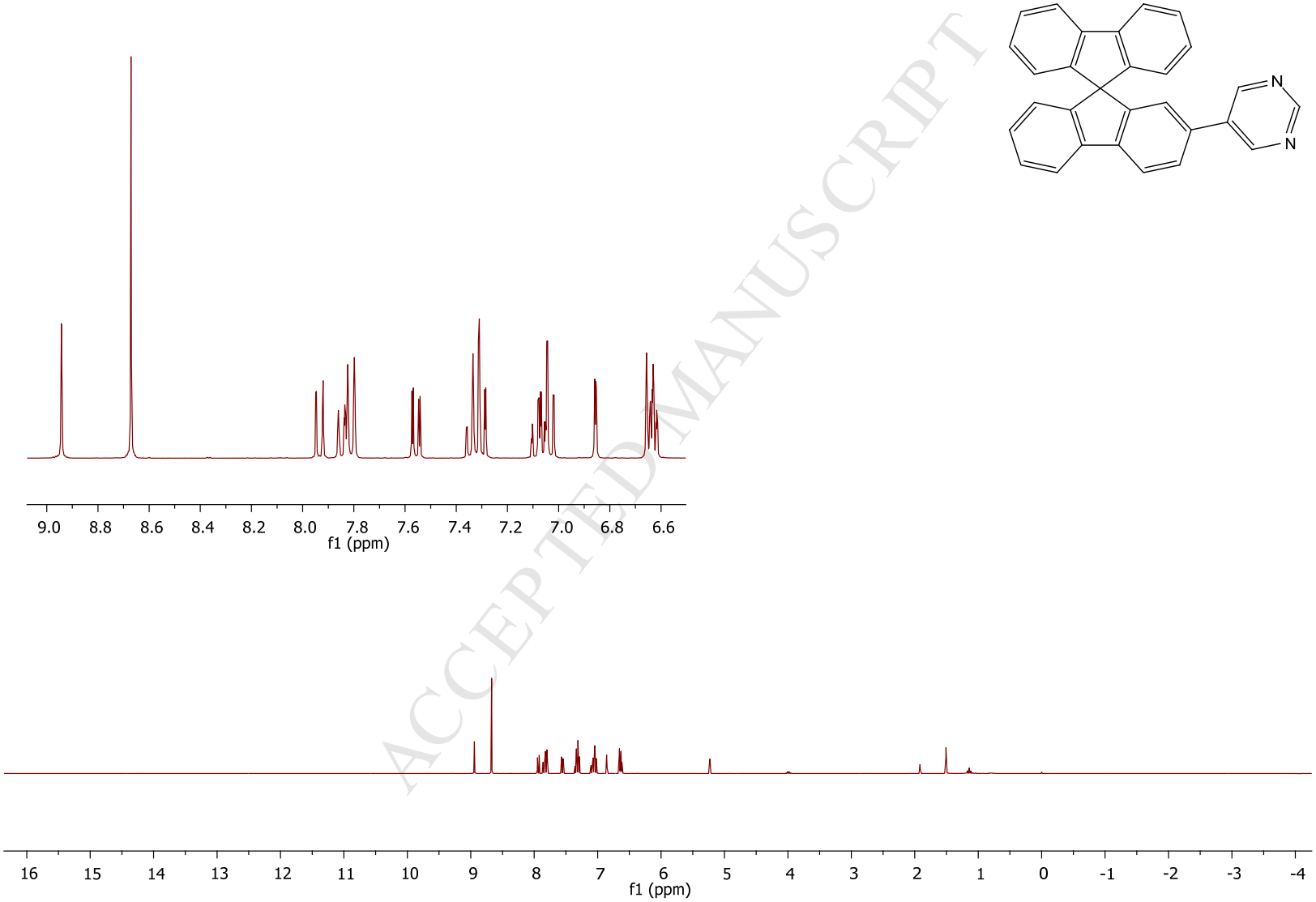

2-5Pm-SBF-^{13}C-CD_2Cl_2

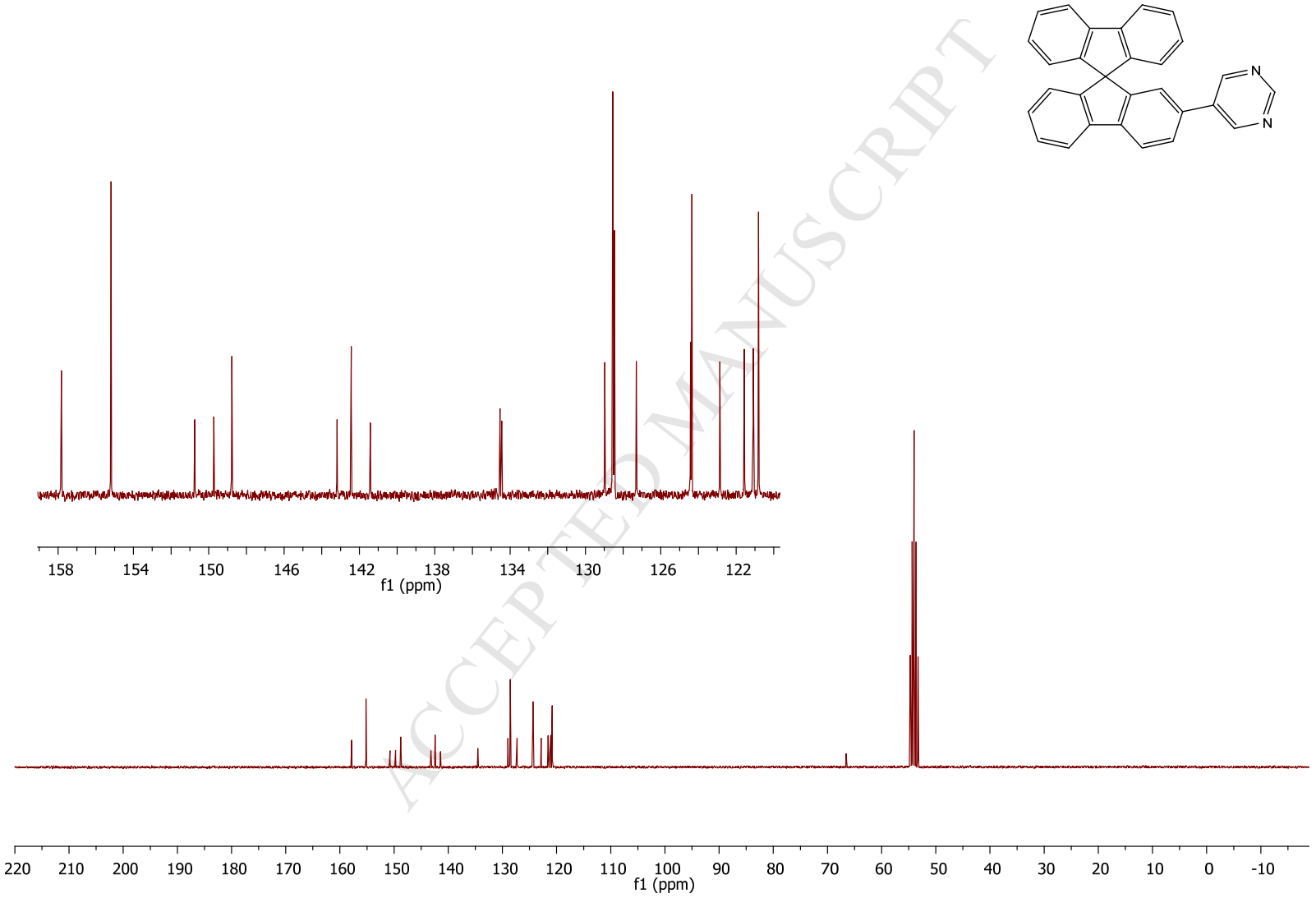

2-5Pm-SBF-DEPT-CD_2Cl_2

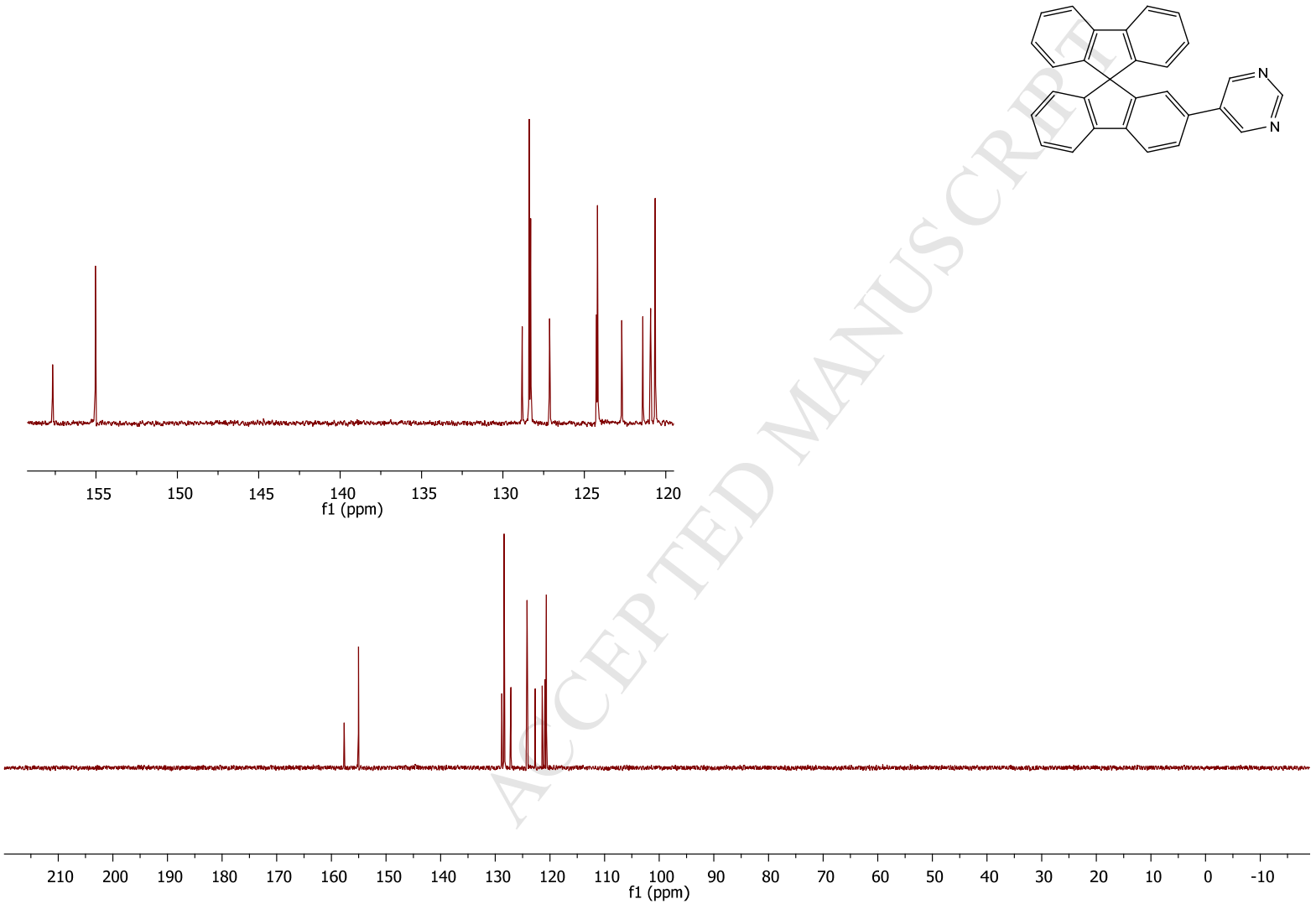

COPY OF MASS SPECTRA

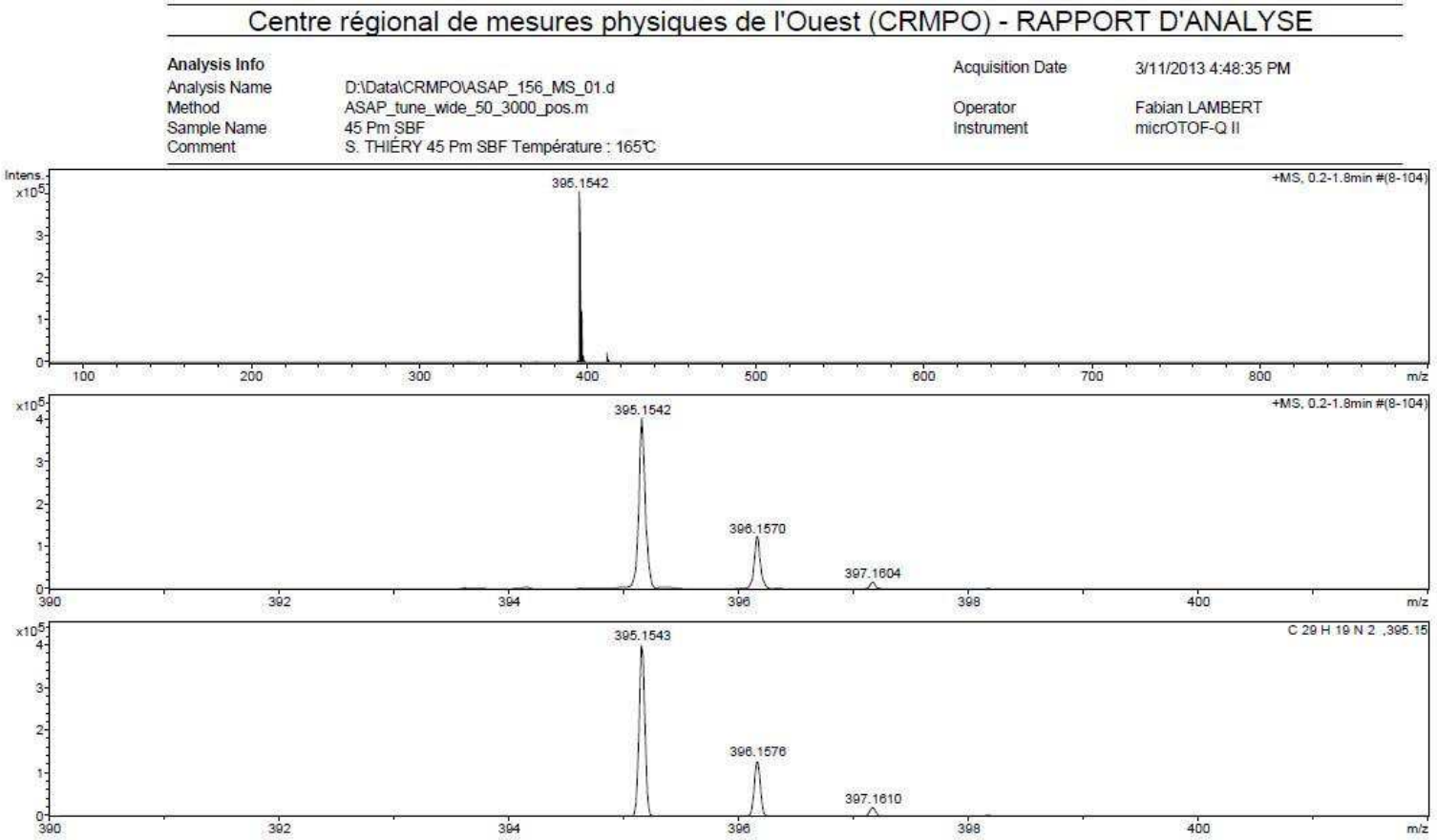

S 9 High Resolution Mass Spectrum of **4-5Pm-SBF**